Electronic Theses and Dissertations

Theses, Dissertations, and Major Papers

2003

# Integrated durability analysis of a vehicle through virtual simulation.

Craig Wood
*University of Windsor*

Follow this and additional works at: https://scholar.uwindsor.ca/etd

INTEGRATED DURABILITY ANALYSIS OF A VEHICLE
THROUGH VIRTUAL SIMULATION


BY


CRAIG WOOD


A THESIS

SUBMITTED TO THE FACULTY OF GRADUATE STUDIES AND
RESEARCH THROUGH THE DEPARTMENT OF MECHANICAL,
AUTOMOTIVE, AND MATERIALS ENGINEERING IN PARTIAL
FULFILMENT OF THE REQUIREMENTS FOR THE DEGREE OF
MASTER OF APPLIED SCIENCE AT THE UNIVERSITY OF WINDSOR


WINDSOR, ONTARIO, CANADA

AUGUST, 2003


© 2003 Craig Wood

Canada

# ABSTRACT

In a fast-paced industry that demands change, the need to be able to develop an automobile from start to finish in shorter and shorter periods of time is vital. Computer simulation has allowed engineers to overcome many barriers that have been encountered through traditional physical testing. Computer simulation allows for up-front engineering capabilities, where "virtual prototypes" can be constructed long before the physical ones even exist.

Vehicle durability testing is a process that involves proving ground and laboratory testing which evaluates a vehicle's resistance to component failure. This process is very time consuming and is very expensive. The intent of this research is to create a high-fidelity multibody dynamics model of a compact Sport Utility Vehicle (SUV) using CATIA, ADAMS and NASTRAN software suites. These software packages together are used to conduct virtual proving ground simulations. An MTS 329 series Road Test Simulator (RTS), which uses servo-hydraulic actuators to replicate vehicle proving ground is used to correlate results. The overall objective is to be able to predict component failure earlier in the design process, and to reduce the amount of time spent conducting physical durability tests. This thesis builds on research currently being conducted by many auto manufacturers in the area of virtual road test simulation.

The development of a complete durability model is very complex, and involves many steps in simulating physical phenomena. This research focuses primarily on model creation techniques that are used to build a virtual multibody dynamics model, with an emphasis being placed on the construction, implementation and background theory of flexible bodies. Model verification techniques are presented, illustrating how to correlate virtual forces and accelerations to values measured on an actual test vehicle.

Various methods were attempted as a means of input to the virtual modal that was created. After performing preliminary simulations, a method incorporating vertical

iii

displacements, lateral forces and longitudinal forces was adapted. Static validations were performed to validate weight distribution of the model, and then dynamic simulations were run using data obtained from an RTS rig representing real road data.

Rigid body simulations produced strong correlation in all vertical channels related to force and acceleration, and in general all force channels correlated within an acceptable level. The implementation of flexible bodies into the dynamic system proved to be influential on the overall vehicle response, and showed great promise in regards to acceleration correlation. The addition of the rear stabilizer bar as a flexible body in this model improved the lateral acceleration correlation dramatically. Documentation regarding flexible body creation using ADAMS was found to be practically non-existent based on an extensive review of literature. Consequently, these procedures are cited in greater detail within.

Two different rear suspension configurations were analyzed using ADAMS, where suspension vibration modes, forces and acceleration were compared between the two designs. Simulations dictated a reduction in forces transmitted to the body, which confirms that it may be necessary to use independent datasets in order to assess durability concerns, since the forces and accelerations are significantly different.

Process automation techniques were employed where custom menus were created within the ADAMS environment. These specialized functions allow component configurations to be rapidly changed, sensitivity analyses to be performed with ease, and allow for rapid data export. This is done to further decrease the amount of simulation time required, and also to allow for more configurations to be tested in a shorter amount of time.

For virtual simulation to be considered worthwhile, it has to be cheaper, faster, robust, and at the same time produce dependable, consistent results.

iv

v

# TABLE OF CONTENTS

## CHAPTER 3 – THEORETICAL BACKGROUND

## CHAPTER 4 - VIRTUAL MODEL CREATION

# LIST OF FIGURES

xi

xiv

# LIST OF TABLES

xv

# LIST OF ABBREVIATIONS

**2WD** - Two Wheel Drive
**4WD** - Four Wheel Drive
**ADAMS** - Automatic Dynamic Analysis of Mechanical Systems
**ARDC** - Automotive Research and Development Centre
**ASD** - Auto spectral Density
**ASTM** - American Standard for Testing Materials
**BCS** - Body Coordinate System
**BIW** - Body in White
**CAD** - Computer Aided Design
**CAE** - Computer Aided Engineering
**CAM** - Computer Aided Manufacturing
**CAT/ADAMS** - CATIA to ADAMS Conversion Module
**CATIA** - Computer Aided Three-Dimensional Interactive Application
**CMS** - Component Mode Synthesis
**cg** - Centre of gravity, centre of mass
**DAC** - Digital to Analog Conversion
**DADS** - Dynamics Analysis and Design System
**DAE** - Differential-Algebraic Equation
**DAQ** - Data Acquisition
**Deg** - Degrees
**DFT** - Discrete Fourier Transform
**DMU** - Digital Mock-Up
**DOF** - Degrees of Freedom
**EDM** - Empirical Dynamic Model
**EOM** - Equations of Motion
**FEA** - Finite Element Analysis
**FEM** - Finite Element Model
**FFT** - Fast Fourier Transform
**FRF** - Frequency Response Function
**FRL** - Full Rated Load
**ft, '** - Feet / foot
**Fx** - Force measured in the x (longitudinal) direction
**Fy** - Force measured in the y (lateral) direction
**Fz** - Force measured in the z (vertical) direction
**g** – Acceleration due to gravity
**GCS** - Global Coordinate System
**HOT** - Higher order terms
**HP** - Hewitt Packard
**HRL** - Half Rated Load
**Hz** - Hertz
**in, "** - Inches
**K&C** - Kinematics and Compliance
**kg** - Kilograms
**lb, lbs** - Pound(s) force

**LAP** - Light as Possible
**LCA** - Lower Control Arm
**LF** - Left Front
**LR** - Left Rear
**LT** - Light Truck
**LVDT** - Linear Variable Differential Transformer
**MART** - Arithmetic Manipulation Module (MSC.Patran)
**MASD** – Auto spectral Density Module (MSC.Patran)
**MMFD** - Multifile Display Module (MSC.Patran)
**MREMDAC** - Remote Parameter Control to DAC File Conversion (MSC.Patran)
**MDACREM** - DAC File to Remote Parameter Control Conversion (MSC.Patran)
**MDI** - Mechanical Dynamics Incorporated
**mm** - Millimeters
**MSR** - Modal Stress Recovery
**MTS** - Mechanical Testing and Simulation Inc.
**Mx** - Moment about an axis running in the x (longitudinal) direction
**My** - Moment about an axis running in the y (lateral) direction
**Mz** - Moment about an axis running in the z (vertical) direction
**MSC** - MacNeil-Schwendler Corporation
**MPC** - Multi-Point Constraint
**MPH** - Miles per Hour
**NASA** - National Aeronautics and Space Administration
**NASTRAN** - NASA Structural Analysis
**NVH** - Noise, Vibration, and Harshness
**ODE** - Ordinary Differential Equation
**PATRAN** - Patches for NASTRAN
**PSD** - Power Spectral Density
**RBE** - Rigid Body Element
**RF** - Right Front
**RPC** - Remote Parameter Control
**RR** - Right Rear
**RTS** - Road Test Simulation
**RVDT** - Rotary Variable Differential Transformer
**SAE** - Society for Automotive Engineers
**s, sec** - Seconds
**SGI** - Silicon Graphics Incorporated
**SLA** - Short Long Arm
**SPC** - Single Point Constraint
**SUV** - Sport Utility Vehicle
**SWIFT** - Spinning Wheel Integrated Force Transducer
**TI** - Transducer Interface
**UCA** - Upper Control Arm
**VIMF** - Vehicle Inertial Measurement Facility
**VPM** - Virtual Product Modeler
**VTL** - Virtual Test Lab
**WFT** - Wheel Force Transducer

$a$ - Acceleration

$A_{313}$ - Euler angle transformation matrix

$^G A^B$ - Euler angle transformation matrix used in converting from body to ground coordinates

$^G A^J$ - Euler angle transformation matrix from the reference marker J, to the ground coordinate system

$^G A^L$ - Euler angle transformation matrix from the reference marker L, to the ground coordinate system

$^B A^P$ - Euler angle transformation matrix relating the orientation change due to body deformation at node P

$^P A^J$ - Euler angle transformation matrix from the user defined marker, J that was manually placed on the body, to the deformed position

$b$ - Distance between I and J markers

$B$ - Body transformation matrix relating the angular velocity of a body and the generalized coordinates

$c_i$ - Damping of mode i

$c_i^{cr}$ - Critical damping

$C_s$ - Damping coefficient of linear spring element

$C_t$ - Damping constant of torsional spring element

$C_1, C_2, C_3$ - Translational bushing damping coefficients\

$D$ - Modal damping matrix, containing damping coefficients

$e$ - Natural Number $\approx 2.7182818$

$\bar{f}$ - Vector of Applied forces

$F(t)$ - Vector of applied forces

$F$ - Force on a body

$f_g$ - Force due to gravity

$F_L$ - Force applied to a marker, L, on a flexible body

$F_{preload}$ - Force preload in linear spring

$F_x, F_y, F_z$ - Translational bushing force components

$F_1, F_2, F_3$ - Constant bushing preload force components

$g$ - Gravitational constant, where $1\ g = 9.80665 m/s^2$, gravitational acceleration vector

$i, j, k$ - Unit vectors in X, Y and Z directions respectively

$I$ - Moment of inertia (MOI)

$I_t$ - Inertia Tensor

$I_{xx}$, $I_{yy}$, $I_{zz}$ - Moments of inertia about X, Y and Z axes respectively

$I_{xy}$, $I_{yx}$, $I_{xz}$, $I_{zx}$, $I_{yz}$, $I_{zy}$ - Products of inertia

$I_p$ - Nodal inertia tensor

$\bar{J}$ - Generalized inertia matrix expressed about the principal reference frame

$k_i$ - Generalized stiffness of mode $i$

$K$ - Kinetic energy in the system, generalized stiffness matrix

$K(\xi)$ - Time variant stiffness matrix for flexible bodies

$\hat{K}_{NN}$ - Stiffness diagonal matrix

$K_s$ - Stiffness coefficient of linear spring element

$K_t$ - Stiffness constant of torsional spring element

$K_1, K_2, K_3$ - Translational bushing stiffness coefficients

$K_{r,t,m}$ - Stiffness matrix components for rotation, translation, and modal DOF. Subscripts are dependant on position of variable in stiffness matrix, $K(\xi)$

$K_4, K_5, K_6$ - Rotational bushing stiffness coefficients

$L$ - The Lagrangian, which denotes L=T-V

*length* - Reference length of spring element (free length when $F_{preload}$ is zero)

$m$ - Mass

$m_i$ - Generalized mass of mode $i$

$m_p$ - Nodal mass

$M$ - Generalized mass matrix

$\dot{M}$ - Time derivative of the flexible body mass matrix

$M(\xi)$ - Time variant mass matrix for flexible bodies

$M_{r,t,m}$ - Mass matrix components for rotation, translation, and modal DOF. Subscripts are dependant on position of variable in mass matrix, $M(\xi)$

$\hat{M}_{NN}$ - Mass diagonal matrix

$M_o$ - Number of mode shapes

$N$ - Nodal transformation matrix

$n$ - Number of degrees of freedom (DOF)

$n_b$ - Number of bodies

$n_c$ - Number of constraints

$n_{gc}$ - Number of generalized coordinates

$n_j$ - Number of joints

$N_o$ - Number of nodes

$p$ - Matrix representing the position of a rigid body

$q$ - Matrix representing the generalized coordinates of a system

$\dot{q}$ - Velocity

$q^*$ - Orthogonalized modal coordinates

$q_C$ - The modal coordinates of the constraint modes

$q_f$ - Generalized coordinates of the flexible body

$q_i$ - i-th modal scaling factor

$q_m$ - Vector of modal coordinates

$q_N$ - The modal coordinates of the normal modes

$Q$ - Generalized forces acting on a body

$Q_T$ - Generalized translational force

$Q_R$ - Generalized rotational force

$Q_M$ - Generalized modal force

$r$ - Distance between markers on linear spring elements

$\vec{r}_p$ - The instantaneous location of a marker attached to a mode, P, on a flexible body

$\vec{s}_p, s_p$ - Position of the undeformed point P with respect to the local body reference frame in vector and matrix form respectively

$t$ - Time

$\vec{t}$ - Vector of applied torques

$\Delta t$ - Time step

$T$ - Kinetic Energy

$\vec{T}_b$ - Sum of torques applied to the body

$T_{preload}$ - Torque preload in torsional spring

$T_{total}$ - Total resultant torque on a body

$T_L$ - Torque applied to a marker, L, on a flexible body

$T_x, T_y, T_z$ - Rotational bushing torque components

$T_1, T_2, T_3$ - Constant bushing torque preload components

$u$ - Matrix of body translational velocities

$u_b$ - Boundary DOF

$u_i$ - Interior DOF

$u_n$ - Linear physical nodal displacements

$\vec{u}_p$ - Translational deformation of the point P from the point's undeformed position, to the deformed position

$u_x, u_y, u_z$ - Direction cosines

$v_0$ - Initial velocity

$v_p$ - The velocity of the point of application, p, of the external force

$v$ - Volume

$V$ - Potential energy

$V_g$ - Gravitational potential energy

$V_x, V_y, V_z$ - Time derivatives of $x_b, y_b, z_b$, respectively for bushings

$x$ - Coordinate along x-axis

$\bar{x}$ - Position vector from the origin of the ground coordinate system to the local body coordinate system

$x_b$ - Bushing deformation in x-direction

$y$ - Coordinate along y-axis

$y_b$ - Bushing deformation in y-direction

$y_n$ - Solution Calculated at Time = $t_n$

$y_{n+1}$ - Solution Calculated at Time = $t_{n+1}$

$z$ - Coordinate along z-axis

$\Lambda_1, \Lambda_2, \Lambda_3...$ - Inertia invariants

$\alpha$ - Angular Acceleration

$\varepsilon$ - Matrix of Euler angles

$\eta$ - Nodal damping ratio

$\Im$ - Energy dissipation function

$\lambda$ - Lagrange multipliers of a system

$\lambda_{eig}$ - Eigenvalues of system

$\theta_o$ - Reference angle for torsional spring element (free angle when $T_{preload}$ is zero)

$\theta_t$ - Angle between markers using torsional spring elements

$\theta_1, \theta_2, \theta_3$ - Small-angle bushing rotational displacements

$\phi_i$ - i-th mode shape vector

$\phi_i^*$ - Orthogonalized Craig-Bampton modes

$\Phi$ - Constraint equation

$\Phi_m$ - Modal matrix

$\Phi_{IC}$ - Physical displacement of the interior DOF in the constraint modes

$\Phi_{IN}$ - Physical displacement of the interior DOF in the normal modes

$\Phi_p$ - Matrix of partial derivatives of constraint equations with respect to position, p

$\Phi_P$ - Portion from the modal matrix that corresponds to the translational DOF of the node P

$\Phi_P^*$ - Portion from the modal matrix that corresponds to the rotational DOF of the node P

$\Phi_q$ - Matrix of partial derivatives of constraint equations with respect to generalized coordinates, q

$\Phi_\varepsilon$ - Matrix of partial derivatives of constraint equations with respect to Euler angles, $\varepsilon$

$\psi$ - Algebraic constraint equation

$\varphi, \theta, \phi$ - First, second and third Euler angles

$\pi$ - Pi $\approx 3.1415926$

$\mu\varepsilon$ - Microstains

$\zeta$ - Matrix of body angular velocities

$\xi$ - Generalized coordinates of a flexible bodies

$\Pi^P, \Pi^R$ - Projection operators

$\Gamma$ - Angular momenta

$\Delta^{(j)}$ - Correction factor used with Newton-Raphson method

$\sim$ - Skew operator, as defined in Equation 3.54

$\omega$ - Frequency of Vibration

$\omega_d$ - Damped Natural Frequency

$\omega_f$ - Frequency of Force in Forced Vibration (Driving Frequency)

$\omega_n$ - Natural Frequency of Vibration

$^{G}\omega_B^{B}$ - Angular velocity of the body relative to the ground coordinate system, expressed in body coordinates

$^{G}\omega_B^{J}$ - Angular velocity of the body relative to the ground coordinate system, expressed at a marker, J

$^{B}\omega_B^{P}$ - Angular velocity of the body relative to the body coordinate system, expressed at a deformed node, p

$\omega_x, \omega_y, \omega_z$ - Bushing angular velocity components

$\varpi$ - Body angular velocity

# CHAPTER 1 INTRODUCTION

## 1.0 General

Reducing the time to market for production vehicles has long been one of the primary goals for automobile manufacturers. Computer simulation has allowed engineers to reduce the vehicle development time by using up-front Computer Aided Engineering (CAE) techniques, such as the procedures presented in this research. The ability to produce a high quality product in less time and at lower cost allows products to get to market faster, and carry less risk of failure, which translates to less liability for the manufacturer. Each manufacturer also strives to be the first to market for new vehicle segments, which further emphasizes the importance on time constraints.

Vehicle durability measures the ability of a vehicle's components to withstand the loading placed on them under typical driving conditions. Durability is also synonymous with quality in the eyes of a buyer. To evaluate vehicle durability, instrumented vehicles are rigorously tested at proving ground facilities, as well on a Road Test Simulator (RTS), both of which allow accelerated vehicle testing over a wide range of conditions.

1

The RTS is able to simulate real world testing in the controlled environment of a laboratory, by exciting a vehicle in order to replicate forces, accelerations and movements encountered at the proving ground. This allows engineers to evaluate the life of the components, and also allows comparisons to be made based on changes made to components during the design and testing phase. This portion of the vehicle design cycle can be very time consuming and expensive, but is critical in determining how long the vehicle can endure without component failure. If a method could be devised to simulate these procedures in the virtual realm using high speed computers, it could further reduce the amount of time and money spent testing and building physical prototypes, and allow the evaluation of many more "what-if" configurations.

## 1.1 Project Overview

In the current research, a model has been devised to simulate a compact Sport Utility Vehicle (SUV) vehicle on a RTS machine undergoing a conventional durability test. Software suites including CATIA, ADAMS and NASTRAN have been used for model construction, simulation and validation. A full vehicle model has been created using ADAMS software, which is a commercially available multibody dynamics software package. A computer model of the vehicle's suspension was built up from a manufacturer's database and assembled to create a virtual model. Properties for elements such as springs, shock absorbers and bushings were acquired from appropriate manufacturers and suppliers for all necessary components on the test vehicle. Process automation was addressed, and techniques were developed to rapidly change component configurations in the virtual model using ADAMS multibody dynamics software. Custom menus were devised in the ADAMS environment to further automate the virtual simulation process.

2

Two different types of suspension configurations were tested for a compact Sport

Utility Vehicle (SUV) using these methodologies. Flexible bodies were used to

investigate the stress distribution in specific parts under dynamic loading conditions, as

well as to generate files to be used in fatigue analysis. A full model has been created for

the entire testing apparatus itself in addition, all of which will be described in detail

within the chapters to follow.

This research was conducted at the University of Windsor / DaimlerChrysler

Automotive Research and Development Centre, which is located in Windsor, Ontario,

Canada. The ARDC facility is home to over 200 personnel, which includes students,

engineers, technicians and support staff members. This project was done in partial

collaboration with Ferry {16} at this facility, and involves simulating an additional

vehicle, as well as building on the concepts and methodologies that were used in that

earlier thesis investigation.

## 1.2 Ground Vehicle Testing

Ground vehicle testing has been used for decades to evaluate reliability, structural

defects, and performance characterization of a vehicle under a range of operating

conditions. Three unique testing methods currently exist including proving ground

testing, road test simulation (RTS), and virtual simulation. These three methods will be

compared in detail within the sections to follow.

## 1.2.1 Proving Ground Testing

Proving ground testing is conducted on specially made closed-circuit on and off-

road courses which are designed specifically for the testing of vehicles. These courses

can include off-road terrain, high speed tracks, and worn road sections to test a vehicle in

its expected environment. This process is *very* time consuming, as it requires the test

vehicles to be driven for weeks or months on end. The results are also dependant on the

3

competence and driving style of the actual driver of the test vehicle, since a vehicle must be driven literally thousands of kilometers.

Proving ground testing is used to excite a vehicle using obstacles that are known to be damaging to the vehicle's structure. For example, a vehicle driving over a pothole is more likely to sustain damage than a vehicle driving on smooth pavement. By running a vehicle over harsh obstacles like these rather than driving it over many kilometres of smooth pavement, the durability cycle of the vehicle can be shortened dramatically.

A proving ground also enables engineers to test environmental conditions such as temperature and humidity extremes, as many of the components may behave differently in varying temperature regimes. Manufacturers typically operate proving grounds in several climates, ranging from hot deserts, to the northern snow belt, to test vehicles in a variety of conditions. Tests conducted at these facilities tend to be very time consuming and expensive, but are indicative of how a vehicle will behave in the real world.

Changes in configuration to vehicles at a proving ground can be difficult to address, and usually require full re-testing to observe effects and trends. A test generally requires many weeks to complete, as well as extensive set up and vehicle preparation time. In this atmosphere, investigating what-if scenarios is not cost effective, and tends to fall back to trial and error methodologies. If components on the vehicle fail early into the durability cycle, the cost and time spent escalate even further. Virtual simulation attempts to foresee these problem areas earlier on in the design cycle, so component failures can be predicted and corrected before the first prototypes are even built.

With proving ground testing, it is difficult to reduce the time required to run a single durability test, as vehicles have to be driven a certain distance at certain speeds to replicate the life cycle of a given vehicle. Proving grounds themselves also require regular maintenance when vehicles are driven over these terrains repetitively. Testing at these facilities is weather dependant, which can cause further delays in testing. The

4

overall objective with virtual simulation is not to eliminate the proving ground from the loop, but to predict vehicle performance ahead of time to minimize the number of tests that have to be conducted, and to eliminate testing that depends on trial and error techniques.

### 1.2.3 Road Test Simulation

Documentation from MTS Corporation {30} explains that the purpose of a Road Test Simulator (RTS) is twofold:

- To gather dynamic loading data that represents the real-time inputs experienced by a vehicle's suspension under driving conditions

- Reproduce the real time inputs in the test laboratory

The RTS machine consists of computer controlled hydraulic actuators that are capable of exciting a vehicle in certain directions, and are categorized by the degrees of freedom (DOF) of which they are capable of replicating. Two common types of simulators that exist are tire-coupled and spindle-coupled. Road coupled simulators apply forces and displacements to a vehicle at the tire contact patch, meaning the vehicle is not physically attached to this machine. Figure 1.1 shows a common 4 poster simulator which has one DOF per wheel. This type of simulator which allows for the accurate replication of vertical forces and accelerations. Spindle coupled simulators involve removing the wheels from the vehicle, and attaching the vehicle directly to the testing apparatus as shown in Figure 1.2. These are commonly referred to as 4 DOF simulators. The four degrees of freedom available at each wheel are: translation in the vertical, longitudinal, and lateral directions, and braking torque about the centreline of the wheel. Each of these movements can be controlled independently.
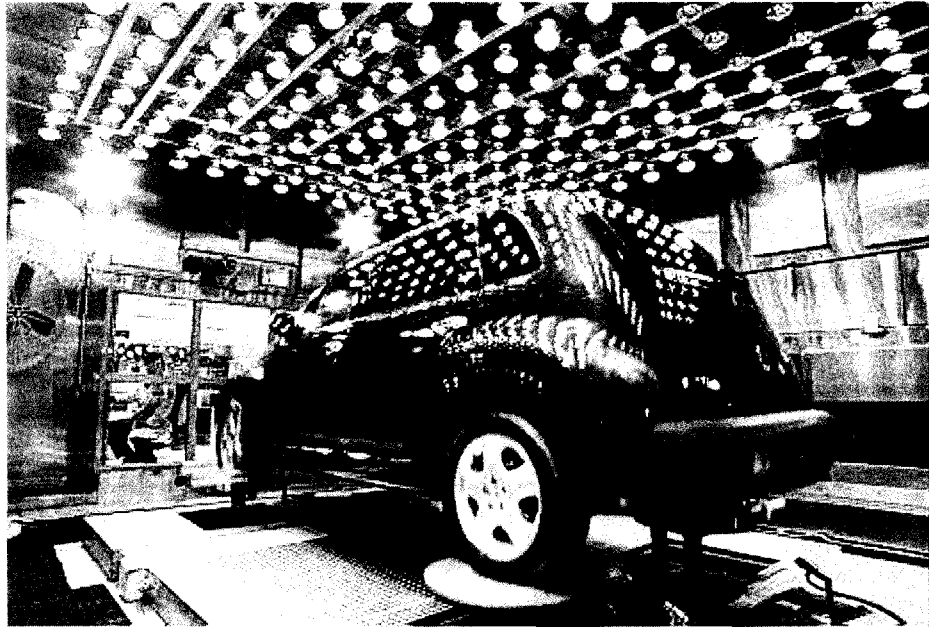
**Figure 1.1**: Vehicle mounted on a 4 poster Road Test Simulator (RTS), which is
commonly used to run vertical durability tests as well as NVH tests (noise,
vibration, and harshness). The model shown above is an MTS 320
simulator, which allows environmental conditions to be tested in addition.
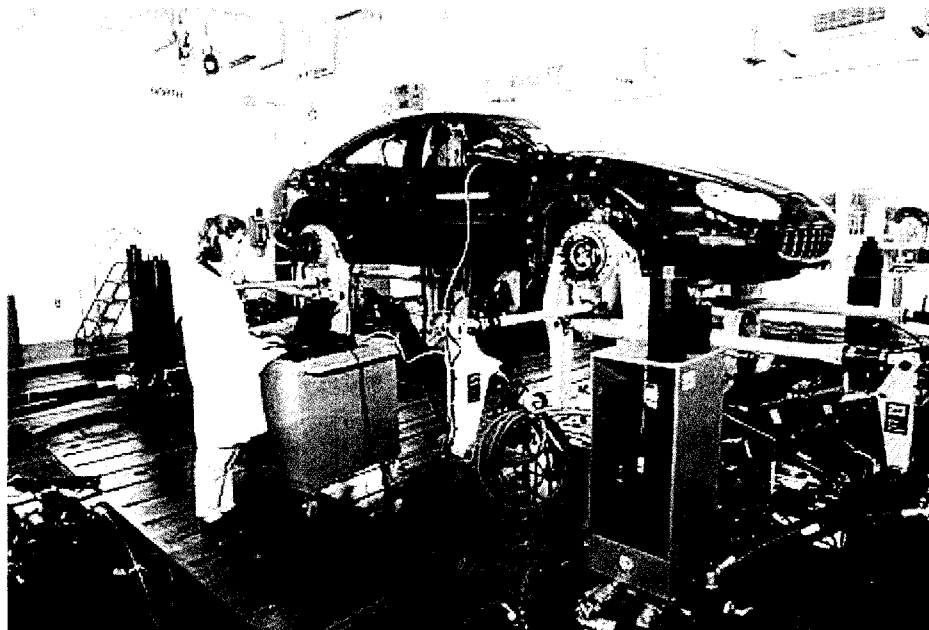


**Figure 1.2**: Vehicle mounted on a 4 DOF Road Test Simulator (RTS), which is used to
simulate durability schedules in a controlled laboratory environment. This
particular apparatus, the MTS 329 passenger car simulator, was used
specifically for virtual model validation in this project.

6

The RTS machines can be used to test separate portions of a vehicle, such as front or rear suspension assemblies, which do not require an entire vehicle to be present. Rigs used in this configuration are commonly referred to as half rigs. Rigs that provide two additional DOF at each wheel in comparison to the 4 DOF models are also commercially available. The units are referred to as 6 DOF machines and provide two additional moments (torques) at each wheel in addition to braking torque. These RTS rigs provide precise control of all translational and rotational DOF at each spindle. Degrees of freedom of a body will be described in greater detail in Section 2.4.1.

A fully instrumented vehicle is run on a durability course several times at the proving ground to generate data that is used for these test rigs. This information is conveyed to the laboratory, where test engineers create "drive files" which command the simulators to excite the vehicle in the same manner as at the proving ground. The process in creating a drive file to be run on an RTS rig will be explained in Section 2.3. Once this stage is complete, damaging data can be replicated over and over again in the test lab.

Environmental effects such as temperature and humidity and/or solar exposure can be simulated as shown in Figure 1.1, but are commonly available only on four-poster rigs. Testing of this nature is very expensive and is complex. Set-up, testing and regular maintenance of these rigs is also expensive, as are the actual test rigs themselves. Neither the effects of power/drive train operations, aerodynamics nor corrosion are considered in the laboratory. It is difficult to further reduce test time once a process is optimized because this process is limited to real time analysis, as with proving ground testing.

The objective of virtual simulation is not to replace this step in the durability process. It can make this process more efficient and can potentially predict component issues earlier in the design phase. This way, the test cells can be used to run fewer tests

7

of the same vehicle, the cell can be allocated to other test programs, and the RTS rigs will require less maintenance per vehicle run.

### 1.3 Vehicle Prototyping and the Design Cycle

Campbell {7} notes that product improvement using CAE has been shown to save more than a billion dollars on major automotive programs, while reducing time to market. Computer simulation acts to reduce the amount of time taken in the development of a new vehicle. By using computer simulation, the efforts in design and analysis are concentrated up-front in the process. The further along in the design cycle the vehicle progresses, the higher the cost of change is, and the more difficult changes are to implement as is shown in Figure 1.3.
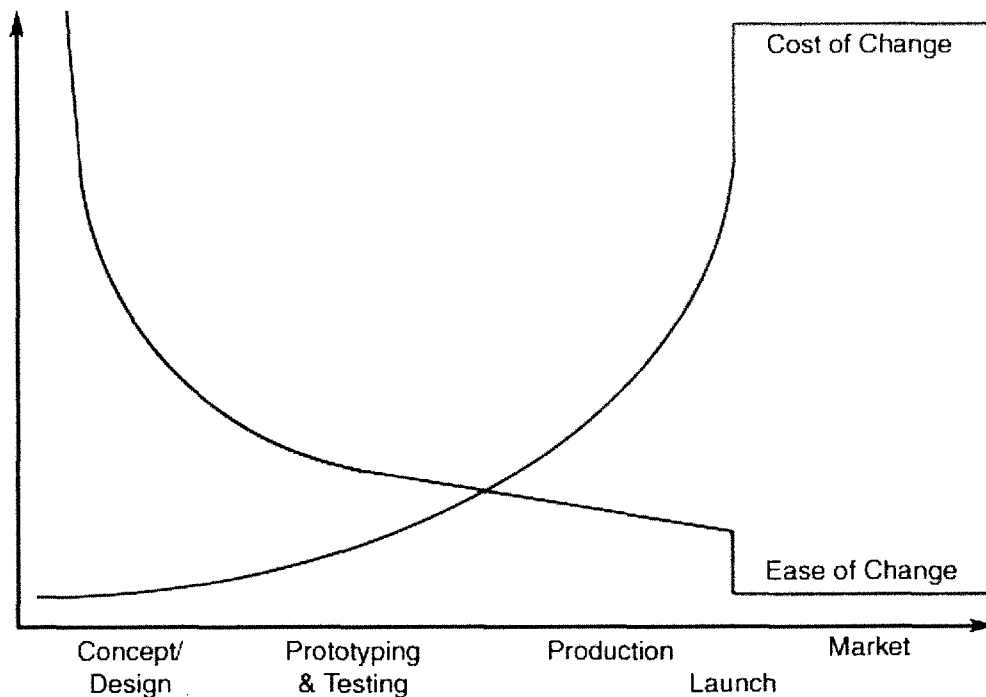


**Figure 1.3:** Illustration of how the cost of change increases dramatically throughout the product lifecycle of a vehicle. As time progresses into vehicle development and into production, the ease of making a change decreases inversely with the cost. At the point of launch, the cost of change increases instantly, and it becomes much more difficult to make changes from this point on.

8

In the conceptual and design stage, the cost of change may be as simple as the time it takes to alter the design on a computer or on drawings, which is very modest in comparison to later on. In the prototyping stage, the cost of change begins to rise, where new prototypes may have to be made, and testing apparatus have to be altered. In this stage, change is less acceptable, since it will require significant investment. The ease of change continues to decrease as a result of this. Once production begins, the cost of change increases dramatically; tooling may have to be changed, assembly lines may have to be altered, and manufacturing processes may have to be changed. Once the vehicle is launched into the market, the cost of change escalates even further. Change during the customer usage period comes in the form of recalls and warranty claims, which Nasser et al. {31} states can cost the company hundreds of millions of dollars.

### 1.3.1 Physical Prototyping

It is very common in pre-production and in the production phase to have several different configurations for components that are being considered for implementation. To execute a change such as a full rear suspension system would require prototypes to be built, new bushings to be developed, and would require the vehicle to be run through a durability cycle once again. It is easy to see that this would be very time consuming, as well as being very costly, especially if the end result shows that the change actually has negative effects. If a validated virtual prototype could be created up-front, this could potentially save the task of constructing multiple physical prototypes, and would allow many more of these "what-if" configurations to be examined.

### 1.3.2 Virtual Prototyping

Campbell {7} explains that computer simulation has been shown to be effective for many engineering tasks such as: 1) determining structural loading 2) predicting vibration and noise and 3) determining stiffness/resonance of components or systems.

9

Virtual prototyping constitutes performing all the processes that were traditionally conducted on a physical mockup using a digital computer model. The construction of virtual prototypes follows the same progression used in physical prototyping. A system is designed, rigorous testing is conducted, and results are examined. The design is then refined based on results, and iterations are conducted until the performance of the system has been optimized. The main difference with virtual prototyping is that all of the analysis is done using a computer system. What used to take weeks or even months to design, manufacture and analyze physically can now be achieved in just hours.

Simulation of a vehicle's suspension system has many advantages over physical testing for several reasons. Bushing, spring and damping (shock absorber) properties can be changed with ease, which is particularly useful in tolerancing and sensitivity studies. Ultimately, a nearly unlimited number of possible configurations can be investigated. Model geometry can be changed with ease in comparison, and can be optimized based on results from simulations.

One significant benefit to virtual simulation is that each time a new computer simulation is run, it can be run with a "brand new" vehicle. With physical tests, "mule" vehicles are used to test various component configurations. Each time a configuration is changed, a new dedicated mule vehicle is required. These mule vehicles are often one of a kind prototype test vehicles, which are very costly, especially when several of them are required to test different configurations.

Another crucial element in the design analysis is determining the loading to which components are subjected to. A physical vehicle can be instrumented to measure only the loads on a vehicle where sensors can be viably placed, such as at the spindle (using wheel force transducers (WFT's)), and at ball-joints. These loads are used to correlate the virtual model.

10

With a calibrated virtual model, loads and stresses can be measured almost anywhere on components, when flexible bodies are used. In many cases, dynamic loads would be impossible to measure using traditional sensors on physical vehicles, where these properties can be measured with ease on a virtual model. This alone saves a great deal of time and money in instrumentation, data acquisition, and data editing on a physical vehicle. An unlimited number of sensors can be placed on a virtual model, as they do not occupy volume like physical ones do, and they will not affect the dynamic response of the virtual vehicle by adding mass.

## 1.4 Virtual Simulation and Design Considerations

As computer simulation continues to gain acceptance in industry, the applications of simulation also continue to increase. Simulation time is dependant on computational power; the faster the computer, the faster the simulations. The speed at which simulations can be prepared and run is also dependent on the knowledge and training of the individual users. Simulations are already being conducted today that a decade ago would not have been thought to be possible. Looking ahead to the future, the speed at which these simulations can be run will only continue to increase.

### 1.4.1 Process Validation

A computer model is only as accurate as the component properties, and requires validation with physical data to confirm its precision. Sensor responses, both physical and virtual, are used in order to correlate the virtual model behavior to the physical equipment. It must be noted that the objective of computer testing and simulation is not to render physical testing obsolete, as testing and simulation complement each other.

To validate a computer model, clean and reliable dynamic data is needed from instrumented test vehicles. These are used as virtual model inputs. Detailed component information about the specific test vehicles is critical in the validation process. This

11

includes physical component geometry, mass, and inertial properties, as well as rate properties of bushings, springs, shock absorbers and jounce bumpers. Detailed records of the data acquisition process is also necessary, including specifics on sensor placement, calibration and polarity of channels, vehicle payloads used, and durability schedules that are run. Using more accurate information in the model creation results in more reliable predicted behavior of the model.

Rao {35} explains that a well correlated model can be used to study the behavior of the vehicle under different conditions with reasonable confidence. A well validated model forms the baseline for evaluating the effect of design changes. This reduces the need to go through the expensive and time-consuming process of building several physical prototypes and carrying out tests at proving ground facilities and on RTS machines. Iterations can be performed on several "virtual prototypes", and one physical prototype can be built based on the optimized design.

## 1.4.2 Drawbacks to Virtual Simulation

Despite approaches used in virtual prototyping, systems that include friction, elastomeric components, complex fluid dynamic behavior, wear and corrosion can be difficult to model accurately in a short amount of time. Incorporating environmental effects would be very difficult, and are not considered. In reality, specimens are not always perfect, as they will have surface imperfections and irregularities. They will not have uniform material properties and will wear and degrade with usage. Fatigue simulation software allows for many of these factors to be accounted for, such as surface finishes, which help to give a more accurate prediction of fatigue life.

With these systems, numerous engineering assumptions have to be made, as many of these phenomena cannot be easily characterized, measured or even understood. Wear and tribology effects that result from mechanical clearances and corrosion issues are also

12

very difficult to characterize. The engineer's goal is to determine which assumptions are valid, and what degree of simplification a system can be made which still gives favourable and useful results. Simulation is always an approximation, the effectiveness of which is a measure of how close the results relate to physical testing.

## 1.5 Motivation for Virtual Simulation Research

There are many driving forces behind this project, some of which are as follows:

- Reduce the amount of time taken to develop a vehicle from design to production
- Reduce the amount of time spent at a proving ground and on road test simulators
- Reduce the number of physical prototypes that have to be constructed
- Measure stress and strain in components under *dynamic* loading conditions
- Produce a superior vehicle by predicting failures and correcting them early in the design process
- Detect areas of high stress or high force locations that may not be evident through measurement or visual inspection (inside components)
- Test "what-if" scenarios and perform sensitivity analysis
- Optimize component properties based on findings

## 1.6 Project Objectives

Several project objectives were stipulated for investigation in this research, and are as follows:

- Generate a high-fidelity multi-body dynamics model of a Sport Utility Vehicle (SUV) using CATIA and ADAMS software suites.
- Simulate this vehicle using data acquired from proving ground and a Road Test Simulator (RTS).
- Devise methods to attain correlation between the physical and virtual tests using time histories and frequency response data.

13

- Test two different rear suspension configurations on the same vehicle and observe differences. This is to determine whether the loadings on separate components are significantly different on the vehicle when the same spindle forces/displacements are input into the model.

- Devise methods to partially automate this simulation process using tools such as ADAMS/Durability and through creating user interfaces within the ADAMS environment.

- Devise methods for generating flexible bodies and determine methodology for incorporating flexible bodies into the ADAMS rigid body model.

- Determine the effects of replacing rigid components with flexible (deformable) components by creating finite element models (FEM) using CATIA, PATRAN, and NASTRAN software packages.

# CHAPTER 2 REVIEW OF CURRENT TRENDS, FUNDAMENTAL CONCEPTS, AND SOFTWARE SUITES

## 2.0 General

This chapter addresses current trends in multibody dynamics, involving both rigid and flexible body analysis. Research in the area of road test simulation, as well as the software being used to create the virtual model is highlighted. A background on multibody and vehicle dynamics is given with an overview of flexible body modeling and analysis.

## 2.1 Durability Testing

Durability testing is conducted to test the ability of vehicle's components to withstand the loading placed on them under typical driving conditions. The performance of a component diminishes when flaws develop, and they are required to be replaced. Failure can occur from a number of different mechanisms including fatigue, creep, wear, corrosion and the general degradation of the component as a whole. The principal failure mode of concern is fatigue, which refers to the cracking and subsequent failure of components under dynamic loading conditions. Fatigue life results are commonly expressed in terms of number of cycles or repetitions of specific loading sequences in

15

order to achieve failure criterion at certain locations. Failure can be expressed in terms such as hours, miles, or cycles depending on how the testing is conducted.

A durable vehicle is one that remains free of flaws for a greater amount of time. Durability also affects the reputation of auto manufacturer, and is a factor to customers who tend to buy from a company again and again if their products have less durability related problems. By producing a vehicle that is more durable, several other aspects following the design cycle also benefit. A more durable vehicle will tend to have fewer warranty claims and recalls. Recalls are very expensive to a company in that a simple design problem, which may have cost very little in the design process, can cost millions of dollars to resolve after the vehicle has been produced. Warranty claims also consume valuable company resources, since parts and labor have to be allocated at little cost to the consumer. As manufacturers continue to extend their warranty periods to attract customers, durability issues become more relevant than ever.

## 2.2 Review of Literature

Subramanyam et al. {40} stipulates that with vehicle dynamics refinement taking centre stage, it has become increasingly accepted that use of well developed, Computer Aided Engineering (CAE) models present the best approach for early stage prediction of vehicle behavior. They also state that meaningful results can be derived, and projections made from the CAE model only if the CAE results are correlated against physical tests. A majority of the documented literature stressed the importance on model correlation, but also stressed how difficult and time consuming this process can become.

Suh et al.{41} explains that much time and money is required to develop a new vehicle because the durability of a vehicle structure must be analyzed through actual driving on roads, proving grounds, or road simulators. For computer simulation to be beneficial to automotive manufacturers, it must be quick, efficient, and provide

16

meaningful results at faster rate than traditional methods. Although it was found that most simulation groups could provide impressive visual representations from computer simulation, many still could not claim close correlation with physical tests.

Virtual durability analysis of full vehicle was found to be a recent engineering development, which is partially due to the increase in computing power in the past decade, as well as the recent availability of powerful and reliable commercial software. It was established that research conducted in this area is highly confidential within corporations, and is rarely released into public domain. In the case that any proprietary information is released, the methodology is typically very general, and does not include any details as to how the models were built, or how the simulations were conducted. The following section outlines recent advances in the field of multibody dynamics and durability analysis, which have been influential towards this project.

Rao et al. {35} presented a study outlining developing an ADAMS model using physical test data. This research illustrated the methodology involved in acquiring parameters such as characterizing springs, shock absorbers, bushings, and associated parameters. Geometry and key hard point positions were measured using a Coordinate Measuring Machine (CMM). This was a private study performed by a parts supplier who did not have access to geometric data, but wanted to study the dynamic movements of a certain vehicle. Ride and handling were the parameters they desired to investigate, as well as braking and acceleration effects. Tire models were used to model the tire to road interface. Preliminary results show close correlation using numerous validation tests.

Kinematics and Compliance (K&C) tests were performed to validate vehicle behavior using an MTS K&C machine. These machines were used to perform two types of tests as the machine's name states: kinematic tests, and compliance tests. Precisely controlled displacements and forces are input to the tires of the vehicle using four independent platforms, while the body is held fixed. Wheel displacements and forces are

17

measured, which are used for validating the ADAMS model. Kinematic testing includes measuring wheel position changes under varying input conditions, such as ride height and roll while the longitudinal and lateral forces are zero. Compliance testing allows measurement of the wheel position using lateral, longitudinal, and aligning moment inputs.

Dittmann et al. {12} demonstrated methods of validating virtual prototypes though a Virtual Test Laboratory (VTL). A validated model of a physical test rig was used to simulate a virtual vehicle model, in order to validate the vehicle model itself. ADAMS software was used for the simulations, and in-house software was used for result validation and manipulation. This particular research represents the position of many manufacturers in the area of virtual road test simulation.

The operation of the virtual test lab was explained, and interpretation of model output data was highlighted. This study concluded that the VTL was able to generate load sequences, which allowed for correlation between the physical and virtual models. As was mentioned earlier, detailed results and analysis procedures are not generally released to the public domain, so many specific techniques, as established in the study above, are required to be written in-house for specific applications.

Krishna et al. {25} presented a paper outlining the effects of adding flexible bodies into computer models in place of rigid bodies using ABAQUS and ADAMS software. The components of concern in this study were primarily those of a front independent suspension. Components were tested as separate entities, and were then considered as a system, for flexible and rigid bodies in both cases.

Results showed that flexibility of the control arms did not significantly alter the load path, although the local distribution of the forces were notably different. They concluded that retaining rigid bodies in this case would be sufficiently accurate in predicting the overall forces in the system. They also commented that flexibility effects

18

were more prominent in the lower control arms, and that simulation time is much higher, and is a critical factor to be considered when adding flexible bodies.

Ewanochko et al. {15} investigated durability and fatigue issues of a heavy duty rotary cutter using specific CAE tools. The components of the rotary cutter were modelled as flexible bodies using a combination of Pro-E, ADAMS, and ANSYS and FE-Fatigue software packages. Separate finite element models were prepared for components of the assembly, and they were assembled in ADAMS. Inputs were applied to both a physical and a virtual model. Throughout the physical testing, component cracking was observed, and the number of cycles to failure was noted. The results from the ADAMS simulation were then output to FE-Fatigue, where the fatigue life was computed.

This particular study presented very favourable results to support the application of virtual durability assessment, and showed correlation with failures observed with physical testing. This paper and the project served as a major stepping-stone in the application of virtual durability using ADAMS/Flex and ANSYS.

## 2.3 MTS 329 Passenger Car Road Test Simulator Operation

MTS Corporation {30} states that the purpose of road test simulation is to gather dynamic loading data that represents the real time inputs experienced by a vehicle's suspension under typical driving conditions, then it aims to reproduce these inputs in the test laboratory. The primary objective of these machines is to test component life, which will depict the durability of the vehicle.

The road test simulator used in this project is a 4 DOF spindle coupled, multi-axial system. It can accurately simulate forces and accelerations on a test vehicle in the vertical, longitudinal, and lateral directions. Before the drive file creation process is explained in detail, an overview of the physical operation of the MTS 329 passenger car

19

road test simulator is presented. A CATIA computer model of the machine is shown in Figure 2.1 illustrating the basic components and motions of the fixture.
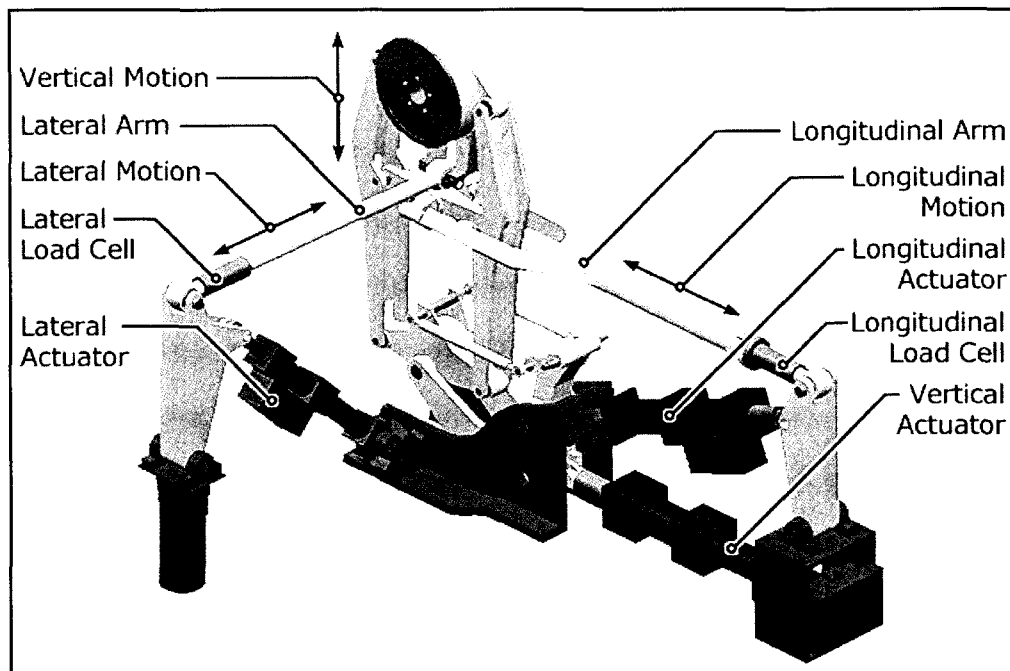


**Figure 2.1**: Schematic representation of the MTS 329 Passenger Car RTS machine. Directions of motion, as well as the physical actuators and arms are shown for the vertical, longitudinal, and lateral directions. The locations of the longitudinal and lateral load cells are noted. This diagram represents only one of the four fixtures that are required in total to excite the vehicle (one at each wheel). The three remaining fixtures operate in the same manner.

Each fixture uses three servo-hydraulic actuators to apply motions to the test vehicle, in each of the vertical, longitudinal, and lateral directions. Each of these actuator assemblies contains an LVDT (Linear Variable Differential Transformer) that records the position of the actuator. The longitudinal and lateral arms have load cells mounted on them to measure the forces in these directions. The four degrees of freedom for each fixture come from the number of possible inputs, which in this case are vertical, longitudinal, lateral, and braking torque. The actuator used for braking torque is not shown in the above figure, as braking torque was not applied to the test vehicle in this study.

20

MTS Corporation {30} defines six steps that are required in the drive file development process. These steps are outlined in the sections to follow:

- Record Field Data

- Transfer, Analyze and Edit the Data

- Measure System Frequency Response Function

- Estimate the Drive File

- Execute Durability Sequences

- Calculate Error and Iterate

### 2.3.1 Record Field Data

Vehicles are fully instrumented and are driven over pre-defined road courses at a proving ground facility. Critical parameters are measured, including acceleration, forces and strain values at various positions on the vehicle. Wheel Force Transducers (WFT) are used to measure the forces at the spindles, which are also used later on in the iteration process. Vehicles must be instrumented by hand, including strain gauge application, accelerometer mounting, and WFT attachment. Data is collected via an onboard data acquisition system.

The vehicles are tested at several load ratings such as Full Rated Load (FRL), HRL (Half Rated Load), and Light as Possible (LAP). These load ratings depend on the type of vehicle, and its load capacities. The vehicle is tested on many road courses that are representative of the most damaging surfaces that a vehicle will undergo based on its expected usage. This testing is done several times to ensure repeatability in the results, and is done with the above variances, as to replicate different conditions during the life of the vehicle. This stage is very critical in the durability process, as all steps following it will be ultimately dependant on the acquired data. This step can take months to execute

21

and consumes a great deal of resources and person hours. The data collected in this stage shall be referred to as "raw data" herein.

## 2.3.2 Transfer, Analyze, Edit, and Filter the Data

Once the vehicle has endured the proving ground, road data is downloaded from the data acquisition system, to be analyzed in a laboratory. Remote Parameter Control (RPC) software, which is produced by MTS Systems Corporation, is used to manipulate data in this process. During this stage, the data is analyzed, and edited to determine the appropriate data to be used to for drive files creation. Steering correction is performed since the vehicle is unable to steer as it would at the proving ground while it is on the RTS machine. Special algorithms have been created by MTS for this purpose. Events such as sensor spikes and non-damaging data are removed during this stage. This is one of the great benefits in using RTS methods. Data that is determined not to be an influence in damaging the vehicle can be removed, reducing the amount of physical testing time involved. The process is executed using specific software and is based on in-house experience and statistical information. The data output during this stage shall be referred to as "edited data" herein. One last step remains: filtering the edited data, to remove the DC and very low frequency content that cannot be simulated. The resultant file is referred to as the "desired" data since this is what is desired to be replicated on the rig.

## 2.3.3 Measure System Frequency Response Function

The instrumented vehicle that was used at the proving ground is now placed on the RTS machine, where random excitation is input to the test rig to excite the vehicle. This allows a Frequency Response Function (FRF) of the test vehicle to be determined. The FRF determines the response of the vehicle to known inputs from the rig, using feedback from certain sensors on the vehicle, as well as feedback from the wheel force

22

transducers. Once the FRF has been determined, the inverse FRF matrix can be used to predict the behavior of the system based on known inputs, such as road data from the proving ground testing.

### 2.3.4 Estimate the Drive File

Using the computed FRF from the previous step, the RPC software takes a given road course, and predicts the necessary input required from the MTS test rig that will match the reading from sensors on the vehicle for that specific road course. This drive file estimate represents a linear approximation that gives an initial starting point for the iterations that will be carried out in the following step. Iterations are required to determine the exact input that will be required to simulate the motion of the vehicle, as this is an initial estimate. Certain channels, referred to as control channels as will be discussed further in Chapter 4, are used to match signals from the proving ground to that of the signals monitored in the laboratory. Common control channel data includes accelerometers, lower control arm angles, and wheel forces. The iteration process becomes more difficult and will consume more time as the number of control channels increases.

### 2.3.5 Calculate Error and Iterate

After the initial drive file has been collaborated, the iteration process can begin. Each time an iteration is performed, the outputs from the control channel sensors on the MTS rig are compared to the desired data derived from the proving ground testing. A certain amount of error will exist between these signals. The objective of this process to bring this error (differences between the signals) below specified tolerances. The error measured is then added back to the inverted FRF, and a new corrected drive file is created. The process is repeated until the outputs from the control channels match to

within a defined range of the edited data. This step is very time consuming as it must be done for each road course, and for each load rating.

### 2.3.6 Execute Durability Sequences

At this stage, the RPC controller incorporates the specific inputs required to excite the vehicle in order to replicate certain road courses on the RTS machine. Instrumentation is no longer required on the vehicles to be tested, so production models that are similar to the test vehicles can now undergo durability tests. The durability sequences are run exactly as they would be on the damaging sections at the proving ground, and road courses can be run as many times as required in a specified durability sequence. The failure of certain components can now be monitored, and additional instrumentation can be added to monitor other critical aspects of the vehicles behavior. Slight changes can be made, such as spring or shock absorber rates, to determine their effect on the response and durability of the vehicle. If any extensive modifications are required based on the results of durability testing, this entire process may have to be repeated from step one. This entire six step process could potentially benefit greatly from virtual simulation.

### 2.4 Multibody Dynamics

Meirovitch {29} explains that the oldest and most fundamental part of physics is concerned with the equilibrium and motion of material bodies. The multibody method utilizes a finite set of elements including rigid bodies, joints, springs, dampers, and actuators to represent a physical system. The movement of a multibody system is represented using ordinary differential equations (ODE's) that are determined from the fundamental equations of motion. Mechanical joints are used in these multibody dynamic models to constrain relative motions, and are represented by non-linear

24

algebraic equations. The differential equations are expressions based on classic physical laws presented by Newton and Euler that describe the motion of these multibody systems.

The study of multibody dynamics encompasses two main fields; rigid multibody systems, and flexible multibody systems. In rigid body systems, the mass and inertia properties are fixed in time and the body is unable to deform with loading. Two arbitrary points on a rigid body cannot move with respect to one another. Meirovitch {29} states that the concept of a rigid body is more of a mathematical idealization than a physical reality. Flexible multibody systems can contain both rigid and flexible bodies. Flexible bodies have distributed inertia and elasticity properties, which are dependant on the deformation of the bodies. As the body deforms with respect to time, the shape of the body will change, which will cause the mass distribution and inertia to vary accordingly. Two arbitrary points on a flexible body are able to change position relative to one another.

By adding flexibility into the system, the equations of motion become much more complicated, and as a result, are more computationally intensive. The usage of flexible bodies should be limited to cases where deformations are too large to be considered negligible, or when the stress is required in a specific component. Mathematical expressions for defining the motion and constraints on these systems will be presented in Chapter 3 for both rigid and flexible systems, with specific application to the ADAMS software package.

### 2.4.1 Degrees of Freedom

Shabana {38} states that six coordinates that define the location of a point on a body and the orientation of a coordinate system rigidly attached to the body are required to describe the unconstrained motion of a rigid body in space. Three degrees of freedom represent the translational degrees of freedom, and three represent the rotational degrees

25

of freedom as shown in Figure 2.2. Mechanical systems can be defined according to the

number of degrees of freedom (DOF) that they have. Norton {33} states that a system's

DOF is equal to the independent parameters (measurements) that are needed to uniquely

define its position in space at any instant in time. The number of degrees of freedom in a

system is dependant on the number of bodies being used, and on the constraints that are

placed on their relative movement.
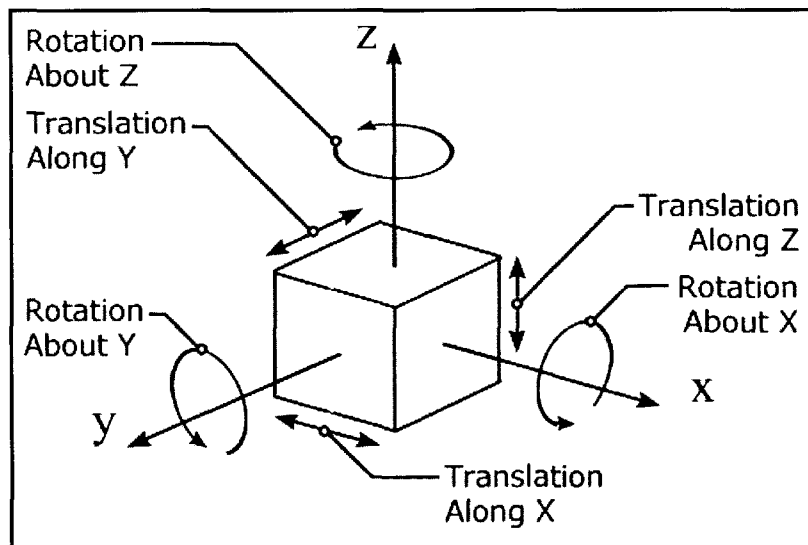


**Figure 2.2:** An unconstrained rigid body in space has 6 degrees of freedom. Three of these represent translational DOF in the x, y, and z directions. Three represent rotational degrees of freedom about the x-axis, y-axis and z-axis as is shown. Degrees of freedom can be removed by adding mechanical joints, which limit the relative movements between two rigid bodies.

### 2.4.2 Mechanical Joints and Constraints

Mechanical joints are used to define relative movement between bodies. These

joints reduce the total degrees of freedom in a system and dictate how the motion of one

body is transmitted to another. A few joint examples that will be detailed in the

following section are shown in Figure 2.3. The analysis conducted within this research is

in three dimensions, so joints related to spatial (three-dimensional) kinematics will be

addressed.

26
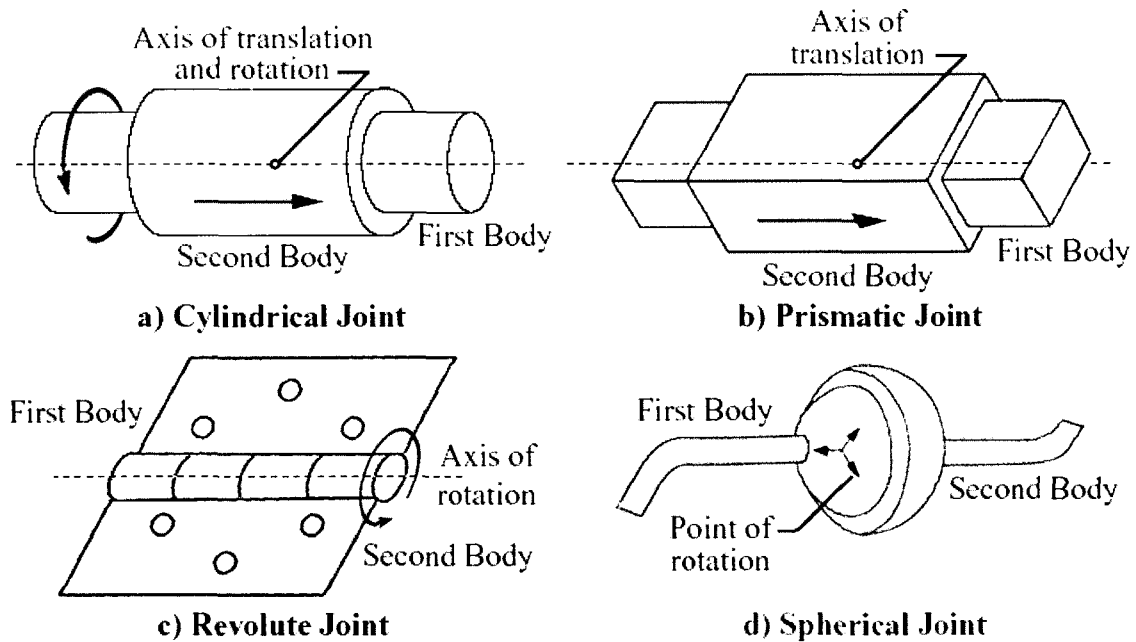
**Figure 2.3**: Various joints used in constraining the relative motion of rigid and flexible
bodies. Cylindrical (a), prismatic (b), revolute (c), and spherical (d) joints
are shown, and their relative movements are displayed.

A *cylindrical joint* provides two degrees of freedom between two bodies, which
dictates translation and rotation about a common axis. A *revolute joint* can be thought of
as a special case of a cylindrical joint, where the translational motion is not permitted.
This allows relative rotation between two parts about a specific axis and provides one
degree of freedom. A *prismatic*, or *translational joint* as it is also called, is also a special
case of the cylindrical joint, where the rotational motion is not permissible. The
movement allows relative translation between two parts along a specified line, resulting
in one degree of freedom.

A *spherical joint* allows for relative rotation between two parts with respect to
another. The bodies cannot translate relative to one another, resulting in three degrees of
freedom. *Fixed Joints* are used to rigidly connect components to one another. No
relative movement is allowed between the two bodies. Six degrees of freedom are
removed, resulting in zero degrees of freedom between the two bodies. A *ground link*

27

has zero degrees of freedom, and is fixed in space. Every system is required to have a ground link, which the Global Coordinate System (GCS) is located on.

A *universal*, or *Hooke joint*, allows relative rotation between two parts about two separate axis. Since only two rotations are allowed, two degrees of freedom are present. A *point/curve constraint* restricts a fixed point defined on one part to lie on a curve defined on a second part. This constraint can be thought of as a translating spherical joint, and as a result allows four degrees of freedom.

### 2.4.3 Kinematic Analysis

Kinematic analysis refers to the study of a system without the consideration of the forces that produce the motion of the body. Displacement, velocity and acceleration relationships are used to describe the motions of the system, irrespective of the forces on the system itself. In position analysis, the kinematic relations are solved based on the degrees of freedom in the system, which are dictated by joint constraints. The velocity and acceleration equations of the system can be found by taking the time derivative of the displacement once, and twice respectively.

### 2.4.4 Forward and Inverse Dynamics

There are two main types of analysis that can be performed for mechanical systems: forward and inverse dynamics. With forward dynamics, the forces on the system are known, and the objective is to determine the positional coordinates, velocities, and accelerations with respect to time. Using fundamental equations of motion, the acceleration of the individual bodies can be determined. The velocities and displacements of these bodies can be found by integrating the accelerations, using the appropriate numerical integration techniques. Using inverse dynamics, the motions of the bodies are known, and the forces on them are required. Numerical integration is not required as in the case of forward dynamics, since the position, velocities, and

28

accelerations are known. The forces can be determined through the use of equations of motion.

## 2.5 Mechanics of Deformable Bodies

Shabana {39} states that a body in the system can be treated as rigid when the deformation is small enough that it can be neglected. Where the deformation is considered significant, these rigid bodies must be replaced by flexible ones. Deformable bodies are also particularly useful where the stress in the body is required, and also for use in fatigue analysis. Meirovitch {29} further explains that a deformable body of finite dimensions can be described as having an infinite number of particles, such that it possesses an infinite number of degrees of freedom (DOF). Finite element methods (FEM) are used to discretize these bodies into a finite number of DOF, for which equations of motion can be derived. Techniques such as superelement analysis use mathematical matrix reduction techniques to significantly decrease the amount of computation necessary. The deformation of certain components can have a significant effect on the dynamic behavior of the system.

Shabana {37} states the most widely used method in computer simulation of flexible bodies is the floating frame of reference. Ambrósio et al. {2} affirms that when using a floating frame of reference, two sets of coordinate systems are required; one to describe the location and orientation of a selected body coordinate system, while the other describes the deformation of the body with respect to its coordinate system. These techniques are described in further detail in Chapter 3, as ADAMS uses floating frame of reference formulation to describe the position and deformation of flexible bodies.

### 2.5.1 Superelement Analysis

Finite element models involving large assemblies are often made up of many sub-assemblies and components, and as a result, the finite element models are large, and can

be computationally intensive. Gockel {18} notes that superelement analysis is a form of substructuring, where assemblies are broken up into separate components as can be seen in Figure 2.4, each of which having their separate reduced mass, stiffness and damping matrices. Finite element models of the components are solved separately, and solutions are used to solve the entire model. In the current research, these techniques are used to connect flexible bodies to rigid bodies using ADAMS.
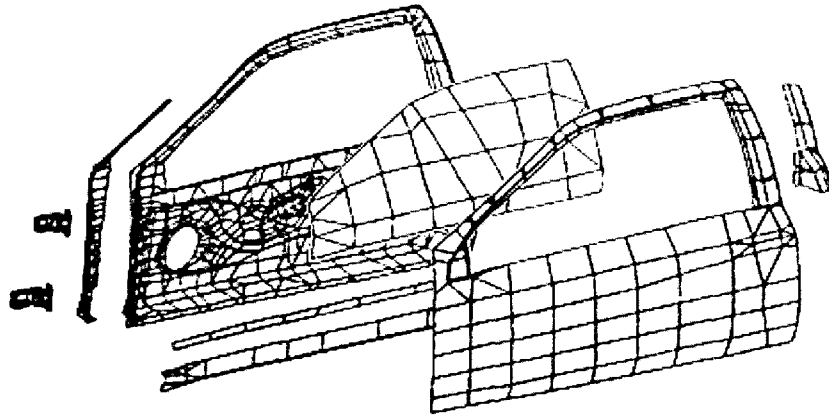


**Figure 2.4**: An application of superelements being used to model an automotive door assembly. Superelement analysis is a form of substructuring, where an assembly of components are broken up to be analyzed individually. Mathematical matrix reduction methods are used to significantly decrease computational times using this technique. Illustration adapted from Blakely {5}.

Superelement analysis has many advantages in addition to reducing simulation times. Literally hundreds of external suppliers are involved in the design, testing, and analysis of a vehicle assembly. Rather than providing each company access to an entire model which may be highly confidential, the parent company can request a model for an individual component that is suitable for superelement analysis. A system of these components can then be assembled and solved, reducing the risk of revealing proprietary information. If portions of a model need to be altered, or varied as in the case of the rear suspension in this research, only the affected superelements need to be modified, and then the final analysis can be repeated.

30

### 2.5.2 Modal Analysis

Blakely {5} states that the deformed shape of a structure at a specific natural frequency is termed a normal "mode" of vibration. Each mode shape corresponds to a certain natural frequency. The natural frequencies of a component are the specific frequencies of vibration at which the structure tends to vibrate if subjected to a disturbance. The deflection of a flexible body under certain loading can be described by the combination of a number of mode shapes. Primary modes can consist of pure bending and pure torsion, while higher order modes (which also correspond to higher frequencies) are a combination of very complex shapes and movements.

Each deformable body will have a unique set of mode shapes that will determine the overall shape of the body under dynamic loading. The deformation of a body can usually be described using a finite number of mode shapes. This is possible because some higher order modes will be outside the range of attainable frequencies in the system, and may be beyond the frequency range of interest. These higher order modes can be neglected if they do not significantly affect the response of the system. The point at which these higher modes can be truncated is based on the specific model. Techniques used in modal truncation will be discussed further in Chapter 4.

### 2.5.3 Component Mode Synthesis

Craig {10} comments that Component Mode Synthesis (CMS) involves dividing a structure into a number of substructures, and components, obtaining reduced-order models of components, and then assembling a reduced-order model of the entire structure. It is a form of superelement dynamic reduction where matrices are defined in terms of modal coordinates, which correspond to the superelement modes, and physical coordinates, which relate to the grid points of the superelement boundaries. The advantage of component mode synthesis is that there are fewer modal coordinates than

31

physical coordinates, which Blakely {5} states can be as few as one percent of the original number. The process of creating a model using these modal techniques, as well as superelement analysis is highlighted in Chapter 4.

A detailed synthesis into multibody dynamics, both rigid and flexible, is beyond the scope of this thesis, and interested parties are encouraged to refer to specific references following this document.

## 2.6 Vehicle Dynamics

Vehicle dynamics is specific application of rigid and flexible body dynamics, and is the focus of this research project. Gillespie {17} states that vehicle dynamics concerns the movements of vehicles, from automobiles, trucks, and buses to special purpose vehicles such as all-terrain vehicles or race cars on a road surface. Barak {3} further notes that a vehicle represents a complex vibration system with many degrees of freedom, and it is possible to simplify the system considering only some of its major motions and components. Vehicle dynamics encompasses many areas of a vehicle's performance, from drivetrain and powertrain, to braking, aerodynamic loading, and in the case of this project, suspension dynamics. Suspension dynamics can be further broken up in to several areas including ride, handling, rollover, road loading, tires, steering systems and durability.

Gillespie {17} explains the primary function of a vehicle's suspension is to:

- Provide vertical compliance such that wheels can follow an uneven road, isolating the chassis from roughness in the road

- Resist roll of the chassis

- Keep the tires in contact with the road with minimal load variations

- React to the control forces produced by the tires – longitudinal (acceleration and braking forces), lateral (cornering forces), and braking and driving torques.

32

Suspension linkages not only dictate the path of motion of the components, but they also control the amount of force that is transferred through these separate components. The dynamic behavior is determined by the forces that are imposed on the vehicle from gravity, tire loadings, and aerodynamics. Load path analysis is a critical step in determining where high force areas are located in the suspension components, which is vital for durability analysis. Fatigue and durability design of any component requires reliable information about the loads that the components are subjected to.

The particular vehicle being analyzed in this research uses a front double-wishbone independent suspension, and both a three and four link rear suspension are investigated. Gillespie {17} states that with three and four link rear suspension configurations, the lower control arms act to provide longitudinal control of the vehicle, while the upper control arm(s) act to absorb braking/driving torques and lateral forces. With independent front suspension using upper and lower control arms, the lateral and longitudinal loadings are distributed through both arms.

Vehicle motions are typically characterised according to the SAE Standard J670e {36}, which defines vehicle dynamics terminology. Roll, pitch, and yaw rotations are illustrated in Figure 2.5. In the case of this figure, the x-axis runs longitudinally, the y-axis runs laterally, and the z-axis runs vertically. The right hand rule is used to determine sign conventions.

33
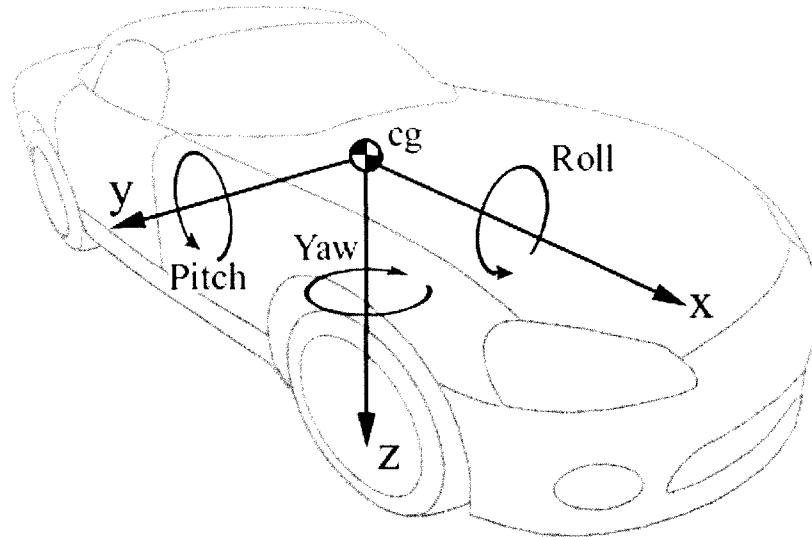
**Figure 2.5**: Diagram illustrating the basic motions associated with vehicle dynamics including roll, yaw and pitch about their respective axis according to the SAE Vehicle System included in SAE Standard J670e {36}.

**2.7 Software Suites**:

A number of different software packages were used in creating the computer models for this research. These models were created, assembled and simulated on SGI and HP UNIX platform based workstations. The following is a listing of the software suites, their primary usages, and their impact on the project at hand.

**2.7.1 CATIA**

Computer Aided Three-Dimensional Interactive Applications, CATIA for short, is a very powerful CAD package, which is widely used in industry around the world. CATIA integrates all aspects of product design: Computer Aided Design (CAD), Computer Aided Machining (CAM), and Computer Aided Engineering (CAE). CATIA was used extensively for research at hand, and was a dominant tool used for model assembly, refining geometries, calculating moments of inertia, and performing basic kinematic analysis. CATIA can also be used for creating initial finite element meshes for

34

use with PATRAN and NASTRAN software suites. CATIA is the flagship product of Dassault Systemes, and was established through a strategic partnership with IBM.

### 2.7.2 ENOVIA Virtual Product Modeler (ENOVIA/vpm)

The function of VPM is to enable users to access, manage, and synchronize all aspects of the design process, from start to finish using a single software product. One of the main tools with which this information is organized is the Product Structure Navigator (PSN). This portion of the software graphically organizes and displays the product assembly and manufacturing structures as shown in Figure 2.6. These graphs can be used to manage the assembly and detail configurations for product information. Another application of VPM is configuration, which allows the product structure to be organized and displayed according to different available options (4WD vs. 2WD versions for example). In this, an assembly can be shown configured for a desired option and the resulting graph will display only those versions of detail parts that apply. VPM was used to compile, access, and assemble a majority of the vehicle model in this research project, and is used in conjunction with CATIA. This software package is also a product of Dassault Systemes.
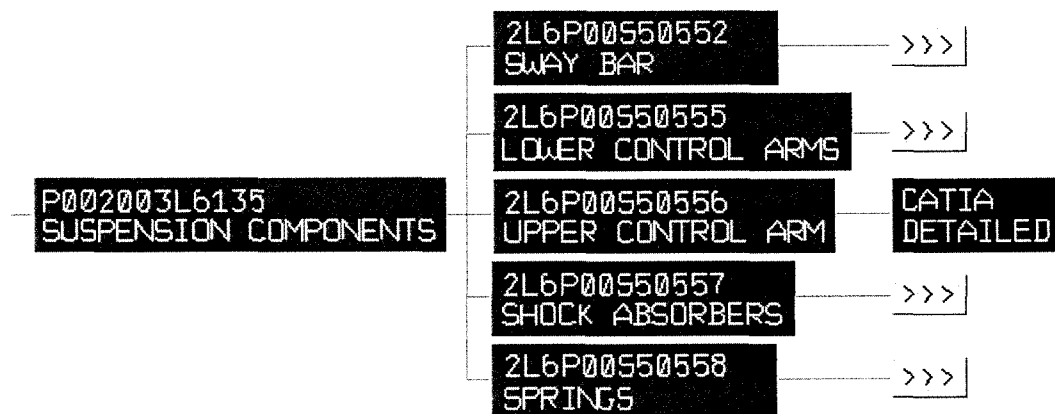


**Figure 2.6**: ENOVIA/vpm user interface showing the detail of a suspension system. In each case, the arrows following each entry can be selected to either show more components within the sub-system, or allow access CATIA drawings. The numbers above the components are their assembly reference numbers.

35

### 2.7.3 MSC.ADAMS (View/Post/Solver)

Automatic Dynamic Analysis of Mechanical Systems, or ADAMS as it is commercially known, is multi-purpose dynamics software package which is widely used for multi-body dynamics simulation. The core suite in ADAMS consists of three main operators; ADAMS/View, ADAMS/Solver and ADAMS/Post.

ADAMS/View allows one to build mechanical systems and simulate the dynamic behavior of the models. It acts as a pre-processor and is used to generate virtual models. ADAMS/Solver is the backbone of the ADAMS software package, and is used to solve the necessary equations of motion and the constraint equations. ADAMS/Solver runs concurrently with ADAMS/View, where ADAMS/View automatically generates necessary mathematical equations and uses ADAMS/Solver to solve them. ADAMS/View also allows users to create project specific user menus and dialog boxes through ADAMS' own unique programming language. Simulation using ADAMS software was the primary focus of this current research.

ADAMS/Post is used to analyze simulation results, and allows playback of simulations, plotting desired system outputs, and allows for basic frequency domain analysis. Any mentioned instances of these three products will simply be referred to as ADAMS herein. ADAMS/Durability and ADAMS/Flex are both add-on programs to the core ADAMS suite as will be discussed below. ADAMS software is a product of Mechanical Dynamics Incorporated (MDI), which has recently been acquired by MacNeil-Schwendler Corporation (MSC).

### 2.7.4 ADAMS/Durability

ADAMS/Durability is a powerful tool that allows durability simulations to be conducted in ADAMS and can be used to drive fatigue prediction tools such as MSC.Fatigue and nCode Fatigue. ADAMS/Durability software provides the ability to

36

input and output time history data in leading durability file formats, including nCode International's DAC format, and RPC® III format from MTS Systems Corporation. Outputs in these formats can be compared to physical data using ADAMS/Post or other commercially available products for the purpose of model correlation and analysis. When flexible bodies are implemented, ADAMS/Durability allows fringe plots of stress and strain to be viewed using ADAMS/Post. Mode shapes can be exported for analysis using NASTRAN or ABAQUS, and nodal information such as stress and strain can be exported for external analysis.

### 2.7.5 MSC.ADAMS/Flex

ADAMS/Flex is a tool for adding flexible bodies into ADAMS simulations, and allows integration of finite element models from many preferred Finite Element Analysis (FEA) programs. This feature allows the stress and strain at specific nodes to be analyzed, as well as the deformation of the parts to be monitored. It also allows frequency analysis to be preformed on components as a system, allowing the vehicles frequency behavior to be fine tuned.

ADAMS/Flex Toolkit is a file translator included within the ADAMS/Flex package that allows finite element analysis files to be converted into ADAMS recognized flexible bodies formats, and is a stand alone program. ADAMS/Flex uses interfaces within ADAMS/View to allow for these translated files to be inserted into the virtual model itself. In the case of this research project, NASTRAN is the FEA solver being used.

### 2.7.6 CATIA to ADAMS Conversion Software (CAT/ADAMS)

CAT/ADAMS is a software attachment used to translate solid geometric models created in CATIA to ADAMS format, so that dynamic analysis can be performed on the system. Component properties, such as mass, inertia, and centre of gravity are

37

transformed, as well as joints created using CATIA's kinematics module. The interface is contained within the CATIA package, and upon converting the files, the model is shown in ADAMS format. The file can then be exported and saved in ADAMS format. CATIA has far superior geometric modeling capabilities to that of ADAMS, and all of the manufacturer's databases are linked to CATIA files. This allows for the strength of each program to be combined to produce a superior end result.

### 2.7.7 MSC.PATRAN

MSC.Patran is a multi-purpose finite element program used for both pre- and post- processing tasks. MSC.Patran serves as a powerful tool for stress analysis as well as for vibration analysis as used in this project. Finite element models can be created using CAD generated models, and the necessary forces and constraints can be applied to the components using PATRAN prior to solving using NASTRAN.

The post-processing capabilities allow flexible bodies representations in ADAMS to be verified by comparing normal mode frequencies and their associated mode shapes as computed using PATRAN and NASTRAN alone. This will confirm whether the approximations made when importing the deformable bodies into ADAMS were sufficient for analysis.

### 2.7.8 MSC.NASTRAN

MSC.NASTRAN is multi-purpose, multi-discipline finite element solver that is widely used in industry for finite element analysis. NASTRAN offers a wide variety of analysis types, including linear statics, normal modes, and buckling. Optional modules support heat transfer, dynamics, frequency response, transient response, random response, and response spectrum analysis. MSC.NASTRAN was used in the present research for solving finite element models, both for usage in ADAMS as well as

38

MSC.PATRAN. Normal mode, dynamic stress analysis, and superelement analysis problems were solved using this software.

### 2.7.9 nCode International nSoft

Large volumes of data can be processed automatically using nSoft by nCode International. This software is specifically designed for use in Fatigue analysis and is backed by powerful macro language capabilities. Batch files were composed in order to process large amounts of data though simple commands accessed through a UNIX command prompt. This allowed for otherwise time consuming and repetitive tasks to be automated and specifically tailored for this project as will be discussed in Chapter 4. The main modules used in this research are described below.

### MART: Arithmetic Manipulation

The arithmetic manipulation module does just that, it allows mathematical manipulations to be done to time history data. This is particularly useful for converting engineering units on large data sets and for renaming files within these large datasets. While this may seem like a simple task, the raw data alone for each road course contains over 90 channels of data, which would require countless hours to convert manually, and would hinder actual timesaving through a repetitive process.

### MASD: Auto Spectral Density

The Auto Spectral Density module is used in order to generate an output file that dictates the frequency content of a time history input. This is achieved through Fast Fourier Transforms, which act to transfer the dataset from the time to the frequency domain. Batch commands were used to automate the conversion from the time to the frequency domain of large datasets using the MASD function.

### MFFF: Frequency Domain Fourier Filter

The MFFF module acts as a Finite Impulse Response (FIR) filter, which is used to apply filters to frequency domain datasets. This is particularly useful for removing low and

39

high frequency content in these datasets, through using high and low pass filters as well as band pass and band stop filters.

**MMFD: Multifile Display**

Multifile Display can be used to plot time and frequency domain datasets. Files can be plotted separately, overlaid, and cross plotted. By overlaying the plots, frequency analysis can be done to compare results from physical models, to that of virtual models. Batch files were also used to automate the post-processing of data, to further reduce the amount of time required during analysis.

**MREMDAC: RPC to DAC Conversion**

The REMDAC module allows Remote Parameter Control (RPC) Files to be extracted into separate Digitized Analogue Channel (DAC) datasets. Although ADAMS software recognizes the RPC format, post processing is done more efficiently when the files are in the DAC format, so that they can be compared separately as files.

**MDACREM: DAC to RPC Conversion**

This module performs the opposite operation to that of the MREMDAC module, where it allows DAC files to be packaged into RPC format. RPC format allows for more efficient storage of DAC files as entire analysis sets can be stored as channels in a single RPC file.

40

# CHAPTER 3 THEORETICAL BACKGROUND

## 3.0 General

This chapter outlines the theoretical operation of both ADAMS/Solver and ADAMS/Flex

for use in multibody dynamic analysis. Details on how ADAMS defines constraints,

motions and solving theories will be presented. An explanation of how ADAMS/Flex

treats flexible body analysis will be discussed in detail, including the derivation of the

governing equations of motion for both rigid and flexible bodies.

## 3.1 Multibody Dynamics of Rigid Bodies Using ADAMS

As noted in earlier chapters, ADAMS is multi-purpose dynamics software

package widely used for computer simulation of mechanical systems such as vehicle

suspensions. This section addresses theoretical concepts employed in defining and

solving mechanical models using this software for rigid body analysis. Flexible body

mathematics will be addressed in following sections.

### 3.1.1 Euler Angles

ADAMS/Solver uses Euler angles to establish the initial orientation of the local

body coordinate system (BCS) with respect to the ground coordinate system (GCS). The

41

body-fixed 3-1-3 (or z-x'-z'') rotation sequence method is used. The rotation angles used in this rotation sequence are often referred to as Euler angles. By using these successive rotations as illustrated in Figure 3.1 below, a specific axis orientation can be reached.



| a) initial orientation (GCS) | b) after first rotation | c) after second rotation | d) after third rotation (BCS) |
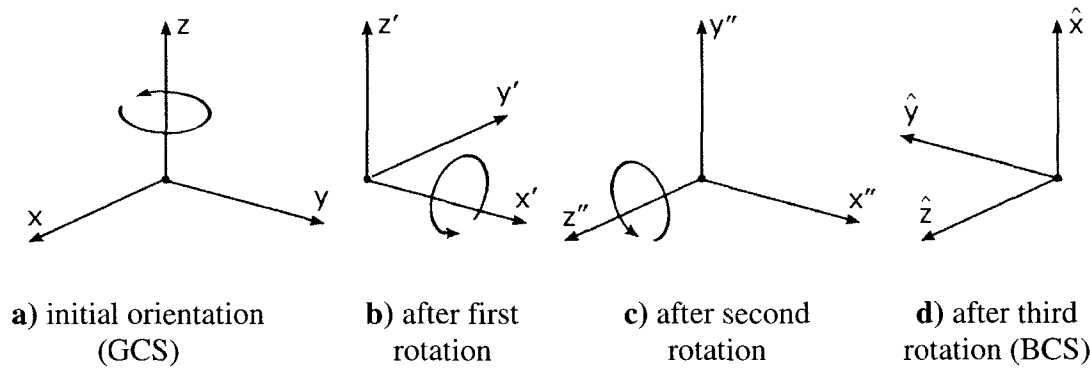
**Figure 3.1**: Euler angle rotation sequence for orienting local axis systems relative to the global coordinate system. In this illustration, the Euler angle representation is (90,90,90). Image a) represents the orientation of the GCS. The first rotation is 90° about the z axis, the second rotation is 90° about the x' axis, and the third rotation is 90° about the z'' axis. The final BCS is show in d).

Initially, the body coordinate system is positioned with the same orientation as the base coordinate system. The first Euler angle rotation is about the z axis, and as a result, the new temporary x', y' and z' axis relationship is created. The second Euler angle rotation is about the relocated x' axis, and a repositioned x'', y'' and z'' axis configuration is established. The third Euler angle orientation is defined by rotating about the repositioned z'' axis. The final body coordinate system is established after the third sequence of rotations ( $\hat{x}, \hat{y}, \hat{z}$ ). It must be noted the direction of rotation is always defined by the standard right rand rule. CATIA allows the axis coordinate system orientation in the 3-1-3 (Z-X-Z) sequence of local axis systems to be displayed, which aids in the creation of ADAMS models.

### 3.1.2 Generalized Coordinates

ADAMS uses a set of generalized coordinates to position each body in space relative to the ground coordinate system. The position, $p$, of a rigid body can be defined by three Cartesian components x, y and z as noted by Harris et. al. {21}.

$$p = \begin{bmatrix} x & y & z \end{bmatrix}^T \qquad\qquad 3.1$$

The orientation of a body is described by Euler angles as described earlier that correspond to a 3-1-3 sequence of rotation: $\psi$, $\theta$ and $\phi$ respectively. These three angles are stored in an array in the following form.

$$\varepsilon = \begin{bmatrix} \varphi & \theta & \phi \end{bmatrix}^T \qquad\qquad 3.2$$

The set of generalized coordinates in ADAMS is associated with rigid body $i$ as follows in equation 3.3.

$$q_i = \begin{bmatrix} p_i \\ \varepsilon_i \end{bmatrix} \qquad\qquad 3.3$$

Using these generalized coordinates, the body translational and angular velocity are expressed by taking the time derivatives:

$$u = \dot{p} \qquad\qquad 3.4$$

$$\omega = B\dot{\varepsilon} = B\zeta \qquad\qquad 3.5$$

The notation $\omega$ denotes the angular velocity of the body, expressed in the local body coordinate system, and $B$ is the transformation matrix that defines the relationship between the angular velocity of the body and the choice of generalized coordinates which is expressed as:

$$B = \begin{bmatrix} \sin\theta\sin\phi & 0 & \cos\phi \\ \sin\theta\cos\phi & 0 & -\sin\phi \\ \cos\theta & 1 & 0 \end{bmatrix} \qquad\qquad 3.6$$

For an entire mechanical system that contains $n_b$ bodies, the following array

43

$$q = \begin{bmatrix} q_1^T & q_2^T & \cdots & \cdots & q_{n_b}^T \end{bmatrix}^T = \begin{bmatrix} q_1 & q_2 & \cdots & \cdots & q_{n_{gc}} \end{bmatrix}^T \qquad 3.7$$

describes the position and orientation of each body in the system, where $n_{gc}$ denotes the

generalized coordinates. Note that $n_{gc} = 6 \cdot n_b$.

### 3.1.3 Mechanical Joints and Constraints

Joints in ADAMS act to constrain the motion of one body relative to another.

These joints can be thought of as constraints that act among some of the coordinates $q_1$

through $q_n$ from Equation 3.7. Harris et al. {21} describes that mathematically:

$$\Phi(q) = 0 \qquad 3.8$$

A prismatic joint would create a set five constraints resembling Equation 3.8, to

allow one degree of freedom between the two bodies, which is translation along one axis.

The combined constraint expressions produced by joints present in the model are denoted

by:

$$\Phi(q) = \begin{bmatrix} \Phi_1^T(q) & \Phi_2^T(q) & \cdots & \cdots & \Phi_{n_j}^T(q) \end{bmatrix}^T$$

$$= \begin{bmatrix} \Phi_1(q) & \Phi_2(q) & \cdots & \cdots & \Phi_{n_c}(q) \end{bmatrix}^T \qquad 3.9$$

Where $n_j$ denotes the number of joints in the model, and $n_c$ represents the number of

constraints induced by each joint in the model. Typically $n_c < n_j$, meaning that the total

number of constraints in the system is less than the total number of generalized

coordinates. In the case where $n_c \geq n_j$, the system may be either over-constrained ($n_c \geq$

$n_j$), or is kinematically driven ($n_c = n_j$).

By taking the derivative of the position kinematic constraint equation, Equation

3.9, the velocity kinematic constraint equations are obtained:

$$\Phi_q \dot{q} = 0 \qquad 3.10$$

44

Taking the derivative of Equation 3.10, the acceleration kinematic constraint equations are obtained:

$$\Phi_q \ddot{q} = -(\Phi_q \dot{q})_q \dot{q}$$

3.11

The generalized coordinate array, Equation 3.7, along with its first and second time derivatives, must be able to satisfy the conditions imposed by Equations 3.9 through 3.11. This will guarantee that that the constraints are obeyed at every period in time.

## 3.1.4 Motions

Motions in general indicate that mathematically, a generalized coordinate of the system, or an expression depending on generalized coordinates, depends explicitly on time. For example, the translational motion of a hydraulic cylinder in the case of an RTS machine might impose that the linear motion associated with its unique degree of freedom will vary in time based on the equation $x = \sin(2\pi*t)$. Harris et al. {21} state that a motion in ADAMS is represented as a time dependent constraint equation as follows:

$$\Phi(q,t) = 0$$

3.12

Bearing in mind the definitions of position, velocity and acceleration kinematic constraint equations, for constraint equations induced by either joints or motions as described earlier, the following equations must be satisfied at any time, t.

$$\Phi(q,t) = 0$$

3.13

$$\Phi_q(q,t) \cdot \dot{q} = -\Phi_t(q,t)$$

3.14

$$\Phi_q(q,t) \cdot \ddot{q} = -(\Phi_q \dot{q})_q \dot{q} - 2\Phi_{qt}\dot{q} - \Phi_{tt}(q,t)$$

3.15

In this case, Equations 3.14 and 3.15 represent the time derivatives of the kinematic constraint formulation, Equation 3.13.

### 3.1.5 Kinematic Analysis

In general, for a kinematic analysis to be performed on a system, the number of independent constraint equations must equal the number of generalized coordinates in the model. If the system is to change its configuration in time, some of these constraints must be in the form of motions (a kinematically driven system), such that their position is a function of time.

*Position Level Kinematics* is used to determine the position of the system at a time $t_1 > t_0$, given the system is at time $t_0$. The constraint equations from Equation 3.13 are non-linear, so a Newton-Raphson iterative method is used to compute $q_1$ at time $t_1$. Shabana {38} explains that using a Taylor series expansion based linearization of the non-linear constraint equations yields:

$$\Phi(q_1, t_1) = \Phi(q_0, t_1) + \Phi_q(q_0, t_1)(q_1 - q_0) + HOT \qquad 3.16$$

Since the number of independent constraint equations equal the number of generalized coordinates in the model, this produces a square matrix. The constraint equations are assumed to be independent, and as a result, the matrix is also invertible. Using an explicit integrator, an initial starting configuration $q_1^{(0)}$ is determined, and the iterative algorithm proceeds at each iteration $j \geq 0$ by finding the correction $\Delta^{(j)}$:

$$\Phi_q(q_0, t_1)\Delta^{(j)} = -\Phi(q_1^{(j)}, t_1) \qquad 3.17$$

Which leads to:
$$q_1^{(j+1)} = q_1 + \Delta^{(j)} \qquad 3.18$$

The iterative process is stopped once $\Delta^{(j)}$ and/or the residual $\Phi(q_1^{(j)}, t_1)$ becomes small enough based on acceptable tolerances.

*Velocity Level Kinematics Analysis* is much easier to compute than the positional variant, as the velocity kinematic constraint equations are linear in velocity. Since $q_1$ is available from the positional analysis, the non-singular matrix $\Phi(q_1^{(j)}, t_1)$ can be evaluated, where the linear system is dictated by Equation 3.14 for the new velocity vector, $\dot{q}_1$.

46

*Acceleration Level Kinematics Analysis* can be determined at time $t_1$ as the solution of Equation 3.15. The matrix that is used in the velocity kinematic analysis is used as forward/backward substitution sequence, which allows the generalized equations $\ddot{q}$ to be solved. Once $\ddot{q}$ has been equated, the Lagrange multipliers acting on the system are computed for the linear system, giving:

$$\Phi_q^T \lambda = F - M\ddot{q} \qquad 3.19$$

Specifics on how this equation is derived will be addressed in the following section.

## 3.1.6 Dynamic Analysis

Several additional quantities are required to describe the dynamic motion of a system, as will be discussed below. The following quantities are used in forming the rigid body equations of motion as noted by Harris et al. {21}:

$$K = \frac{1}{2}u^T M u + \frac{1}{2}\varpi^T \bar{J}\varpi \qquad 3.20$$

Several variables are defined as:

$M \equiv$ generalized mass matrix

$\bar{J} \equiv$ generalized inertia matrix expressed about the principal local reference frame

$K \equiv$ kinetic energy

$\lambda \in R^m \equiv$ an array of Lagrange multipliers. The number of Lagrange multipliers is given by the number of constraint equations (denoted m) induced by joints connecting a body to other bodies in the system.

$F(q,\dot{q},t) = \begin{bmatrix} \bar{f} \\ \bar{t} \end{bmatrix} \in R^6 \equiv$ the vector of applied forces, where $\bar{f}$ represents the applied forces, and $\bar{t}$ the applied torques

$Q(q,\dot{q},t) \in R^6 \equiv$ the generalized force acting on the body which are obtained by projecting the applied force upon the generalized coordinates.

47

Typically,

$$Q = \begin{bmatrix} \left(\Pi^P\right)^T \bar{f} \\ \left(\Pi^R\right)^T \bar{t} \end{bmatrix}$$

3.21

The projection operators are calculated as follows:

$$\Pi^P = \frac{\partial v^P}{\partial u}$$

3.22

$$\Pi^R = \frac{\partial \bar{\omega}}{\partial \zeta}$$

3.23

Where $v^P$ represents the velocity of the point of application, $p$, of the external force, F.

### 3.1.7 Equations Of Motion (EOM)

The Lagrange formulation of the equations of motion are used to obtain the following second-order differential equations:

$$\frac{d}{dt}\left[\left(\frac{\partial K}{\partial \dot{q}}\right)^T\right] - \left(\frac{\partial K}{\partial q}\right)^T + \Phi_q^T \lambda = Q$$

3.24

Recalling the definitions for the generalized coordinates from Equation 3.1, the above equations are rewritten giving:

$$\frac{d}{dt}\begin{bmatrix} \left(\frac{\partial K}{\partial u}\right)^T \\ \left(\frac{\partial K}{\partial \zeta}\right)^T \end{bmatrix} - \begin{bmatrix} \left(\frac{\partial K}{\partial p}\right)^T \\ \left(\frac{\partial K}{\partial \varepsilon}\right)^T \end{bmatrix} + \begin{bmatrix} \Phi_p^T \lambda \\ \Phi_\varepsilon^T \lambda \end{bmatrix} = \begin{bmatrix} \left(\Pi^P\right)^T \bar{f} \\ \left(\Pi^R\right)^T \bar{t} \end{bmatrix}$$

3.25

Since:

$$\frac{d}{dt}\left(\frac{\partial K}{\partial u}\right)^T = M\dot{u}$$

3.26

$$\left(\frac{\partial K}{\partial p}\right)^T = 0$$

3.27

Where the angular momenta is defined by:

48

$$\Gamma = \frac{\partial K}{\partial \zeta} = B^T \bar{J} B \zeta \qquad\qquad 3.28$$

The equations of motion from Equation 3.25 are reformulated in ADAMS as:

$$M\ddot{u} + \Phi_p{}^T \lambda = \left(\Pi^p\right)^T \bar{f} \qquad\qquad 3.29$$

$$\dot{\Gamma} - \frac{\partial K}{\partial \varepsilon} + \Phi_\varepsilon{}^T \lambda = \left(\Pi^R\right)^T \bar{t} \qquad\qquad 3.30$$

These first order differential equations are called the kinetic differential equations. They indicate how external forces determine the time variation of the translational and angular momenta as Harris et al. {21} notes. The time variation of the generalized coordinates is directly related to the translational and angular momenta by means of kinematic differential equations. The kinetic and the kinematic differential equations are used by ADAMS to generate a set of equations, Equations 3.31 through 3.35, that provide the information necessary to find a numerical solution for the dynamic analysis of a given mechanical system.

$$M\ddot{u} + \Phi_p{}^T \lambda = \left(\Pi^p\right)^T f \qquad\qquad 3.31$$

$$\dot{\Gamma} - \frac{\partial K}{\partial \varepsilon} + \Phi_\varepsilon{}^T \lambda = \left(\Pi^R\right)^T \bar{t} \qquad\qquad 3.32$$

$$\Gamma - B^T \bar{J} B \zeta = 0 \qquad\qquad 3.33$$

$$\dot{p} - u = 0 \qquad\qquad 3.34$$

$$\dot{\varepsilon} - \zeta = 0 \qquad\qquad 3.35$$

## 3.2 Force Elements in ADAMS

Three main types of force elements were used in ADAMS, which represent an applied force to the system based on either relative displacement or velocity.

*Linear Spring/Damper Elements:* Mechanical Dynamics Incorporated {28} defines these as action-reaction single-component force elements. These elements apply a force

49

between two bodies based on their relative displacement and velocities which are defined in Equation 3.36. The force applied to the bodies is along the line between the two markers that the element is connected to, which uses the SPRINGDAMPER function in ADAMS, and is defined as:

$$Force = -C_s\left(\frac{dr}{dt}\right) - K_s(r - length) + F_{preload} \qquad 3.36$$

Where:   $C_s$   ≡   damping constant of linear spring element

$K_s$   ≡   stiffness constant of linear spring element

$\dfrac{dr}{dt}$   ≡   relative velocity between two bodies

$r$   ≡   distance between markers

$length$   ≡   reference length (free length when $F_{preload}$ is zero)

$F_{preload}$   ≡   force preload in spring


*Torsional Spring Elements:* Mechanical Dynamics Incorporated {28} defines these action-reaction single-component torque elements. These elements apply a force between two bodies based on their relative rotation and angular velocities which are defined in Equation 3.37.

$$Torque = -C_t\left(\frac{d\theta}{dt}\right) - K_t(\theta - \theta_o) + T_{preload} \qquad 3.37$$

Where:   $C_t$   ≡   damping constant of torsional spring element

$K_t$   ≡   stiffness constant of torsional spring element

$\dfrac{d\theta}{dt}$   ≡   relative velocity between two bodies

$\theta_t$   ≡   angle between markers

$\theta_o$   ≡   reference angle (free angle when $T_{preload}$ is zero)

50

$$T_{preload} \equiv \text{torque preload in spring}$$

*Bushing Elements:* The BUSHING statement in ADAMS defines a massless bushing with linear stiffness and damping properties. Translational stiffness, including radial, axial and normal, are used, as well as the rotational stiffness values, which are torsional and two conical values. Damping is required for each of the stiffness directions. Bushing forces are applied based on the relative movement between two bodies, each having a reference marker. The motion of one body relative to the other is resisted by linear and torsional forces between the two markers.

$$
\begin{bmatrix} F_x \\ F_y \\ F_z \\ T_x \\ T_y \\ T_z \end{bmatrix} =
\begin{bmatrix}
K_{11} & 0 & 0 & 0 & 0 & 0 \\
0 & K_{22} & 0 & 0 & 0 & 0 \\
0 & 0 & K_{33} & 0 & 0 & 0 \\
0 & 0 & 0 & K_{44} & 0 & 0 \\
0 & 0 & 0 & 0 & K_{55} & 0 \\
0 & 0 & 0 & 0 & 0 & K_{66}
\end{bmatrix}
\begin{bmatrix} x \\ y \\ z \\ \theta_1 \\ \theta_2 \\ \theta_3 \end{bmatrix}
$$

$$
-
\begin{bmatrix}
C_{11} & 0 & 0 & 0 & 0 & 0 \\
0 & C_{22} & 0 & 0 & 0 & 0 \\
0 & 0 & C_{33} & 0 & 0 & 0 \\
0 & 0 & 0 & C_{44} & 0 & 0 \\
0 & 0 & 0 & 0 & C_{55} & 0 \\
0 & 0 & 0 & 0 & 0 & C_{66}
\end{bmatrix}
\begin{bmatrix} V_x \\ V_y \\ V_z \\ \omega_z \\ \omega_y \\ \omega_z \end{bmatrix}
+
\begin{bmatrix} F_1 \\ F_2 \\ F_3 \\ T_1 \\ T_2 \\ T_3 \end{bmatrix}
$$

3.38

Where:  $F_x, F_y, F_z \equiv$ translational force components

$x_b, y_b, z_b \equiv$ bushing deformation vector

$V_x, V_y, V_z \equiv$ time derivatives of x, y, and z, respectively

$F_1, F_2, F_3 \equiv$ constant preload force components

$T_x, T_y, T_z \equiv$ rotational force components (torque)

$\theta_1, \theta_2, \theta_3 \equiv$ small-angle rotational displacements

$\omega_x, \omega_y, \omega_z \equiv$ angular velocity components

51

$T_1, T_2, T_3$ $\equiv$ constant preload torque components

$C_1, C_2, C_3$ $\equiv$ translational damping properties

$C_4, C_5, C_6$ $\equiv$ rotational damping properties

$K_1, K_2, K_3$ $\equiv$ translational stiffness properties

$K_4, K_5, K_6$ $\equiv$ rotational stiffness properties

## 3.3 Flexible Body Analysis using ADAMS

When rigid bodies are replaced with flexible bodies, the governing equations of motion change due to the variance in inertia and relative coordinates of the body itself. Two points on a given body are now able to move relative to one another. The methodology utilized by ADAMS software to adapt to the usage of flexible bodies will be explained in this section.

## 3.3.1 Modal Superposition

Flexible body formulation in ADAMS is dependent on small linear body deformations with respect to a local reference frame, while the entire body is experiencing large, non-linear global motion. Components are discretized into finite elements, which allow a finite number of DOF to be assigned to the flexible body. The deformations of each node are approximated as a linear combination of mode shapes as shown by Blakely {5} in Equation 3.39.

$$u = \sum_{i=1}^{M_o} \{\phi_i\} q_i \qquad\qquad 3.39$$

Where:    $u$ $\equiv$ linear physical nodal displacements

$\phi_i$ $\equiv$ i-th mode shape vector

$q_i$ $\equiv$ i-th modal scaling factor

$M_o$ $\equiv$ the number of mode shapes

52

Ottarson {34} notes that this can be expressed in matrix form as:

$$u = \Phi q_m \qquad\qquad 3.40$$

Where:    $u$   $\equiv$   linear physical nodal deformation

             $\Phi$   $\equiv$   modal matrix, which transforms the smaller set of modal coordinates into the larger set of physical coordinates

             $q_m$   $\equiv$   vector of modal coordinates

This method, called modal truncation, is used to reduce the nodal DOF into a smaller set of modal DOF, but at the same time allow the deformations of the bodies to be completely defined. A simple schematic illustration of how modal superposition works can be seen in Figure 3.2 below:
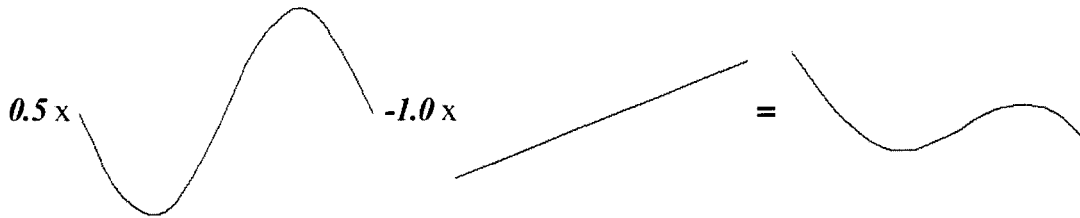
**Figure 3.2:** A demonstration of modal superposition, where an arithmetic combination of two mode shapes are used to create a specific body deformation.

### 3.3.2 Component Mode Synthesis

Recalling Component Mode Synthesis (CMS), which was introduced in Section 2.5.3, ADAMS utilizes a specific application of CMS commonly referred to as the Craig-Bampton method {9}.

The degrees of freedom in the system are divided into internal and interface DOF. Interface nodes are typically chosen in the model where external forces or joint constraints are to be applied. Interface DOF, also referred to as external DOF or boundary DOF, are not subjected to modal superposition, and as a result, do not suffer any loss of resolution when higher order modes are truncated. The system's DOF are

53

broken into boundary DOF, $u_B$, and the interior DOF, $u_I$, from which 2 types of mode shapes are defined as described by Ottarson {34}:

*Constraint Modes*: With these modes, each boundary DOF is given a unit displacement, while the other boundary DOF are held fixed. This method spans all of the possible motions of the boundary DOF.

*Fixed Boundary Normal Modes*: To obtain these modes, the boundary DOF are fixed, and an eigensolution is obtained. The number of desired modes must be selected, either based on a number of nodes, or for frequency areas of interest. The quality of the modal representation is proportional to the number of modes retained.

The physical DOF, the Craig-Bampton modes and modal coordinates are shown in the following equation:

$$u = \begin{Bmatrix} u_B \\ u_I \end{Bmatrix} = \begin{bmatrix} I & 0 \\ \Phi_{IC} & \Phi_{IC} \end{bmatrix} \begin{Bmatrix} q_C \\ q_N \end{Bmatrix} \qquad 3.41$$

Where:   $u_B$   $\equiv$  boundary DOF

$u_I$   $\equiv$  interior DOF

$\Phi_{IC}$  $\equiv$  the physical displacement of the interior DOF in the constraint modes

$\Phi_{IN}$  $\equiv$  the physical displacement of the interior DOF in the normal modes

$q_C$  $\equiv$  the modal coordinates of the constraint modes

$q_N$  $\equiv$  the modal coordinates of the normal modes

Using these modal coordinates, the mass and stiffness matrices corresponding to the Craig-Bampton modal methodology are obtained, as shown by Ottarson {31}, where Equation 3.42 represents the stiffness transformation and Equation 3.43 denotes the mass transformation:

54

$$\hat{K} = \Phi^T K \Phi = \begin{bmatrix} I & 0 \\ \Phi_{IC} & \Phi_{IN} \end{bmatrix}^T \begin{bmatrix} K_{BB} & K_{BI} \\ K_{IB} & K_{II} \end{bmatrix} \begin{bmatrix} I & 0 \\ \Phi_{IC} & \Phi_{IN} \end{bmatrix}$$

$$= \begin{bmatrix} \hat{K}_{CC} & 0 \\ 0 & \hat{K}_{NN} \end{bmatrix} \qquad\qquad 3.42$$

$$\hat{M} = \Phi^T M \Phi = \begin{bmatrix} I & 0 \\ \Phi_{IC} & \Phi_{IN} \end{bmatrix}^T \begin{bmatrix} M_{BB} & M_{BI} \\ M_{IB} & M_{II} \end{bmatrix} \begin{bmatrix} I & 0 \\ \Phi_{IC} & \Phi_{IN} \end{bmatrix}$$

$$= \begin{bmatrix} \hat{M}_{CC} & 0 \\ 0 & \hat{M}_{NN} \end{bmatrix} \qquad\qquad 3.43$$

Where:   $B$  ≡  boundary DOF

   $I$  ≡  interior DOF

   $N$  ≡  normal mode

   $C$  ≡  constraint mode

   $\hat{M}_{NN}$  ≡  mass diagonal matrix

   $\hat{K}_{NN}$  ≡  stiffness diagonal matrix

Note:   $\hat{K}$  =  block diagonal: There is no coupling between the constraint modes and the fixed-boundary normal modes

   $\hat{M}$  =  not block diagonal: There is inertia coupling between the constraint modes and the fixed boundary normal modes

### 3.3.3 Mode Shape Orthonormalization

The Craig-Bampton modes are not an orthogonal set of modes, since the generalized mass and stiffness matrices are not diagonal, as was noted in Equations 3.42 and 3.43. This can be resolved by solving the eigenvalue problem:

$$\hat{K}q = \lambda \hat{M}q \qquad\qquad 3.44$$

Using these eigenvector solutions, the transformation matrix, N, can be defined, which allows for the transformation from the Craig-Bampton modal basis to an orthogonal basis with modal coordinates $q^*$:

$$Nq^* = q \qquad\qquad 3.45$$

This alters the superposition formula of Equation 3.39 to the following:

55

$$u = \sum_{i=1}^{M} \phi_i q_i = \sum_{i=1}^{M} \phi_i N q^* = \sum_{i=1}^{M} \phi_i^* q^* \qquad 3.46$$

Where: $\phi_i^* \equiv$ orthogonalized Craig-Bampton modes

The orthogonalized modes are not the eigenvectors of the original system, but are eigenvectors of the Craig-Bampton representation of the system, and they have a natural frequency associated with them. Orthonormalization generates the modes of an unconstrained system. Of these modes, six are rigid body modes, which can be disabled. These are discarded since ADAMS provides its own large motion rigid body DOF.

### 3.3.4 Modal Flexibility

**Position**

The instantaneous location of a marker that is attached to a node, P, on a flexible body is a vector sum as shown by Ottarson {34}, which is illustrated in Figure 3.3:

$$r_p = \vec{x} + \vec{s}_p + \vec{u}_p \qquad 3.47$$

Where: $\vec{x} \equiv$ the position vector from the origin of the ground coordinate system to the local body coordinate system

$\vec{s}_p \equiv$ the position of the undeformed point P with respect to the local body reference frame

$\vec{u}_p \equiv$ the translational deformation of the point P from the point's undeformed position, to the deformed position

56
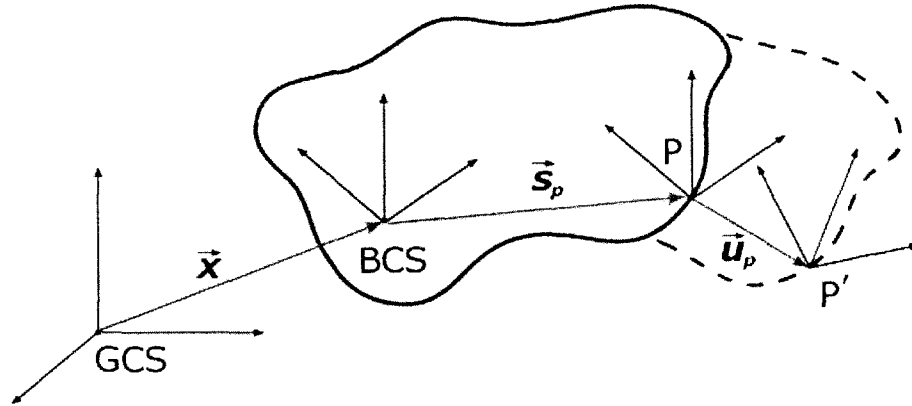
**Figure 3.3** Coordinate system illustration of a point, P' on a flexible body, which is measured relative to an undeformed point P, body coordinate system (BCS), as well as the global coordinate system (GCS). The shaded region is the original unreformed body, while the dotted impression represents the deformed state. The arrows show the vectors that relate the coordinates.

This equation can then be written in matrix form, giving:

$$r_p = \bar{x} + {}^{G}A^{B}(s_p + u_p)$$ 

3.48

Where:  $\bar{x}$  ≡ the position vector from the origin of the ground coordinate system to the local body coordinate system

$s_p$  ≡ the position of the undeformed point P with respect to the local body reference frame, which is a constant

${}^{G}A^{B}$  ≡ the transformation matrix , which is composed of the Euler angles, where superscripts G and B denote ground and body respectively.

$u_p$  ≡ the translational deformation, which is a modal superposition

The vector $u_p$ can be further defined as:

$$u_p = \Phi_p q_f$$

3.49

Where:  $\Phi_p$  ≡ the portion from the modal matrix that corresponds to the translational degrees of freedom of the node P. The matrix has dimensions of 3 X the number of modes being used

$q_f$  ≡ the generalized coordinates of the flexible body

57

From the above equations, the overall set of generalized coordinates for a flexible body

can be expressed as shown by Shabana {37} in equation 3.50:

$$\xi = \begin{Bmatrix} x \\ y \\ z \\ \varphi \\ \theta \\ \phi \\ q_f^i \end{Bmatrix} = \begin{Bmatrix} p^i \\ \varepsilon^i \\ q_f^i \end{Bmatrix} \qquad 3.50$$

### 3.3.5 Orientation

As a flexible body deforms in ADAMS, the marker rotates small angles relative to the

local body coordinate system. These angles are also calculated using modal

superposition as follows:

$$\theta_p = \Phi_p^* q_f \qquad 3.51$$

Where:  $\Phi_p^*$  ≡ the portion from the modal matrix that corresponds to the rotational degrees of freedom of the node P. The matrix has dimensions of 3 times the number of modes being used

$q_f$ ≡ the generalized coordinates of the flexible body

The orientation of the marker J, relative to the ground coordinate system is determined by

the Euler transformation matrix as stated below in Equation 3.52. Ottarson {34} notes

that it is a product of three matrices:

$$^{G}A^{J} = {}^{G}A^{B} \, {}^{B}A^{P} \, {}^{P}A^{J} \qquad 3.52$$

Where:  $^{G}A^{J}$  ≡ Euler transformation matrix (overall)

$^{G}A^{B}$ ≡ transformation of the local body coordinate system to the ground coordinate system, which is simply referred to as "A" herein

$^{B}A^{P}$ ≡ transformation matrix relating the orientation change due to body deformation at node p, an identity of which is shown in Equation 3.53.

58

$${}^{P}\!A^{J}$ ≡ transformation matrix from the user defined marker, J that was manually placed on the body, to the deformed position

The transformation matrix used to account for the orientation change due to the body deformation, ${}^{B}\!A^{P}$, can be simplified for small angles as, where I is the identity matrix, and the tilde denotes the skew operator:

$$
{}^{B}\!A^{P} = \begin{bmatrix} 1 & \theta_{pz} & -\theta_{py} \\ \theta_{pz} & 1 & \theta_{px} \\ -\theta_{py} & \theta_{px} & 1 \end{bmatrix} = I + \tilde{\theta}_{p} \tag{3.53}
$$

An example of how the tilde operator works is shown in Equation 3.54 for clarification, as the tilde is used in many equations throughout this chapter.

$$
a \times b = \begin{bmatrix} 0 & a_{z} & -a_{y} \\ a_{z} & 0 & a_{x} \\ -a_{y} & a_{x} & 0 \end{bmatrix} b = \tilde{a}b = -\tilde{b}a \tag{3.54}
$$

### 3.3.6 Velocity Equations

*Translational Velocity*

To calculate the kinetic energy in the system, the velocities of the points are required. The positional coordinates are differentiated to give the following equation:

$$
v_{p} = \dot{x} + \dot{A}(s_{p} + u_{p}) + A\dot{u}_{p} \tag{3.55}
$$

Using the relationship:

$$
\dot{A}s = A({}^{G}\omega_{B}^{B} \times s) = A^{G}\tilde{\omega}_{B}^{B} = A\tilde{s}\,{}^{G}\omega_{B}^{B} \tag{3.56}
$$

Where:    ${}^{G}\omega_{B}^{B}$ ≡ the angular velocity of the body relative to the ground, expressed in body coordinates

     ~ ≡ skew operator as noted in Equation 3.54

Gives:      $v_{p} = \dot{x} - A(s_{p} \mp u_{p})B\dot{\varphi} + A\Phi_{p}\dot{q}_{f}$      3.57

Where:    ${}^{G}\omega_{B}^{B}$ ≡ $B\dot{\varphi}$, which relates the angular velocity to the time derivative of the angular orientation state

59

*Angular Velocity*

The angular velocity of the user positioned marker J, can be seen below in Equation 3.58. This calculation represents a sum of the angular velocity of the body, and the angular velocity due to the deformed state.

$$^{G}\omega_{B}^{J} = {}^{G}\omega_{B}^{P} = {}^{G}\omega_{B}^{B} + {}^{B}\omega_{B}^{P} = {}^{G}\omega_{B}^{B} + \Phi_{p}^{*}\dot{q}_{f} \qquad 3.58$$

### 3.3.7 Point Forces and Torques

Forces and torques present in a flexible system must be projected onto an external node, at an external marker, and must be projected on the generalized coordinates of the system. It is important to note that the modal matrix is defined only at interface nodes, so as a result, they can only be applied to these noted in the ADAMS model. Ottarson {34} remarks that the Force, $\vec{F}$, and the Torque, $\vec{T}$, applied to a marker, L, can be expressed as follows:

$$F_{L} = \begin{bmatrix} f_{x} & f_{y} & f_{z} \end{bmatrix}^{T} \qquad 3.59$$

$$T_{L} = \begin{bmatrix} t_{x} & t_{y} & t_{z} \end{bmatrix}^{T} \qquad 3.60$$

These above equations can be used to represent the total force, Q, as show in Equation 3.61 for which the terms will be detailed below shown is by Ottarson {34} as:

$$Q = \begin{bmatrix} Q_{T} & Q_{R} & Q_{M} \end{bmatrix}^{T} \qquad 3.61$$

Where: $Q_{T}$ $\equiv$ generalized translational force

$Q_{R}$ $\equiv$ generalized rotational force

$Q_{M}$ $\equiv$ generalized modal force

The *general translational force* must be transformed from the force at marker L, to the global coordinate reference frame by using Equation 3.62. In this format, the generalized force becomes independent of the point of application.

60

$$Q_T = {}^G A^L F_L \qquad\qquad 3.62$$

Where: ${}^G A^L \equiv$ transformation matrix from the ground reference, to the
reference marker, as noted in equation 3.52 for a similar marker

The *generalized torque* on the system can be derived from the Equation 3.63 which is the
torque on the body relative to it's local coordinate system.

$$\vec{T}_{total} = \vec{T}_b + \vec{p}_b \times \vec{F}_b \qquad\qquad 3.63$$

Where: $T_{total} \equiv$ total resultant torque on the body

$\vec{T}_b \equiv$ sum of torques applied to the body

$\vec{p}_b \times \vec{F}_b \equiv$ sum of the torques created as a result of force
application at a distance $\vec{p}_b$ from the BCS.

The generalized torque must also be expressed with respect to the ground coordinate
system, which Ottarson {34} shows as giving:

$$T_{total} = {}^G A^L T_L + p \times {}^G A^L F_L \qquad\qquad 3.62$$

Applying total torque and representing it with respect to the generalized torque on the
body Euler angles from the B matrix of Equation 3.6 gives:

$$Q_R = \left[ {}^G A^B B \right]^T T_{total} = \left[ {}^G A^B B \right]^T \left[ {}^G A^L T_L + p \times {}^G A^L F_L \right] \qquad\qquad 3.63$$

The *generalized modal forces* applied at a point due to forces and torque are calculated
by projecting them onto the mode shapes. Assuming a point application at marker L as
before, the can be translated to the local reference frame of the body:

$$F_l = {}^G A^{B^T} {}^G A^L F_L \qquad\qquad 3.64$$

$$T_l = {}^G A^{B^T} {}^G A^L T_L \qquad\qquad 3.65$$

The forces are translated onto the translational mode shapes, and the torques are
translated onto the angular mode shapes as expected, and shown in Equation 3.66:

61

$$Q_F = \Phi_p^T F_I + \Phi_p^{*T} T_I \qquad\qquad 3.66$$

Where:  $\Phi_p$  $\equiv$  portion of modal matrix corresponding to translation
DOF at point p

$\Phi_p^*$  $\equiv$  portion of modal matrix corresponding to rotational
DOF at point p

### 3.3.8 Flexible Body Equations of Motion

To describe the motion of a flexible body, Ottarson {34} notes that the governing

ordinary differential equations (ODE's) for the body are derived using the Lagrange

equation as shown in Equation 3.67

$$\frac{d}{dt}\left(\frac{\partial L}{\partial \dot\xi}\right) - \left(\frac{\partial L}{\partial \xi}\right) + \left(\frac{\partial \Im}{\partial \dot\xi}\right) + \left[\frac{\partial \Psi}{\partial \xi}\right]^T \lambda - Q = 0 \qquad\qquad 3.67$$

$$\Psi = 0 \qquad\qquad 3.68$$

Where:  $L$  $\equiv$  the Lagrangian , which denotes $L = T - V$, where T and
V are the kinetic and potential energies

$\Im$  $\equiv$  energy dissipation function

$\Psi$  $\equiv$  the constraint equations

$\lambda$  $\equiv$  the Lagrange multipliers for the constraints (constraint
Jacobian matrix)

$\xi$  $\equiv$  the generalized coordinates as defined in Equation 3.50

$Q$  $\equiv$  the generalized forces (the applied forces that are
projected on the generalized coordinates)

To formulate the ODE using the Lagrange's equations, the Lagrangian (L) of the

system is required. The kinetic and potential energy of a body is obtained by integrating

the kinetic and potential energy of unit volume on the flexible body over the entire

volume of the body. In order to derive the kinetic and potential energy of a flexible body,

the position and velocity vectors of an arbitrary point on the elastic body are needed.

Ottarson {34} notes that the variables involved in the Lagrangian as stated above in

Equation 3.67, are calculated using the formulations to follow.

62

### Kinetic energy and the mass matrix:

The kinetic energy for a flexible body can be expressed as:

$$T = \frac{1}{2} \int_V \rho v^T v \, dV \qquad\qquad 3.69$$

$$T \approx \frac{1}{2} \sum_p v_p^T m_p v_p + {}^G w_P^{BT} I_p {}^G w_P^{BT} \qquad\qquad 3.70$$

Where $m_p$ and $I_p$ are the nodal mass and nodal inertia tensor of the node P. Ottarson {34} states that $I_p$ is often a negligible quantity, which can be neglected. Shabana {39} remarks that the kinetic energy of the system can be reduced to the quantity shown in Equation 3.71:

$$T = \frac{1}{2} \dot{\xi}^T M(\xi) \dot{\xi} \qquad\qquad 3.71$$

The mass matrix is in the form of a 3x3 matrix as seen below in Equation 3.72:

$$M(\xi) = \begin{bmatrix} M_{tt} & M_{tr} & M_{tm} \\ M_{tr}^T & M_{rr} & M_{rm} \\ M_{tm}^T & M_{rm}^T & M_{mm} \end{bmatrix} \qquad\qquad 3.72$$

Where:  r,t,m $\equiv$ rotation, translation and modal DOF respectively

$$M_{tt} \equiv \Lambda^1 I$$

$$M_{tr} \equiv -A\left[\Lambda^2 + \Lambda_j^3 q_j\right] B$$

$$M_{tm} \equiv A\Lambda^3$$

$$M_{rr} \equiv B^T \left[\Lambda^7 - \left[\Lambda_j^8 + \Lambda_j^{8T}\right] q_j - \Lambda_{ij}^9 q_i q_j\right] B$$

$$M_{rm} \equiv B^T \left[\Lambda^4 + \Lambda_j^5 q_j\right]$$

$$M_{mm} \equiv \Lambda^6$$

Note that the variables represented as $\Lambda$ represent inertia invariants as will be defined below. The mass matrix is dependant on the modal coordinates, and the dependence on

63

orientation coordinates is due to the transformation matrices, $A$ and $B$. The inertia

invariants are computed from the $N_o$ nodes of the finite element representation, based on

their undeformed location, $s_p$, their component modes, $\Phi_p$, and the nodal masses, $m_p$.

Ottarson {34} shows that the inertia invariants are defined as:

Where: $\Lambda^1 \equiv \displaystyle\sum_{p=1}^{N_o} m_p$ (The total mass of the flexible body)      Scalar

$\Lambda^2 \equiv \displaystyle\sum_{p=1}^{N_o} m_p s_p$, $j=1,..,M_o$      (3 x 1)

$\Lambda^3_j \equiv \displaystyle\sum_{p=1}^{N_o} m_p \Phi_p$      (3 x $M_o$)

$\Lambda^4 \equiv \displaystyle\sum_{p=1}^{N_o} m_p \tilde{s}_p \Phi_p + I_p \Phi_p$      (3 x $M_o$)

$\Lambda^5_j \equiv \displaystyle\sum_{p=1}^{N_o} m_p \tilde{s}_p^T s_p + I_p$, $j=1,..,M_o$      (3 x $M_o$)

$\Lambda^6 \equiv \displaystyle\sum_{p=1}^{N_o} m_p \Phi_p^T \Phi_p + \Phi_p^T I_p \Phi_p$ (The generalized mass)      ($M_o$ x $M_o$)

$\Lambda^7 \equiv \displaystyle\sum_{p=1}^{N_o} m_p \tilde{s}_p^T \tilde{s}_p + I_p$ (The moment of inertia)      (3 x 3)

$\Lambda^8_j \equiv \displaystyle\sum_{p=1}^{N_o} m_p \tilde{s}_p \tilde{\Phi}_{pj}$, $j=1,..,M_o$      (3 x 3)

$\Lambda^9_{ij} \equiv \displaystyle\sum_{p=1}^{N_o} m_p \tilde{\Phi}_{pj} \tilde{\Phi}_{pk}$, $j,k=1,..,M_o$      (3 x 3)

Four combinations of invariant usage are possible in flexible body simulation:

*Rigid Body*: ADAMS disables the sixth inertia invariant, which makes the flexible body

behave as a rigid one. This is beneficial to use in comparative studies, and is also useful

while debugging models. Results comparison to a true rigid body may differ slightly.

*Constant*: The third, fourth, fifth, eighth and ninth invariants are disabled. This method

neglects the effects of the changes in the centre of mass location and the moments of

inertia. This is primarily a research tool, and results may be quite inaccurate.

64

*Partial Coupling*: The fifth and ninth inertia invariants are disabled. These invariants serve as a second order correction to the flexible body tensor, and may not be necessary for simulation. Disabling these have little effect on the results and can reduce CPU time.

*Full Coupling*: All invariants are enabled, and this method is used to achieve full accuracy, but at the cost of computational time.

### Potential energy and the stiffness matrix:

Potential energy arises from the contributions from gravity, as well as energy storage (as in springs) and elasticity effects. This relation can be expressed as:

$$V = V_g(\xi) + \frac{1}{2}\xi^T K \xi \tag{3.73}$$

In this equation, K represents the generalized stiffness matrix, which is generally constant. The modal coordinates are the only factors that contribute to the elastic energy, leading K to be expressed as the following:

$$K(\xi) = \begin{bmatrix} K_{tt} & K_{tr} & K_{tm} \\ K_{tr}^T & K_{rr} & K_{rm} \\ K_{tm}^T & K_{rm}^T & K_{mm} \end{bmatrix} \begin{bmatrix} 0 & 0 & 0 \\ 0 & 0 & 0 \\ 0 & 0 & K_{mm} \end{bmatrix} \tag{3.74}$$

In the case of Equation 3.74, $K_{mm}$ refers to the generalized stiffness matrix with respect to the modal coordinates, q. The term $V_g$ represents the gravitational potential energy as shown in the following equation, where $g$ represents the gravitational acceleration vector:

$$V_g = \int_V \rho \ \bar{r}_p \cdot \bar{g} dV = \int_V \rho [x + A(s_p + \Phi_P q_f)]^T g dV \tag{3.75}$$

The force attributed to gravity is:

$$f_g = \frac{\partial V_g}{\partial \xi} = \begin{bmatrix} [\int_V \rho dV] \ g \\ \frac{\partial A}{\partial \xi} \left[ \int_V \rho(s_p + \Phi_P q_f)^T dV \right] g \\ A \left[ \int_V \rho \ \Phi_P^T \ dV \right] g \end{bmatrix} \tag{3.76}$$

65

### Dissipation and the damping matrix:

Damping forces applied to the flexible bodies is brought on by relative velocities, and is assumed to be derivable from the quadratic form which is known as Rayleigh's equation:

$$\Im = \frac{1}{2}\dot{q}^T D \dot{q}$$ 

3.77

Where:   $\Im$  $\equiv$ energy dissipation

$D$  $\equiv$ a matrix containing the damping coefficients, $d_{ij}$

$\dot{q}$  $\equiv$ velocity

With the orthogonal modes, the damping ratio can be different for each of the modes, and can be defined as a ratio of the critical damping for the mode, $c_i^{cr}$, as shown in Equation 3.78:

$$c_i^{cr} = 2\sqrt{k_i m_i}$$

3.78

Where the damping in the system is relating to the critical damping by the equation:

$$c_i = \eta_i c_i^{cr}$$

3.79

Where:   $k_i$  $\equiv$ generalized stiffness of mode $i$

$m_i$  $\equiv$ generalized mass of mode $i$

$c_i$  $\equiv$ modal damping of mode $i$

$\eta_i$  $\equiv$ modal damping ratio

$c_i^{cr}$  $\equiv$ critical damping

66

### 3.3.9 Governing Differential Equation for Flexible Bodies

Ottarson {34} shows that the governing differential equation in its final form in terms of the general coordinates can be seen in Equation 3.80:

$$M\ddot{\xi} + \dot{M}\dot{\xi} - \frac{1}{2}\left[\frac{\partial M}{\partial \xi}\dot{\xi}\right]^T \dot{\xi} + K\xi + f_g + D\dot{\xi} + \left[\frac{\partial \Psi}{\partial \xi}\right]\lambda = Q \qquad 3.80$$

Where the variables represent:

| | | |
|---|---|---|
| $\xi, \dot{\xi}, \ddot{\xi}$ | $\equiv$ | flexible body generalized coordinates and their time derivatives |
| $M$ | $\equiv$ | flexible body mass matrix |
| $\dot{M}$ | $\equiv$ | time derivative of the flexible body mass matrix |
| $\dfrac{\partial M}{\partial \xi}$ | $\equiv$ | the partial derivative of the mass matrix with respect to the body generalized coordinates. The matrix is a $(M_o + 6) \times (M_o + 6) \times (M_o + 6)$ tensor, where $M_o$ is the number of modes. |
| $K$ | $\equiv$ | generalized stiffness matrix |
| $f_g$ | $\equiv$ | generalized gravitational force |
| $D$ | $\equiv$ | modal damping matrix |
| $\Psi$ | $\equiv$ | algebraic constraint equations |
| $\lambda$ | $\equiv$ | Lagrange multipliers |
| $Q$ | $\equiv$ | generalized applied forces |

# CHAPTER 4 VIRTUAL MODEL CREATION

## 4.0 General

This chapter outlines the process in constructing a high fidelity computer model of both the vehicle and the testing apparatus using ADAMS, CATIA, PATRAN and NASTRAN software suites. The initial steps outline the process in creating the rigid body model and details concerning the vehicle itself, while latter steps outline the addition of flexible bodies. The selection and usage of model input data and how it relates to the Road Test Simulation (RTS) process is highlighted. Methods of automation through computer analysis are addressed in order to optimize simulation performance.

The methodology used in the creation of a virtual model is summarized in Figure 4.1. This chart highlights the steps required in creating a virtual model. These steps include the creation of a rigid multibody dynamics model, the addition of flexible bodies, and fatigue analysis The process of creating a rigid body model is presented by Ferry {16} in greater detail.

68

| Load Model | Stress Model | Fatigue Model |
|---|---|---|
| Create or assemble solid model | Create finite element model of component | Generate load history |
| Apply contraints, material properties and inputs | Verify normal modes in ADAMS using FEA software | Finite element model |
| Simulate Validate Refine | Perform modal stress recovery Apply input loads | Material properties (S-N curves, surface finishes) |
| **Rigid Multibody Dynamics Model** | **Flexible Multibody Dynamics Model** | **Fatigue Life and Durability Model** |

**Figure 4.1:** Flow chart showing the simplified process of creating a virtual durability model. This research focuses in on creating a rigid model, as well as creating a model with flexible elements. Fatigue correlation was not performed in this study.

## 4.1 Coordinate System Identification

The coordinate system adopted in constructing this computer model is based on the Global Coordinate System (GCS) used in the CAD drawings from the manufacturer's database. The x-axis of the system runs longitudinally along the wheelbase of the vehicle, the y-axis runs laterally along the track of the vehicle, and the z-axis runs vertically. The vehicle considered in this study is produced for usage in the North American market, thus the driver's side is oriented to the left, and the passenger's side to the right with a line of site towards the front of the vehicle. Figure 4.2 illustrates the global model axis, where the x-axis is positive facing rearward, the y-axis is positive

69

running from the driver's side to the passenger's side, and the z-axis runs with positive

pointing upwards. Note that this differs from the SAE convention shown in Figure 2.5.



**Figure 4.2**: Global Coordinate System (GCS) of computer model as adapted from manufacturer's database. The x-axis runs longitudinally with positive facing rearward. The y-axis runs laterally with positive facing towards the passenger's side of the vehicle and finally, the z-axis runs vertically, with positive facing upwards.

## 4.2 Vehicle Component Overview

The vehicle being modeled in the current research is a four wheel drive compact sport utility vehicle (SUV). This analysis focuses on the accurate modeling and simulation of the independent front suspension and solid rear axle suspension of this vehicle. In the production form, the suspension is composed of a four-link front suspension, and a three-link rear suspension. For a number of reasons, a four-link rear suspension has been proposed for investigation.

A majority of the components to be used in the creation of this model are readily accessible from the manufacturer's database. The vehicle model that has been assembled is based on the exact vehicle that was tested on the proving ground and on the road test simulator. The geometric model has been assembled at curb position initially, which refers to the vehicle on level ground with no occupants or cargo on board. All the fluids in the vehicle are present, and this would represent the vehicle "as delivered". With this

70

base arrangement, various passenger and cargo ratings are added as required based on durability testing sequences.

### 4.2.1 Front Suspension Configuration

The independent front suspension as shown in Figure 4.3 consists of upper and lower wishbone suspension with an SLA (Short upper arm, Long lower Arm) configuration. The lower control arms are constructed using cast iron while the upper control arms and use forged steel. The upper control arms attach to the upper wheelhouse assembly, and the lower control arm attaches to the engine cradle. The steering knuckle is made of cast iron, and is connected to the upper and lower control arms through ball joints. The vehicle has four wheel drive which requires a clevis assembly to allow the half shafts to drive the front wheels without contacting the spring and shock assembly.



**Figure 4.3**: Front independent suspension configuration in CATIA illustrating the left hand side two link configuration. Major elements such as the control arms, steering knuckle, as well as the clevis and spring/shock assembly have been highlighted. Note: The steering as well as the stabilizer bar assembly have been removed for clarity purposes, and can be seen in Figure 4.4 for the identical suspension assembly.

71

The springs used in the front are a fixed rate, meaning that the spring rate is independent of the deflection of the springs themselves. The assembly contains a concentric shock and coil spring combination, and the attachment points are at the lower control arm and the upper wheelhouse. The motion of the suspension is damped using low pressure gas charged shock absorbers. Urethane jounce bumpers are used to limit the travel of the suspension assembly under jounce conditions, and are also used to reduce the harshness due to impact loadings at jounce. Body roll motion of the vehicle is controlled using a sway bar and end link combination that connect the lower control arms together, and ties them to the body itself.

### 4.2.2 Steering System

The steering system consists of a power-assisted rack and pinion configuration and is shown in Figure 4.4. The steering rack allows the rotational motion of the steering wheel to be converted into the translational motion required to steer the drive wheels. The rack travels in the lateral direction, and has two spherical joints on each of its ends. Tierods are used to connect the steering rack assembly to the steering knuckle. The ball joints connecting the steering knuckle to the control arms give the assembly the necessary degrees of freedom to allow the wheels to turn and steer the vehicle.

**Figure 4.4**: Front independent suspension configuration in CATIA illustrating the steering and braking systems, as well as the stabilizer bar assembly. Several components have been removed for clarity. The remainder of the components are shown in Figure 4.3 above.

### 4.2.3 Rear Suspension Configurations

The rear suspension is composed of a coil sprung live solid axle as shown in Figure 4.5. The three link configuration is made up of an upper "A" shaped upper control arm, and uses dual lower trailing arms. The proposed four link configuration uses similar dual lower trailing arms, but uses twin upper control arms instead of the single arm used with the three link configuration. Both configurations use progressive rate coil springs. Progressive rate refers to the fact that the stiffness of the spring varies, depending upon the spring's displacement. They act to provide consistent loading with change in cargo. Low pressure gas charged shock absorbers are mounted outboard of the springs, and forward of the axle assembly to providing damping. To control body roll motion of the vehicle in the rear, a stabilizer bar is used to connect the lower control arms to one another.

**Figure 4.5**: Rear suspension configurations in CATIA. The three-link configuration is shown at the top, while the four-link is at the bottom. The four-link suspension differs from the three-link configuration with its two upper control arms. Different lower control arms are also utilized as well as differing braking systems. The brake drums themselves have been removed in the three-link model to show the degree of detail used in the CAD model.

74

### 4.2.4 Braking System

The braking system is a power-assisted fully hydraulic type, and uses anti-lock braking technology. The front brakes are disc units while the rear brakes vary depending on the type of rear suspension being tested. The three-link rear suspension uses drum brakes, while the four-link suspension uses disc brakes shown in Figure 4.5. The braking system is not functional in the computer model, but separate bodies for the brakes have been used in the model so a functional braking system model can be added if required.

### 4.2.5 Powertrain and Drivetrain Components

The vehicle tested is equipped with a V6 engine and an automatic transmission. It has a 4WD system, which uses a transfer case, additional driveshafts, and a front axle assembly. The rear axle is part of the unsprung weight and is considered a critical component of the suspension system due to its large mass. The front differential on the other hand, is not part of the unsprung weight, since the vehicle incorporates independent front suspension. Due to complexity of modeling the differential assemblies, only the rear axle assembly was modeled. The front differential mass was included as part of the body assembly. The rear driveshaft was included in the model to couple the transfer case to the rear axle assembly.

### 4.2.6 Body Structures

The vehicle utilizes unibody construction, meaning that there is not a full frame under the vehicle. For this research, the body is treated as being rigid, and flexibility effects will not be considered due to the complexity of creating an accurate flexible body model. The body structure encompasses any components that are not contained within the suspension system that has been modeled. The engine, transmission, and transfer case are not included in the body structure, as they are modeled separately.

## 4.3 Geometric Model Creation and Assembly

The first step in building the computer model was identifying all of the parts used on the test vehicle itself. Each of these parts has a corresponding geometric model in CATIA, and can be retrieved from the manufacturer's database. Part numbers are commonly cast into the components, or are easily identified by tags that are affixed to the parts themselves. Identifying numbers of some components, such as bushings, are difficult to get when they are installed on the vehicle. For parts such as these, an in-house computerized assembly manual was used to determine part numbers. It is also crucial to get the correct part numbers certain items, such as springs and shock absorbers, since they can have drastically different rate characteristics, but at the same time are very similar in appearance.

The "virtual" components are located using ENOVIA/vpm, which is a database of CAD models as explained in Section 2.7.2. Most vehicles have several combinations of option packages and powertrain/drivetrain configurations, which makes having the actual part numbers recorded essential in determining which parts to choose. ENOVIAvpm allows the CAD model to be opened on a remote session of CATIA, where they can be saved locally on a workstation. A majority of these parts are already positioned where they would reside on the vehicle at curb position, eliminating the concern of translating or rotating of the parts to locate them in the correct position on the vehicle. Prototype parts (non-production) usually have to be positioned manually.

### 4.3.1 Component Mass Calculation

For the mass properties of the parts to be defined, CAD models of the geometry must contain a volume. Once a volume has been created, a density can be assigned to it, and the mass and inertia properties can be found. Many of the components that were used in this model started out as surfaces, which do not contain a volume. In order to

76

create a volume, a number of surfaces must be combined to form a three dimensional closed volume.

Three different methods were used in assigning a density to the parts, depending on the resources that were available. Many parts for this vehicle were located on site during the testing phase, and for this case the parts were weighed on a precision balance, and the values were recorded. Using the CATIA model of the component, the volume was calculated, and was used to calculate the density using the following fundamental equation, Equation 4.1. The density was entered into CATIA, and the mass and inertia values were calculated and recorded.

$$\rho = \frac{m}{v} \qquad\qquad 4.1$$

Where:   $\rho$  ≡  Density (kg/m$^3$)

           $m$  ≡  Mass (kg)

           $v$  ≡  Volume (m$^3$)

All of the necessary parts were not available on site for physical weighing, so a second method was also used. A list of weights for a majority of the parts on the vehicle was acquired from the manufacturer and suppliers, and was used to characterize a majority of the parts contained within this model.

It may seem obvious at first to enter the density of the part into CATIA using the density based on the type of material. Many times the geometric models are not an exact representation of the part itself, especially in the case of gears and bolts, so the measured weights in CATIA may be slightly in error. By using the exact measured weights, one can be assured that the weights in the model are correct. Where there was no available weight for the parts, the theoretical density of the part was entered into the CATIA model based on the material used.

77

## 4.3.2 Inertia Characterization

Each part or assembly of parts will have their own associated principal moments of inertia ($I_{xx}$, $I_{yy}$, $I_{zz}$), and may have associated products of inertia ($I_{xy}$, $I_{yz}$, $I_{xz}$). These inertial values will depend on the location and orientation of the axis in which the inertia is measured. When the moments of inertia are calculated for the individual components, they are measured on the principal axes and will not contain products of inertia.

In several instances, the inertia must be added or subtracted to represent several bodies together as one assembly, as with the body structure described in Section 4.3.3. The assemblies or bodies require a common reference axis, which allows the inertial values to be added or subtracted directly. If the model exists in CATIA, a reference axis can be created, and the inertia is calculated relative to that axis. In the case where a computer model does not exist, the inertial values at the common axis must be calculated using matrix transformations. The inertia at one axis can be represented at another reference axis using translational and rotational matrix transformations. For in-depth mathematical representation of the inertia transformations, detailed explanations are provided by Ferry {13} and Hibbeler {22}.

## 4.3.3 Full Vehicle Moment of Inertia

During the execution of durability cycles, the vehicle body is free to move, which requires the centre of gravity (cg) and inertial values for the body structure by itself. If a solid model existed for every component of the body, it would be possible to calculate the inertia of the entire vehicle this way. This method is not very practical, as it would be very time consuming, and its accuracy would be questionable due to the vast number of components involved. Alternatively, this information was obtained from a vehicle similar to the one being used in the present study at the Vehicle Inertia Measurement

78

Facility (VIMF). This unique facility is owned and operated by SEA Technologies Inc. of Columbus, Ohio, USA.

The inertia measurement equipment, as described by Heydinger et al. {23}, was used to calculate the centre of gravity position (x,y,z), along with the principal moments of inertia ($I_{xx}$, $I_{yy}$, $I_{zz}$). The roll/yaw product of inertia ($I_{xy}$) is determined, while the roll/pitch ($I_{xz}$) and pitch/yaw ($I_{yz}$) are assumed to be zero based on vehicle symmetry. Data was acquired for the vehicle at three load ratings: light as possible (LAP), half rated load (HRL), and full rated load (FRL).

Once the full vehicle mass and inertial information was known, the inertia values of the suspension components were subtracted from the full vehicle to attain values for the remaining body structures as described in Section 4.3.3. A reference axis was created at the centre of gravity of the entire vehicle with the x axis forward, y axis towards the right (passengers side), and the z axis down, and using the GCS orientation. This was the convention used at the VIMF facility. CATIA was used to calculate the inertia of the suspension bodies about this reference axis, which allowed the inertial values to be subtracted directly. The mass and moments of inertia for the tires and wheels also had to be subtracted from the body, as the wheels/tires are present at the VIMF, but not on the RTS machine.

The centre of gravity of the body alone was also calculated. This was done by summing the mass moments of each individual component on the vehicle other than the body itself about the vehicles GCS in the x, y, and z directions. Using the centre of gravity information from the VIMF along with each individual component, the centre of gravity for the body alone was calculated. This left one issue when representing the model in ADAMS. The inertia values were represented at the centre of gravity of the full vehicle, while the mass of the body is referenced from the centre of gravity of the body alone. In ADAMS, when the body was defined, a marker was created for the body inertia

79

reference, and the mass was referenced to a marker representing the centre of gravity location.

### 4.3.4 Drivetrain and Powertrain Inertia

Mass and inertial properties for the engine, transmission, and transfer case were obtained from an internal database that cataloged various powertrain and drivetrain configurations. The data was acquired experimentally to determine the centre of gravity, mass, and the moments of inertia of each of the three assemblies. This was done utilizing a trifilar pendulum apparatus at the VIMF facility. The inertial values for the slip-yoke and the driveshaft were calculated using geometric models in CATIA.

The data included a reference location on each assembly, which incorporated machined surfaces and rotational centrelines that could be located in a CATIA drawing to establish a datum. These points and axis orientations were positioned in the appropriate CATIA drawing of the assembly, which allowed the principal axis to be located relative to the GCS, and to the body inertial reference. The centre of gravities and their respective axis orientations were computed using translational components, as well as direction cosines provided in the database. These masses and inertias were then subtracted from the body structure by transforming the inertia via matrix transformations as explained in Section 4.3.2. Points and axis were also positioned where the appropriate bushings were located to attach the assemblies to the body. Simplified geometries were created using CATIA to represent these assemblies for visual purposes.

### 4.4 ADAMS Model Creation

This section outlines the transition of CATIA to ADAMS, and also details the steps involved in setting up additional components such as springs and bushings that determine the frequency response of the model. Finally, model statistics are presented that outline the composition of this virtual model.

80

### 4.4.1 CATIA to ADAMS Translation using CAT/ADAMS

In the process of assembling the CATIA model, there are literally hundreds of parts needed to characterize the mass and the inertia of component assemblies. When these parts are exported into ADAMS as rigid bodies, there is no need to have complicated geometry or assemblies such as gear-trains. ADAMS simply treats the geometric shapes as "shell" files, and are used for visualization purposes only. For this reason, a majority of the parts were simplified and entire assemblies were represented by simple geometry.

Components and assemblies were placed in "sets" in CATIA, and each rigid body was assigned to its own unique set. Joints are used to constrain the relative movement between sets. CAT/ADAMS converts these sets into "parts", which are the ADAMS equivalent.

The simplified geometry was assigned the mass and inertial properties of the complicated structure, so the model retains an accurate representation of the system. Each part in CAT/ADAMS is defined by a centre of gravity marker, the mass of the part, and the inertia properties relative to the centre of gravity marker. A marker in ADAMS is used to create a local coordinate system that is defined relative to the global coordinate system, through a specified translation and rotation (x,y,z and Euler angles)

Critical axis and points other than the centre of gravity markers in the CATIA model must be designated as "hard points" in CAT/ADAMS for them to be brought into ADAMS. These hard points are translated using CAT/ADAMS, which places markers in the ADAMS model allowing force elements and constraints can be positioned accurately. Hard points were created to position the following elements:

- Ball joint rotation centres

- Bushing centre locations, and axis orientation (z axis along torsional rotation line)

81

- Shock absorber mounting points

- Coil spring mounting points

- Jounce bumper contact locations

- Sensor positions for the wheel force transducers and accelerometers

CAT/ADAMS converts the CATIA file into a format recognized by ADAMS, and opens a remote session of ADAMS where the model can be saved locally. All of the mass and inertia properties of the parts in ADAMS were compared to the recorded values to assure that the conversion has been done successfully. An ADAMS model of the full suspension and drivetrain of the vehicle can be seen in Figure 4.6 below.
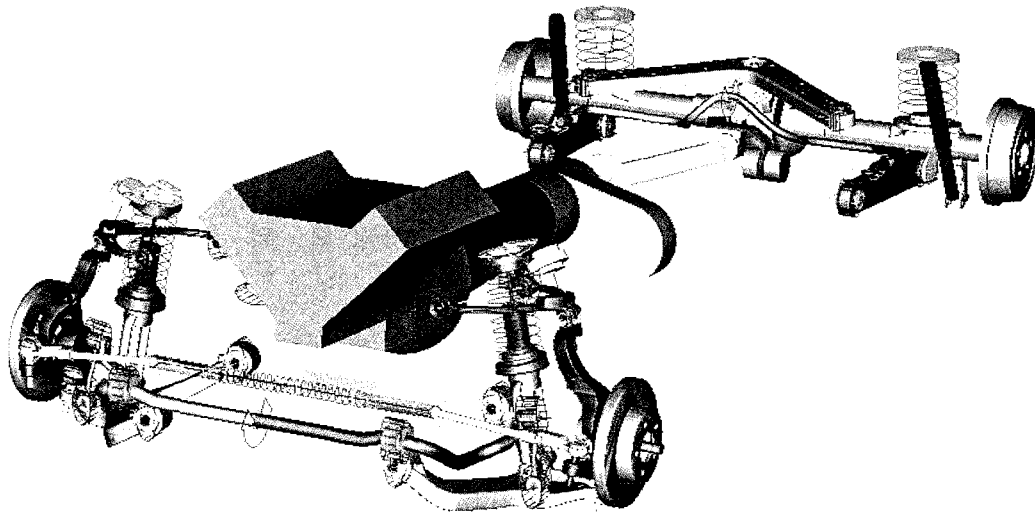


**Figure 4.6**: Virtual ADAMS model representation of test vehicle with 3-link rear suspension configuration. In this illustration, all force elements are present including springs, shock absorbers and bushings. Note the simplified geometry of many of the parts in the model.

The front suspension is composed of the following main rigid bodies: upper and lower control arms, steering knuckle assembly, suspension (clevis) assembly, end links, and stabilizer bar (two halves). Many of these assemblies contain parts that are connected using fixed joints. For example, the steering knuckle assembly includes parts of the knuckle itself, the brake assembly (which includes the hub assembly), physical ball

82

joints, and the input half shafts. While the entire assembly could have been modeled as one part, this would not make the model very robust. If one was to look into making the knuckle a flexible body, then the parts and their relative inertias would have to be recalculated in CATIA and reinserted into the model. With the current arrangement, separate assemblies or individual components can be changed with ease.

The steering assembly is composed of the centre, left and right sections, which allow for a slight flexibility in the system by using force elements. This also allows an additional force element to be added to simulate the tethering of the steering wheel, which is added in the interior of the physical vehicle to resist steering motion of the vehicle during testing. The flexibility in the rack is added to avoid system lockup, and will account for the rack deformation, ball joint play, and gear backlash. Left and right-hand tie-rod assemblies are also represented as rigid bodies to couple the steering rack to the steering knuckle.

The rear suspension assembly contains the rear axle assembly, separate brake systems for each suspension configuration, a vibration isolator, upper and lower control arms for each suspension configuration, stabilizer bar (two halves), and upper control arm mounting brackets (to the rear differential). The drivetrain and powertrain, which attach to the body and rear axle, are composed of the engine, transmission, transfer case, slip-yoke, and driveshaft.

### 4.4.2 Joint Constraints

The first step in assembling the ADAMS model is to add joint constraints to constrain the relative motions between the rigid bodies. The following joints were used in constraining the model:

*Revolute Joints*: The stabilizer bars were split into two separate parts at the centre of the bar, giving a left and right section. Revolute joints were used to allow

relative rotation of the bars at the centre. A torsional spring is used to model the stiffness of the stabilizer bars.

*Spherical Joints*: Ball Joints for upper and lower control arm to steering knuckle interface

Tierod ends for the steering rack to steering knuckle interface

Driveshaft to slip yoke, and driveshaft to rear axle interface

Rear ball joint (upper control arm to rear axle) with the 3-link suspension system

*Translational Joints*: Slip yoke to transmission interface

Left, front and centre sections of steering rack assembly

Rear dummy axle to rear axle assembly (See Section 5.6.2)

*Hooke Joints*: Front steering rack to tierod end (left and right hand sides) prevents the rotation of the tierod ends. In reality, these would be spherical joints, where friction would limit rotation.

*Point/curve*: Front suspension assembly (spring, shock absorber and clevis) to the body to control suspension movement. A point curve constraint was used to allow the spring and shock absorber assembly to compress/elongate, as well as to rotate. A straight line was placed along the centerline of spring, and a point was placed at the body where the assembly was connected. The point and line were tied to one another using the point/curve constraint.

### 4.4.3 Force Element Integration

Forces and force elements are used to model elastic connections between parts, spring and damping elements, actuation and control forces. They do not affect the degrees of freedom of the system, nor do they add mass or inertia to the system. The following sections describe the force element usage in this computer model, examples of which are shown in Figure 4.7.
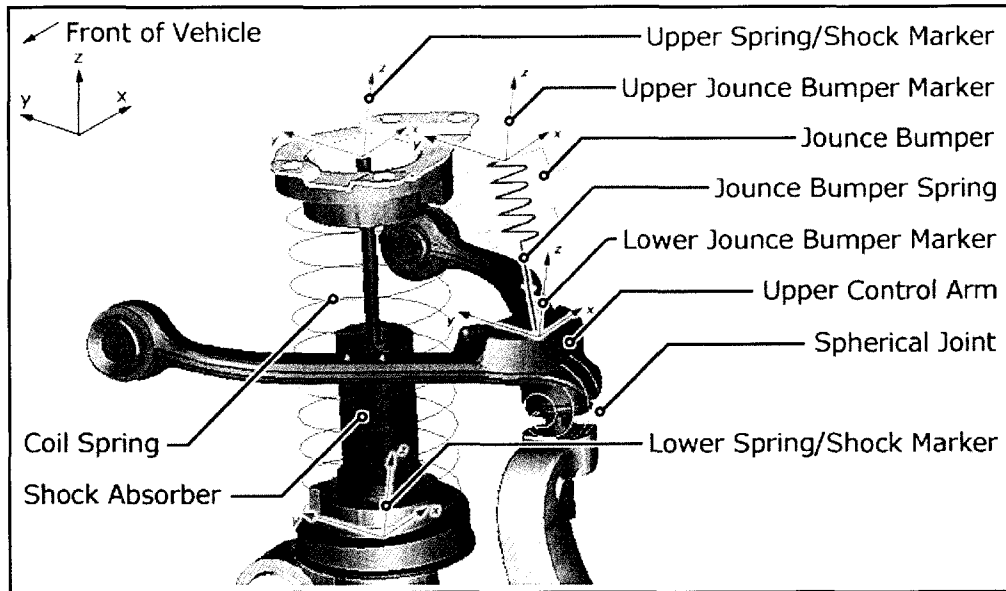
**Figure 4.7**: Front suspension assembly representation in ADAMS showing force element placement and marker locations. Force elements include coil spring, shock absorber, and jounce bumper spring. Also note the spherical constraint for the ball joint.

### 4.4.3.1 Coil Springs / Shock Absorbers

*Coil Springs* are used at both the front and the rear of this vehicle. Four separate springs are used in total. The coil springs were attached to the markers that were brought into ADAMS from CATIA using CAT/ADAMS as is illustrated for the front suspension in Figure 4.7. Properties for these springs were acquired from physical tests conducted by the manufacturer, and were input into the ADAMS model using points from the physical data. The points were input manually into splines, and the default lengths as well as the preloads at curb position were entered into the model. The normalized spring forces as a function of displacement for the front and rear springs can be seen in Figure 4.8, which gives a relative comparison between the two. The front springs are fixed rate units, while the rear ones have progressive rates as noted earlier.

85
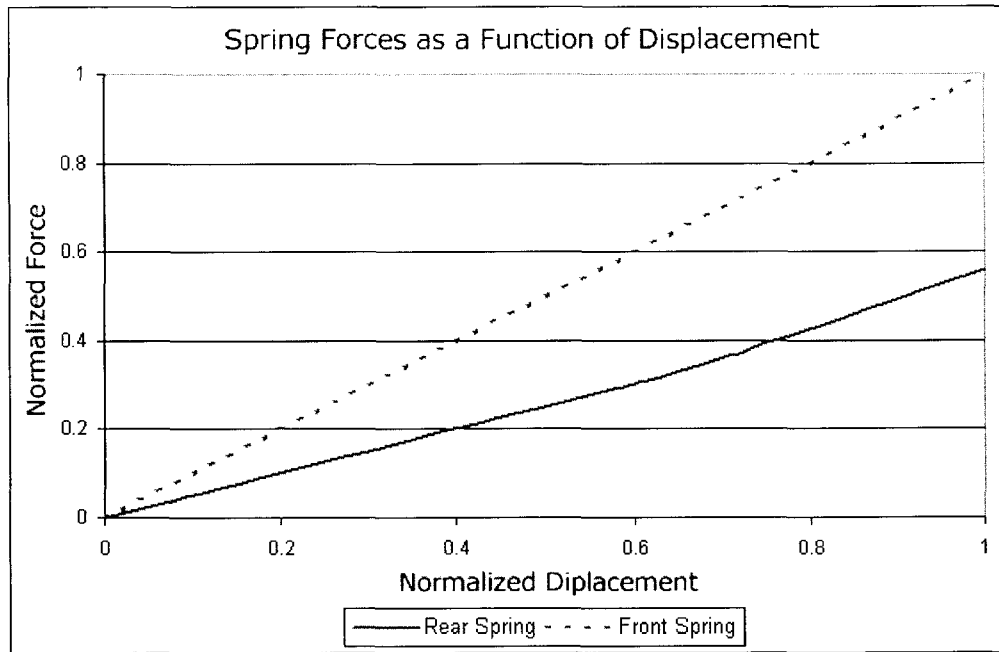
**Figure 4.8:** Normalized spring forces as a function of displacement for both front and rear springs. Clearly, the front springs are nearly twice the stiffness of the rear springs. The front springs are constant rate, while the rear ones are progressive rate, meaning they are a constant rate up until ~0.6 normalized displacement, and ramp up to a higher stiffness that is reached at ~0.75.

*Shock Absorbers* are used to provide damping to the vehicle system. The front shocks are concentric with the coils springs, and use the same markers to attach to as a result. The rear ones on the other hand are separate from the springs, and use their own unique set of markers. The shock forces as a function of velocity for both the front and rear of the vehicle are shown in Figure 4.9. The data was input into ADAMS in the same manner as the springs, through the use of splines. The additional advantage of inputting the data using splines is that springs or shock absorbers can be changed very quickly during design studies.

86
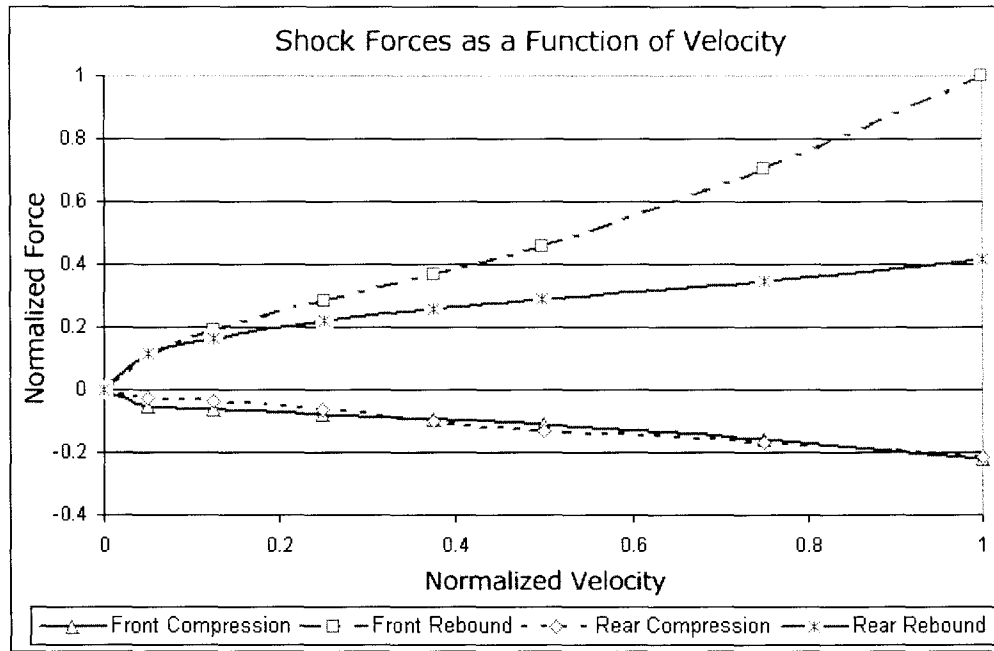
**Figure 4.9**: Normalized shock absorber forces as a function of velocity for compression and rebound. Both front and rear shocks are included to illustrate the differences in damping between the two. Clearly, the compressive damping rates are nearly identical, while the rebound rates vary by a factor of two.

### 4.4.3.2 Jounce Bumpers

*Jounce Bumpers* are "activated" at the upper limits of suspension travel, and in jounce (compression). In reality, the jouncing effect is achieved through contact. For example, with the front suspension, the upper control arms contact the jounce bumper, which is mounted to the body. This contact can be modeled in ADAMS, but this would require defining the properties of the elastomeric materials, and devising a way of representing the bodies as solids or surfaces for contact purposes (recalling that ADAMS treats bodies as visual representations only). Contacts are also very computationally demanding in ADAMS. The contact would also be particularly difficult to model if the control arms were to be replaced with flexible bodies. The effects of contact on flexible bodies may be worth investigating in the future.

Instead, a method was devised to treat the jounce bumpers as springs. The springs that are used in the model have zero stiffness until they reach a displacement where

87

contact occurs. The stiffness that is used at the point of contact onwards is based on a linearized value that was acquired from the manufacturer from jounce bumper compressive tests. An illustration of the spring representation was shown previously on Figure 4.7. A normalized plot of the front jounce bumper force as a function of displacement is shown in Figure 4.10. Both the front and the rear jounce bumpers were modeled in the same fashion.



**Front Jounce Bumper "Spring" Force as a Function of Displacement**
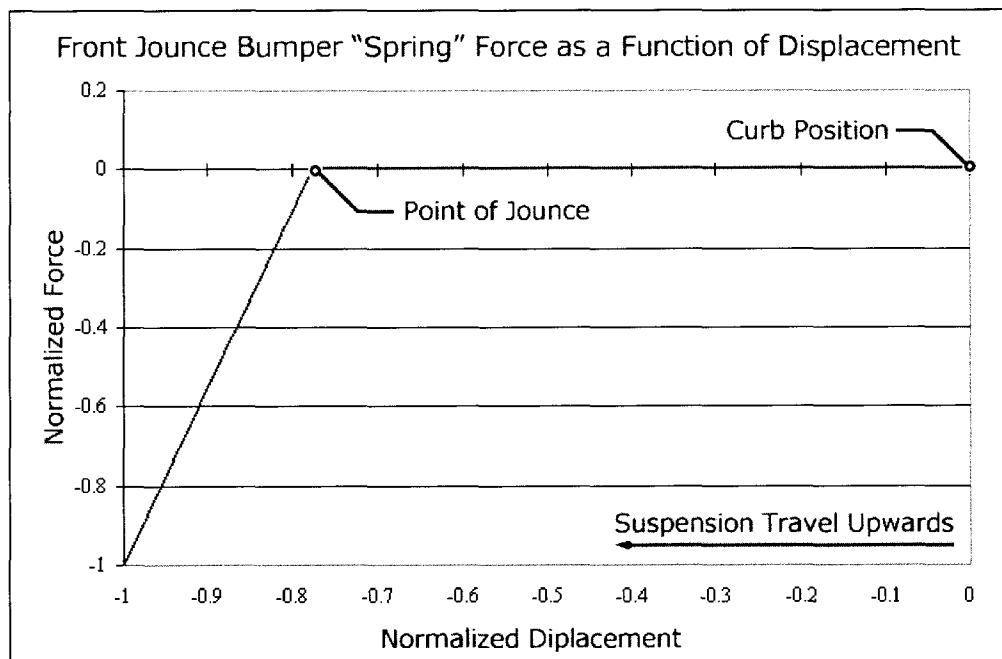
**Figure 4.10**: Normalized front jounce bumper "spring" force as a function of deflection. The zero force condition is a result of the spring only becoming active at the point of jounce. Note that both values are negative, due to the fact that the jounce "spring" is being compressed, and at the point of contact an opposing force is applied.

**4.4.3.3 Stabilizer Bars**

*Torsional Springs* were used to model the deformation and stiffness in the stabilizer bar assemblies. Each bar (front and rear) is split into two separate parts in the middle of the bars, giving a left and right section. A revolute joint is used to allow relative rotation of the bars at their centre, and a torsional spring is used to model the stiffness of the stabilizer bars. ADAMS simply applies a moment relative to the rotation at the revolute joint that connects each half of the stabilizer bars. Stabilizer bar rates

were provided by suppliers and the provided information characterized these bars by representing the force as a function of the tip deflection of the bar (in N/mm). To calculate the stiffness of torsional spring to use, an approximate rotational axis was drawn in CATIA, as is shown in Figure 4.11, showing the front stabilizer bar. An additional axis was drawn between the force input points, and the distance between the two (lever arm) was recorded. This distance along with the loading information from physical stabilizer bar tests was used to convert the units from N/mm at the force input points, to N/deg at the centre of the bar where the torsional spring is located.
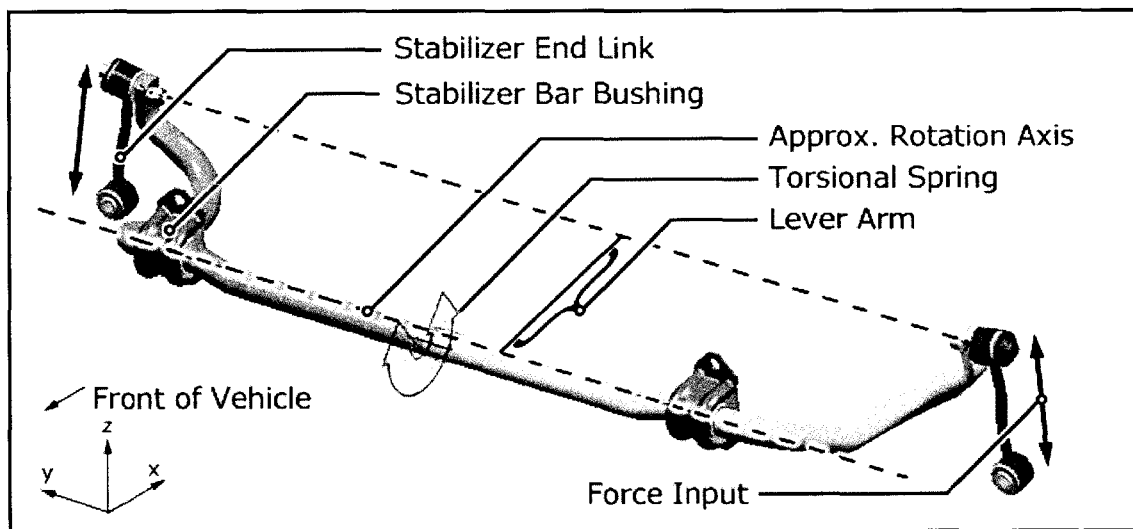


**Figure 4.11**: Illustration in CATIA of the stabilizer bar components and the approximate rotational axis. The lever arm distance is used in calculating an equivalent torsional spring that is placed in the middle of the bar to approximate the stiffness and deflections of the bar itself based on physical tests.

#### 4.4.3.4 Bushings

*Bushings* are undoubtedly the most difficult force element to model, and represent the greatest potential source of error. Bushings are used at many component interfaces, such as the control arms to the body, to give compliance to the assembly, reduce road noise and vibration, and to reduce static friction.

Bushings are commonly made of rubber compounds or other elastomeric materials that behave non-linearly. In viewing several stiffness plots, a trend that bushing

89

stiffness increases with frequency, while the damping tends to decrease was noted. This dictates that the bushing properties will vary, depending upon the frequency at which they are measured. Since the bushings are made up of elastomeric compounds, hysteresis effects are also present. This means that their loading curves are different from their unloading curves. This non-linear behavior is very difficult to model, and even more difficult to measure, so many approximations and assumptions have to be made.

Bushing data was acquired from the manufacturers as stiffness and damping data. Static bushing rates were acquired from the necessary manufacturers for radial, axial, torsional, conical, and normal directions as shown in Figure 4.12. The normal and radial rates are typically equal for most bushings. Several bushings used in this study had differing rates for the normal, or void direction as it is also called. Dynamic rates, which include stiffness and damping rates were only available for the radial direction. The dynamic rates for the axial, torsional and conical direction were approximated by determining the ratio of the dynamic to static rates in the radial direction and multiplying the other directions by this ratio. The damping was calculated by using the ratio of the dynamic stiffness to damping ratio in the radial direction and applying this ratio to the other directions.
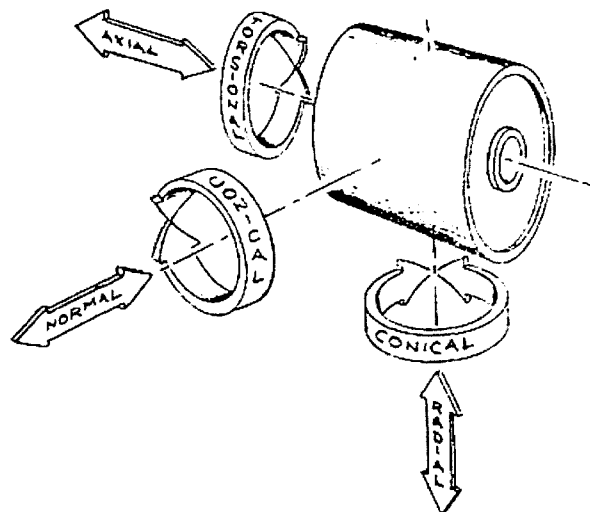
Figure 4.12: Illustration of bushing directional properties. Bushings commonly have stiffness and damping rated in the axial, normal, radial, torsional and conical directions. Image adapted from SAE Standard J670e {36}.

90

The bushing data that was attained represents a linear approximation of the actual rates. Each bushing requires 12 different values to characterize its properties, including 6 stiffnesses and 6 damping rates. Bushings can be treated as being non-linear in ADAMS, but this requires a great deal of information. Splines can be used for each stiffness and damping value, but it would be computationally intensive, and accurate data would be *very* difficult to obtain from the manufacturers. As a result, linear approximations of the values were used. Table 4.1 shows the bushing allocation for both suspension configurations.

| Summary of Bushing Allocation used with Full Vehicle Model in ADAMS | | |
|---|---|---|
| Bushing Description | Bushing Quantity with 3-link rear | Bushing Quantity with 4-link rear |
| Front lower control arms | 4 (2 per side) | 4 (2 per side) |
| Front upper control arms | 4 (2 per side) | 4 (2 per side) |
| Front clevis bushing | 2 (1 per side) | 2 (1 per side) |
| Stabilizer bar bushing | 2 (1 per side) | 2 (1 per side) |
| End link bushings | 4 (2 per side) | 4 (2 per side) |
| Rear lower control arm (body) | 2 (1  per side) | 2 (1  per side) |
| Rear lower control arm (axle) | 2 (1 per side) | 2 (1 per side) |
| Rear lower control arm (body) | 2 (1 per side) | 2 (1 per side) |
| Rear upper control arm (axle) | 0 | 2 (1 per side) |
| Engine mount bushings | 2 (1 per side) | 2 (1 per side) |
| Transmission mount bushing | 1 | 1 |
| **Total number of bushings per vehicle** | 25 | 27 |

**Table 4.1**: Summary of the bushing allocation used with the full vehicle model. Both the 3-link and 4-link configurations are illustrated. The total number of bushings used with each vehicle configuration is noted at the bottom for each case.

91

#### 4.4.4 ADAMS Rigid Body Model Overview

The following is a summary of the ADAMS model of the entire vehicle shown on Table 4.2, which was requested as a list in ADAMS. These values do not account for the methods of force and displacement input, as displacement input will reduce the degrees of freedom in the model.

| Summary of Full Vehicle Model Properties in ADAMS | | |
|---|---|---|
| Item Description | 3-Link Configuration | 4-Link Configuration |
| Moving parts | 63 | 65 |
| Revolute joints | 2 | 2 |
| Spherical joints | 9 | 8 |
| Translational joints | 5 | 5 |
| Fixed joints | 37 | 38 |
| Hooke joints (Universal) | 2 | 2 |
| Point curve | 2 | 2 |
| **Degrees of Freedom (DOF)** | **82** | **91** |

**Table 4.2**: Summary of ADAMS model statistics for full vehicle model with vehicle constrained to ground using 4 bushings representing the road to tire interface at the spindles (6 DOF at each spindle).

Moving parts in this list refers to components that have their own unique mass and inertia properties in ADAMS, and all begin initially with six DOF. These moving parts are then constrained to one another using the joints listed, which act to remove DOF from the system. Based on the way these moving parts are inter-connected, the resultant system has an overall number of DOF as is shown. ADAMS automatically calculates and lists the DOF in the system.

92

## 4.5 Physical and Virtual Correlation: Vehicle Responses

Model correlation is perhaps the most difficult portion of the model creation process. Data recorded by sensors used on the physical vehicle must be in agreement with the virtual results measured on the computer model for correlation to be considered successful. This section will address the instrumentation process, and how the data is used from the start to the finish of the durability process, both in the physical and virtual realms. Vehicle instrumentation, both physical and virtual, is a very critical process in the testing phase, as all of the results from durability testing are based on it. Results from physical durability testing from both proving ground testing and road test simulation were made available for calibration of the computer model in this study.

### 4.5.1 Physical Vehicle Instrumentation

Before being sent to the proving ground, each vehicle is hand instrumented with all the sensors that are required in durability analysis. Additional sensors are also added by request to monitor any additional vehicle responses. Instrumentation on the test vehicle used in this project included four Wheel Force Transducers (WFTs), six strain gauges, 18 accelerometers, four Rotary Variable Differential Transformers (RVDT), one Linear Variable Differential Transformer (LVDT), 22 Load Cells, a speed indicator, a brake indicator and an event marker. Many of the load cells actually contain strain gauges, but their underlying purpose is to measure force transmission. The purpose of the strain gauges listed is to measure the deformation of body panels. A total of 99 channels were used to monitor the motions and forces on the vehicle. A complete listing of all the channels used is presented in Table 4.3.

The SWIFT (Spinning Wheel Integrated Wheel Force Transducer) assemblies, which are manufactured by MTS, were mounted on special rims that allow them to be

93

coupled to the spindles at each corner of the vehicle. Each WFT is able to measure the longitudinal, lateral and vertical loads (x, y and z load respectively) and the resultant moments about the x, y and z axis of the spindle mounting point. They also allow for the measurement of the angle of the wheel about the wheel rotation axis..

The RVDT's were used to measure the control arm angles at each wheel. Each transducer was rigidly mounted to the body of the vehicle, and uses a pivoting arm to measure the angle of the front and rear lower control arm angles. The LVDT was used to measure the linear displacement of the steering rack, which in turn can be used to find the steering wheel angle using the gear ratio of the steering rack.

At each location where acceleration was monitored, three accelerometers were used. Acceleration measurements at each location were in the longitudinal, lateral and vertical directions. The acceleration was monitored at six locations for a total of 18 accelerometers. Accelerometers were located on the front steering knuckle and front lower control arms, as well as outboard of the springs on the rear axle housing for the left and right hand sides of the vehicle.

The load cells, which are noted as "custom" on Table 4.3, are all specially made to measure the force on specific parts. In most cases, strain gauges are used to measure the strain on components, which can then be used to calculate the forces present using the geometry of the component. Load cells are used to measure forces in ball joints, springs, shock absorbers, jounce bumpers, and in numerous links on the vehicle.

Strain gauges were also used to measure the strain on several components on the body. While these measurements are not very useful in the current research, they may be helpful if the body were to be represented as a flexible body for correlation purposes.

94

Finally, a sensor was used to monitor the speed of the vehicle, and one was also included to determine when the brakes are engaged. An event marker was included that the driver could engage to denote that they were beginning a new section of road on the proving ground. This marker places a voltage spike in the dataset to indicate to the test engineers that a new road segment has commenced.

| Compact SUV Vehicle Instrumentation Channel Allocation | | | | | | | |
|---|---|---|---|---|---|---|---|
| Channel Number | Raw Data | Edited Data | Remote Data | Channel Description | Sensor Type | Engineering Axis | Units |
| 1 | ● | ● | ● | LF Wheel Force Transducer Fx | WFT | Fx | lbs |
| 2 | ● | ● | ● | LF Wheel Force Transducer Fy | WFT | Fy | lbs |
| 3 | ● | ● | ● | LF Wheel Force Transducer Fz | WFT | Fz | lbs |
| 4 | ● | ● | ● | LF Wheel Force Transducer Mx | WFT | Mx | ft-lbs |
| 5 | ● | | ● | LF Wheel Force Transducer My | WFT | My | ft-lbs |
| 6 | ● | ● | ● | LF Wheel Force Transducer Mz | WFT | Mz | ft-lbs |
| 7 | ● | | | LF Wheel Force Transducer Angle | WFT | Angle | Deg |
| 8 | ● | ● | ● | RF Wheel Force Transducer Fx | WFT | Fx | lbs |
| 9 | ● | ● | ● | RF Wheel Force Transducer Fy | WFT | Fy | lbs |
| 10 | ● | ● | ● | RF Wheel Force Transducer Fz | WFT | Fz | lbs |
| 11 | ● | ● | ● | RF Wheel Force Transducer Mx | WFT | Mx | ft-lbs |
| 12 | ● | | ● | RF Wheel Force Transducer My | WFT | My | ft-lbs |
| 13 | ● | | ● | RF Wheel Force Transducer Mz | WFT | Mz | ft-lbs |
| 14 | ● | | | RF Wheel Force Transducer Angle | WFT | Angle | Deg |
| 15 | ● | ● | ● | LR Wheel Force Transducer Fx | WFT | Fx | lbs |
| 16 | ● | ● | ● | LR Wheel Force Transducer Fy | WFT | Fy | lbs |
| 17 | ● | ● | ● | LR Wheel Force Transducer Fz | WFT | Fz | lbs |
| 18 | ● | ● | ● | LR Wheel Force Transducer Mx | WFT | Mx | ft-lbs |
| 19 | ● | | ● | LR Wheel Force Transducer My | WFT | My | ft-lbs |
| 20 | ● | | ● | LR Wheel Force Transducer Mz | WFT | Mz | ft-lbs |
| 21 | ● | | | LR Wheel Force Transducer Angle | WFT | Angle | Deg |
| 22 | ● | ● | ● | RR Wheel Force Transducer Fx | WFT | Fx | lbs |
| 23 | ● | ● | ● | RR Wheel Force Transducer Fy | WFT | Fy | lbs |
| 24 | ● | ● | ● | RR Wheel Force Transducer Fz | WFT | Fz | lbs |
| 25 | ● | ● | ● | RR Wheel Force Transducer Mx | WFT | Mx | ft-lbs |
| 26 | ● | | ● | RR Wheel Force Transducer My | WFT | My | ft-lbs |

**Table 4.3**: Physical vehicle instrumentation channel allocation, which shows the channels that were monitored during data acquisition, after editing, and during RTS remote acquisition. Highlighted fields denote control channels, while bold dots indicate that the channels were recorded. In the table below, the number unit "g's" represents the acceleration due to gravity.

95

| Channel Number | Raw Data | Edited Data | Remote Data | Channel Description | Sensor Type | Engineering Axis | Units |
|---|---|---|---|---|---|---|---|
| | | | | **Compact SUV Vehicle Instrumentation Channel Allocation** | | | |
| 27 | • | | • | RR Wheel Force Transducer Mz | WFT | Mz | ft-lbs |
| 28 | • | | | RR Wheel Force Transducer Angle | WFT | Angle | Deg |
| 29 | • | • | • | Left Front LCA Angle | RVDT | Angle | Deg |
| 30 | • | • | • | Right Front LCA Angle | RVDT | Angle | Deg |
| 31 | • | • | • | Left Rear LCA Angle | RVDT | Angle | Deg |
| 32 | • | • | • | Right Rear LCA Angle | RVDT | Angle | Deg |
| 33 | • | • | | Left Front Spindle Acceleration | Accel | X | g's |
| 34 | • | • | | Left Front Spindle Acceleration | Accel | Y | g's |
| 35 | • | • | | Left Front Spindle Acceleration | Accel | Z | g's |
| 36 | • | • | | Right Front Spindle Acceleration | Accel | X | g's |
| 37 | • | • | | Right Front Spindle Acceleration | Accel | Y | g's |
| 38 | • | • | | Right Front Spindle Acceleration | Accel | Z | g's |
| 39 | • | • | • | Left Rear Spindle Acceleration | Accel | X | g's |
| 40 | • | • | • | Left Rear Spindle Acceleration | Accel | Y | g's |
| 41 | • | • | • | Left Rear Spindle Acceleration | Accel | Z | g's |
| 42 | • | • | • | Right Rear Spindle Acceleration | Accel | X | g's |
| 43 | • | • | • | Right Rear Spindle Acceleration | Accel | Y | g's |
| 44 | • | • | • | Right Rear Spindle Acceleration | Accel | Z | g's |
| 45 | • | • | | Left Front Shock | Custom | Axial | lbs |
| 46 | • | • | | Right Front Shock | Custom | Axial | lbs |
| 47 | • | • | • | Left Rear Shock | Custom | Axial | lbs |
| 48 | • | • | • | Right Rear Shock | Custom | Axial | lbs |
| 49 | • | | • | Left Front UCA Ball Joint | Custom | Long | lbs |
| 50 | • | | • | Right Front UCA Ball Joint | Custom | Long | lbs |
| 51 | • | | | Left Front UCA Ball Joint | Custom | Lateral | lbs |
| 52 | • | | | Right Front UCA Ball Joint | Custom | Lateral | lbs |
| 53 | • | | | Left Front LCA Ball Joint | Custom | Long | lbs |
| 54 | • | | | Right Front LCA Ball Joint | Custom | Long | lbs |
| 55 | • | | • | Left Front LCA Ball Joint | Custom | Lateral | lbs |
| 56 | • | | • | Left Front LCA Ball Joint | Custom | Lateral | lbs |
| 57 | • | | | Rear A-Arn Ball Stud | Custom | Long | lbs |
| 58 | • | | | Rear A-Arn Ball Stud | Custom | Lateral | lbs |
| 59 | • | | • | Left Rear LCA Axial Load | Custom | Axial | lbs |
| 60 | • | | • | Right Rear LCA Axial Load | Custom | Axial | lbs |
| 61 | • | | | Left Front Tie Rod | Custom | Axial | lbs |
| 62 | • | | • | Left Front Sway Bar Link | Custom | Axial | lbs |
| 63 | • | | • | RightFront Sway Bar Link | Custom | Axial | lbs |

**Table 4.3**: Physical vehicle instrumentation channel allocation, continued

96

| Compact SUV Vehicle Instrumentation Channel Allocation | | | | | | | |
|---|---|---|---|---|---|---|---|
| Channel Number | Raw Data | Edited Data | Remote Data | Channel Description | Sensor Type | Engineering | |
| | | | | | | Axis | Units |
| 64 | ● | | ● | Left Front Jounce Bumper | Custom | Axial | lbs |
| 65 | ● | | ● | Right Front Jounce Bumper | Custom | Axial | lbs |
| 66 | ● | | ● | Left Rear Jounce Bumper | Custom | Axial | lbs |
| 67 | ● | | ● | Right Rear Jounce Bumper | Custom | Axial | lbs |
| 68 | ● | | ● | Left Front Wheelhouse Front Gage | Rossette | 1 | lbs |
| 69 | ● | | ● | Left Front Wheelhouse Front Gage | Rossette | 2 | με |
| 70 | ● | | ● | Left Front Wheelhouse Front Gage | Rossette | 3 | με |
| 71 | ● | | ● | Left Front Wheelhouse Rear Gage | Rossette | 1 | με |
| 72 | ● | | ● | Left Front Wheelhouse Rear Gage | Rossette | 2 | με |
| 73 | ● | | ● | Left Front Wheelhouse Rear Gage | Rossette | 3 | με |
| 74 | ● | | ● | Left Rear Wheel House Gage | Rossette | 1 | με |
| 75 | ● | | ● | Left Rear Wheel House Gage | Rossette | 2 | με |
| 76 | ● | | ● | Left Rear Wheel House Gage | Rossette | 3 | με |
| 77 | ● | | ● | Right Front Wheelhouse Front Gage | Rossette | 1 | με |
| 78 | ● | | ● | Right Front Wheelhouse Front Gage | Rossette | 2 | με |
| 79 | ● | | ● | Right Front Wheelhouse Front Gage | Rossette | 3 | με |
| 80 | ● | | ● | Right Front Wheelhouse Rear Gage | Rossette | 1 | με |
| 81 | ● | | ● | Right Front Wheelhouse Rear Gage | Rossette | 2 | με |
| 82 | ● | | ● | Right Front Wheelhouse Rear Gage | Rossette | 3 | με |
| 83 | ● | | ● | Right Rear Wheel House Gage | Rossette | 1 | με |
| 84 | ● | | ● | Right Rear Wheel House Gage | Rossette | 2 | με |
| 85 | ● | | ● | Right Rear Wheel House Gage | Rossette | 3 | με |
| 86 | ● | | | Brake Indicator | On / Off | | Volts |
| 87 | ● | | | Event Marker | On / Off | | Volts |
| 88 | ● | ● | | Left Front Spring | Custom | Axial | lbs |
| 89 | ● | ● | | Right Front Spring | Custom | Axial | lbs |
| 90 | ● | ● | | Left Rear Spring | Custom | Axial | lbs |
| 91 | ● | ● | | Right Rear Spring | Custom | Axial | lbs |
| 92 | ● | | | Vehicle speed | I-Box | | MPH |
| 93 | ● | | ● | Left Front Knuckle Acceleration | Accel | X | g's |
| 94 | ● | | ● | Left Front Knuckle Acceleration | Accel | Y | g's |
| 95 | ● | | ● | Left Front Knuckle Acceleration | Accel | Z | g's |
| 96 | ● | | ● | Right Front Knuckle Acceleration | Accel | X | g's |
| 97 | ● | | ● | Right Front Knuckle Acceleration | Accel | Y | g's |
| 98 | ● | | ● | Right Front Knuckle Acceleration | Accel | Z | g's |
| 99 | ● | | | Steering Wheel Angle | LVDT | Angle | Deg |

**Table 4.3**: Physical vehicle instrumentation channel allocation, continued

97

### 4.5.2 Raw Data Acquisition

To execute a durability cycle, the test vehicle is run over a number of separate road courses in a specified sequence and a specified number of times. These road courses are especially designed to test light-duty trucks and SUV's. During the data acquisition process an onboard data acquisition system, as shown in Figure 4.13, records all of the datasets using an MTS Corporation {30} recommended sampling rate of 409.6Hz. This sampling rate is used for several reasons, including studies conducted by Grenier et al. {20} involving fatigue life prediction (FLP). Each of the eight roads must be tested with three different payloads including FRL (full rated load), HRL (half rated load), and LAP (light as possible).
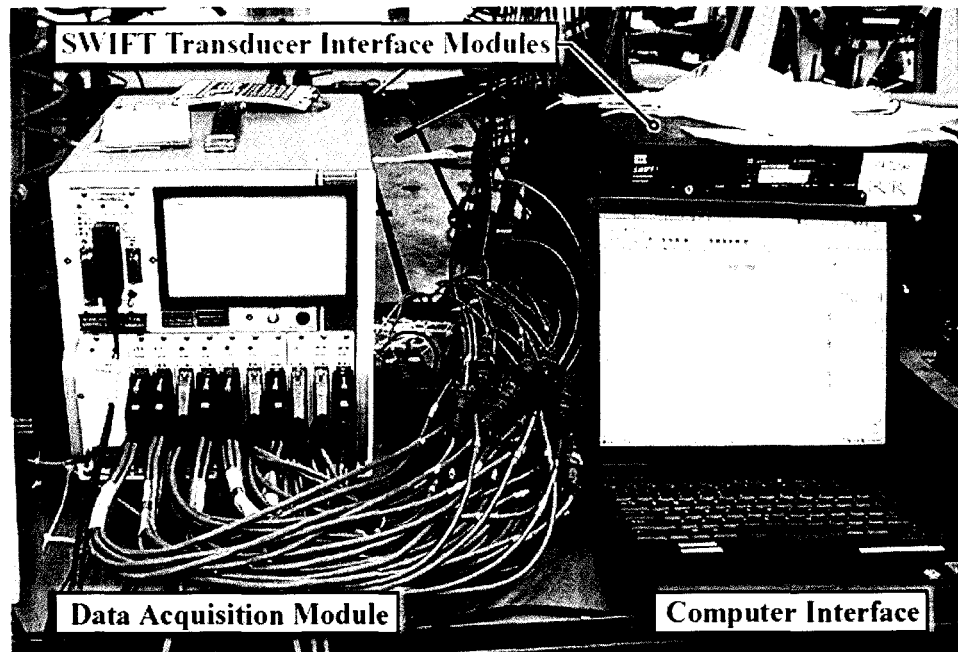


**Figure 4.13**: Data acquisition system that is used to collect sensor data from the test vehicle during proving ground testing, as well as during the iteration process as is shown. Main components include the data acquisition module, which collects the incoming sensor signals, the SWIFT Transducer Interface (TI) modules, which analyze the WFT signals, and the computer interface, which is used to record and calibrate test data.

98

A full durability test on this particular vehicle consists of 24,140 km (15,000 miles) of proving ground driving over these road courses, equally divided over the three payloads. The acquired data for use with the RTS machines is only recorded over a few laps of these road courses, as only one set of results is needed on a given road for each payload.

This data is then brought back to the test laboratory, where it is converted into RPC (Remote Control Parameter) format. The steps as outlined in Section 2.3 are followed, and the process of drive file iteration is commenced. Control channels, which will be briefly described in the following section, are used by the MTS RPC software as feedback control to determine the necessary input displacements of the servo hydraulic actuators to simulate the movement of the vehicle.

### 4.5.3 Drive File Correlation

During the drive file iteration process, specified guidelines are used to determine whether the responses from the vehicle on the RTS machine are within an acceptable range of the measured responses from the vehicle on a proving ground. Control channels are used in generating the drive files, and the channels for this particular vehicle are highlighted in Table 4.3 earlier. The control channels used include WFT's, axle mounted accelerometers, and control arm angles. Once the drive file generation has been successfully completed, the time history for the edited and remote responses will closely match, based upon certain criterion. There are three criteria for convergence of iterations (the error signal referred to is the point-by-point difference between the desired and achieved response):

- The absolute maximum of the error signal must be within a specified percentage of the absolute maximum of the desired time history signal.

99

- The root mean square (RMS) of the error signal must be within a specified percentage of the absolute maximum of the desired time history signal.

- The achieved power spectral density must be within a specified percentage of the desired power spectral density throughout the control band region, except in frequency regions where the power of the desired signal is three decades or more below the peak power of the desired signal.

### 4.5.4 Local and Remote Responses

The local responses that are measured refer to the data collected from instrumentation on the MTS 329 test rig itself. Force transducers are located on the input arms of this machine to measure longitudinal and lateral forces that are input to the vehicle. The displacements at the hydraulic actuators are measured for each direction (longitudinal, lateral and vertical) using LVDT's mounted on each actuator. The displacements output are the approximated displacements at the spindles using the geometry of the rig. These displacements are not the actual displacements of the hydraulic cylinders. A total of 20 channels are recorded corresponding to local responses and can be seen on Table 4.4.

Data that is recorded from the instrumentation onboard the vehicle itself while on the RTS are referred to as the *remote* responses. These 74 data channels, which are indicated on Table 4.3, are very similar to datasets recorded at the proving ground. Fewer channels are recorded than at the proving ground because they may not relevant in the laboratory testing (such as brake and vehicle speed indicators) or they may not have been requested by test engineers.

100

| MTS 329 Road Test Simulator Local Responses | | | | | |
|---|---|---|---|---|---|
| Channel Number | Channel Description | Units | Channel Number | Channel Description | Units |
| 1 | LF Spindle Vert. Disp. | in | 11 | RF Spindle Long. Load | lb |
| 2 | LR Spindle Vert. Disp. | in | 12 | RR Spindle Long. Load | lb |
| 3 | RF Spindle Vert. Disp. | in | 13 | LF Spindle Lat. Disp. | in |
| 4 | RR Spindle Vert. Disp. | in | 14 | LR Spindle Lat. Disp. | in |
| 5 | LF Spindle Lat. Load | lb | 15 | RF Spindle Lat. Disp. | in |
| 6 | LR Spindle Lat. Load | lb | 16 | RR Spindle Lat. Disp. | in |
| 7 | RF Spindle Lat. Load | lb | 17 | LF Spindle Long. Disp. | in |
| 8 | RR Spindle Lat. Load | lb | 18 | LR Spindle Long. Disp. | in |
| 9 | LF Spindle Long. Load | lb | 19 | RF Spindle Long. Disp. | in |
| 10 | LR Spindle Long. Load | lb | 20 | RR Spindle Long. Disp. | in |

**Table 4.4**: Local responses of the MTS 329 Road Test Simulator. The channels that are monitored represent sensors that are located on the machine itself that are used as feedback control to the Remote Parameter Control (RPC) in the test laboratory. These are the channels that are used to drive the virtual model.

## 4.5.5 Virtual Instrumentation

In the correlation phase of the virtual model, the objective is to have the virtual instrumentation imitate the instrumentation on the physical vehicle. This means that virtual sensors must be positioned in the same place on the computer model as they would be in the physical model, both in location and orientation. The choice and selection of this virtual instrumentation is crucial in the validation of the computer model. Virtual sensors are placed on the model to monitor desired values such as acceleration, forces or displacement. One large benefit of using the virtual model is that sensors can be placed anywhere on the model.

A majority of the sensors in the model used the REQUEST function in ADAMS to output data results. Mechanical Dynamics Incorporated {28} states that requests are used to ask for standard displacement, velocity, acceleration, or force information that will help you investigate the results of your simulation. In the case of this project, sets of function expressions that defined the desired output were created manually using ADAMS own programming language. Creating these custom expressions required

101

knowing what quantity was to be measured, and which markers are involved in the calculation. Each request function can contain up to eight sets of data. For example, one request function, REQ_LCA_ANGLES_3LINK, was used to monitor the lower control arm angles with the three link configuration. This request file contained four separate sets of data, one for each corner of the vehicle. Request functions were created for accelerometers, shock and spring forces, wheel force transducers, jounce bumper forces, control arm angles, and various displacements used in correlating the model.

### 4.5.6 ADAMS File Input

Input data in the form of forces and displacements were entered into ADAMS by using the general spline function. The ADAMS/Durability module was used to directly input RPC III and DAC files into the model. For each motion or force that was used as input on the model, an appropriate channel had to be selected to be extracted from the appropriate RPC III file. ADAMS does not store this spline data in the model; it references the RPC III files directly, which greatly reduces the ADAMS file size. The only issue with this is the RPC files are required in addition to the ADAMS model to run simulations. Each force or displacement channel had to be entered into ADAMS as a separate spline. In order to excite the virtual model, either an imposed motion (displacement) or a point force was used.

A finite number of data points are contained within an RPC III file, requiring ADAMS to use an interpolation function. The INTERP function, which is a special function for use with ADAMS/Durability, allows for interpolation between the data points. A simple example of an input command is as follows: INTERP(time,3,Input_Spline_File). In this function, INTERP denotes the interpolation function and time denotes that the input data is indexed with respect to time. The number "3" represents cubic interpolation between data points, and the Input_Spline_File refers

102

to the specific spline in ADAMS to be used. The only additional requirement is that each of the channels require the units to be converted (inches to mm or lb force to N for example), and that in certain cases the initial offset of the channels be subtracted. Alternatively, these files could have been edited using nCode batch file commands, but the objective was to be able to directly input files straight from the RTS output in RPC III format, for ease of use. This also makes the process much faster and more user friendly.

## 4.6 Flexible Body Creation

This section outlines the steps involved in creating flexible bodies for use in an ADAMS model. Superelement techniques are used, which allows direct replacement of rigid bodies with flexible ones, without having to modify entire assemblies. A detailed explanation of NASTRAN input file syntax is beyond the scope of this thesis, and the reader is encouraged to refer to the associated NASTRAN reference manuals by Blakely {5} or Kilroy {24} for further documentation. A detailed explanation outlining the creation of element meshes of complex components is also beyond the extent of this thesis.

## 4.6.1 Geometry Meshing

The first process of creating a flexible body representation of a component is to create a finite element mesh of the specific part. Parameters that affect the creation of this mesh include boundary conditions, loading conditions, areas of concern, and the accuracy and precision of the desired results. Boundary and force conditions include areas where one body is connected to another body through a mechanical joint, and where bodies are attached to one another using force elements. The definition and restraints placed on the models are critical in attaining accurate results when loadings are applied to the bodies. The objective when bringing flexible bodies into ADAMS is to have the exact restraints

103

placed on the model as was the case with rigid bodies. CATIA and PATRAN software suites were both used in the creation of finite element models.

If the geometry is meshed in CATIA, modules such as ANSOLID or ANMESH and ANELFINI are used. ANSOLID is an automated meshing module within CATIA. The ANMESH module is used for manually creating meshes using many element formulations, and the ANELFINI solver within CATIA is used to solve preliminary FEA models. The ANMANAGE module in CATIA is used to convert the file to NASTRAN format. Careful attention should be given to assure that the units being exported are correct, and that the CATIA elements are being correctly converted to an appropriate equivalent NASTRAN element. These files can be edited in PATRAN, or can be created entirely using this pre-processing software. Files that are output from PATRAN can be run immediately after they are output in NASTRAN format. If the flexible bodies are to be used in ADAMS, this NASTRAN file must be manually edited using techniques presented in sections to follow.

### 4.6.2 Modal Selection

The number of normal modes that should be used is dependent on the component being analyzed. A sufficient number of normal modes must be retained to allow the flexible body to have dynamic resolution in the frequency range of interest. Adding too many normal modes will unnecessarily increase the size of the flexible body files (requires more space to store additional modes), and can increase the computational time dramatically. Ottarson {34} states that a general rule of thumb is to multiply the frequency range of interest by two (Nyquist frequency). ADAMS also allows individual modes to be activated or deactivated. This way, one can determine whether the mode significantly affects the output of the system by activating or deactivating certain modes and analyzing and comparing the output responses.

104

Using NASTRAN, the EIGRL (Eigenvalues Lanczos Method) card can be used to specify the frequency range that are of interest, rather than the total number of modes that are required. Alternatively one would run a simple linear analysis using NASTRAN, or an appropriate FEA package for that matter, to determine the number of normal modes. For example, if the simulation only concerned modes smaller than 50Hz, then modes under 100Hz would be retained. Unfortunately there are no true failsafe rules of thumb for predicting what the effects of aggressive modal truncation will be. The effects of modal truncation should not be neglected.

### 4.6.3 Rigid Body Elements (RBE's)

Rigid body elements are a form of multi-point constraint (MPC) used in NASTRAN to tie specified nodes in a model together. Useful applications of these include representing the presence of bushings (outer housings), fasteners, and actual ball joints in finite element models without having to physically include them in the model. Nodes on these RBE's can then be used in superelement analysis, and may be used as points to constrain the flexible bodies to rigid ones in ADAMS. The most common elements being used are the RBE2 and RBE3 element formulations.

Kilroy {24} states that an RBE2 element defines a rigid body with independent degrees of freedom that are specified at a single grid point and with dependent degrees of freedom that are specified at an arbitrary number of grid points.

This means there is one master node (independent ) whose DOF are rigidly attached to many slave (dependant) nodes via these RBE2 elements, as is shown in Figure 4.14. This creates a localized stiffening of the model because the nodes are unable to move relative to one another. Since the master node's DOF are independent, this node can be used as an attachment point (external point). The slave nodes, which would represent the bushing to control arm interface in Figure 4.14 cannot be used as attachment points.

105
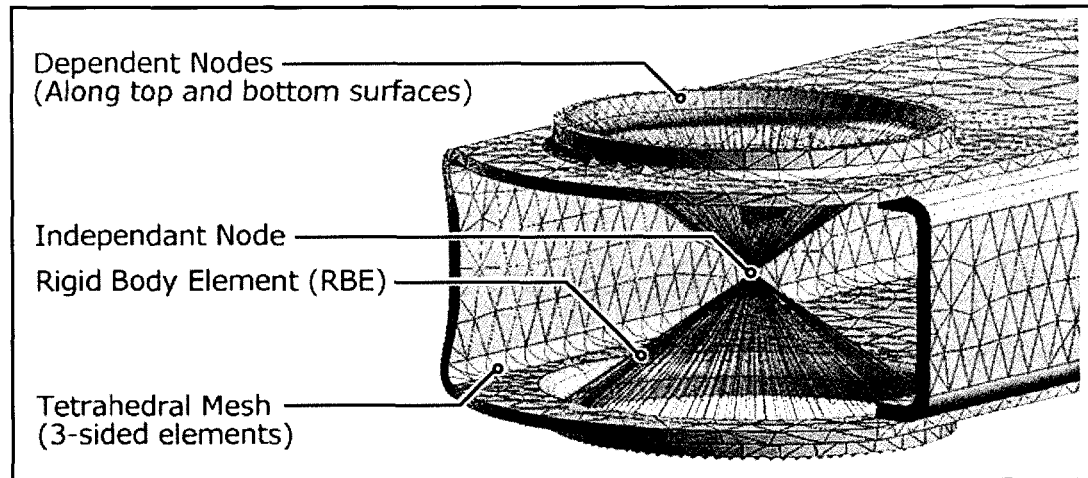
**Figure 4.14**: Illustration of a rigid body element (RBE) that is used in place of a bushing on a control arm. This particular element is an RBE2 element, which has an independent (external) node in the centre, and dependent nodes placed along the bushing-to-control arm contact areas. The independent node is used to attach this flexible body to other rigid bodies in an ADAMS model.

Kilroy {24} notes that an RBE3 element defines the motion at a reference grid point as the weighted average of the motions at a set of other grid points. This reverses the role of the nodes in an RBE2 element. This leaves one slave node whose DOF are dependent upon many master nodes that it is connected to via these RBE3 elements. This greatly decreases any artificial, localized stiffening of the model that are introduced by using RBE2 elements. Since the single dependant node is dependant on the motions of the other nodes, is cannot be used as an attachment point in superelement analysis.

In most cases, RBE2's should be used, unless stress and deformations in the area where the RBE3 is located are critical. RBE3 elements can be used, but require additional elements to be connected to them, such that they can be promoted to attachment points. The rigid body elements used in this research are all RBE2's.

## 4.6.4 Creating Finite Element Models (FEM) using NASTRAN

Many factors must be considered when creating a finite element model (FEM) for NASTRAN, which is used to format output to ADAMS using superelements. These models are created using CATIA and PATRAN as pre-processors. The following list

outlines this process as adapted from Catelani {8}, and assumes that pre-loading of components are not considered. Techniques involving superelement analysis, which was outlined in Section 2.5.1 are utilized in this analysis.

- A single and unique FEM must be created for each and every component to be investigated as a flexible body.

- Boundary conditions, such as single point constraints (SPC's) must not be defined in the FEM. When conducting mode shape validation, loading conditions must be omitted. Constraints will be completely defined in ADAMS.

- Material properties must be assigned to the structural elements of the FEM.

- The external interface (master) nodes have to be defined in the structure. These are the nodes that will be used to constrain or apply forces to in the ADAMS model. All other nodes are internal to the superelement.

- It is not possible to redefine these interface nodes after the NASTRAN analysis has been run.

- It is not possible to apply loads or constraints to nodes in the ADAMS model to internal, non-interface nodes.

- It is important to only define interface nodes to FEM elements that have 6 degrees of freedom in most cases. These include CBEAM, CQUADR, CTRIAR, RBAR and RBE2 elements. To overcome this problem with degrees of freedom there are two options:

  - If a 3 DOF element is used, such as a solid element (3 DOF), an additional node can be created very close to the node of the element in question. These nodes can then be connected using an element such as an RBE2 element, and the newly created node can be made external, giving it 6 DOF.

  - The other alternative is to compensate for these DOF in ADAMS. For example, if the node of a solid element is made external and is to be fixed in ADAMS,

107

then the correct way to attach the element is to use a spherical joint in ADAMS, since solid element nodes only fix translational DOF.

### 4.6.5 Preparing FEM files for ADAMS Verification

ADAMS uses component modal synthesis (CMS) approach to represent the normal modes of a given part in a system. This process involves truncating the number of mode shapes represented in the system, which means normal modes that contain certain frequency bands will be lost. To confirm that the translation into ADAMS format was successful, the identical component is analyzed using NASTRAN for analysis, and then PATRAN for post processing. This test is also done to confirm that the constraints applied in ADAMS match those that would be applied in NASTRAN.

Two types of analysis are run: free-free modal analysis, and constrained mode analysis. Free-free analysis refers to the part being analyzed in free space, with no external loads applied, and no constraints enforced. Constrained mode analysis is the exact opposite, where the component is constrained as it would be in the ADAMS model. PATRAN is used to generate a .bdf file, which is solved using NASTRAN. NASTRAN outputs a .op2 file, for which the results can be viewed in PATRAN. Using these results, the modal frequencies and shapes are recorded so they can be compared to the ADAMS results as outlined in Section 4.7.8.

### 4.6.6 Preparing the NASTRAN Code

Once the model had been created using the appropriate pre-processor, a .bdf file is exported using PATRAN, using a normal modal analysis (SOL 103 in NASTRAN). This .bdf file is now manually edited, making the coding appropriate for translation into ADAMS. A sample NASTRAN code had been included in Appendix A for illustration and clarification purposes. Several steps are required in NASTRAN file creation process, as are outlined below.

108

- A special function, called a DMAP "alter" function, *mnfx.alt*, is used to drive the correct execution of the modal operations and the correct formatting of results for the conversion from NASTRAN to ADAMS. The alter function can either be included within the NASTRAN program, or can be referenced using an INCLUDE statement.

- Ensure that the DMAP function is correct for the software package and release.

- In the Case Control section, METHOD=10 is used. This is used to define the EIGRL card, which defines the eigenvalues calculation. This card is explained in later steps.

- The Bulk Control Section must contain the following PARAM commands:

  PARAM,FIXEDB, -1 (To avoid data recovery on the residual structure)

  PARAM,AUTOSPC,YES (To fix singularity issues in the stiffness matrix)

  PARAM,GRDPNT,0 (To debug mass matrix)

  PARAM,OLDSEQ,3

  PARAM,K6ROT,0 (Specifies stiffness to be added to the normal rotation for
  CQUAD4 and CTRIA3 elements)

- It is critical that the units are defined correctly using the DTI statement, exactly as they are in the ADAMS model. In the case of this study, the statement used was: DTI, UNITS,1,mgg, NEWTON, mm, SECOND.

- It is also important to note that the standard units statement in NASTRAN, WTMASS, is ignored when considering superelement analysis.

- Using the SESET (Superelement Set) command, all of the internal nodes must be defined, where all external points are to be omitted from this statement. This sets the DOF that will be used to represent the modes. Any node that is not included in the SESET statement will be treated as an external node. Alternatively, the CSUPEXT command can be used instead of the SESET command, which allows the declaration of external nodes.

  SESET, ID Super, ID Node, ID Node... (Define nodes one by one)

SESET, ID Super, ID Node, thru, ID Node (Define a consecutive list using THRU)

Or alternatively:

CSUPEXT, ID Super, Node, ID Node... (Define external nodes)

- Define the number of SPOINT (Scalar Points), which is equal to the number of mode

  shapes that are to be calculated for the model. This number must match the value

  defined for EIGRL in the next step.

  SPOINT, 1001, THRU, 1020

  Note: SPOINTS should be defined after the last grid point in the model to avoid

  confusion later on.

  The points must be unique, and must not be contained in the actual model itself.

- Define the EIGRL (Real Eigenvalue Extraction, Lanczos Method) statement, which

  defines the number of mode shapes to be used.

  EIGRL      10           20           0

  In this statement, the number 10 refers to the METHOD=10 statement as outlined

  above, and the 20 references the number of modes to be used in analysis.

With the .bdf edited, it can now be processed using NASTRAN. The output file, which is

in NASTRAN (.out) compact binary format, can be used for translation into ADAMS

after the files have been checked for fatal errors. A sample NASTRAN code had been

included in Appendix A for illustration and clarification purposes.

### 4.6.7 Verifying Mode Shapes and Frequencies in ADAMS

ADAMS/Flex toolkit is used in to convert files from NASTRAN (.out) to

ADAMS format (.mnf). A translator, which is part of the ADAMS/Flex package, is used

in the conversion process, and the default settings are maintained. The conversion

process is as simple as pressing a button in the ADAMS/Flex Toolkit. MDI {27} states

that a modal neutral file (MNF, .mnf) contains the following information:

110

- Geometry, which includes the location of nodes and their connectivity

- Nodal mass and inertia

- Mode shapes

- Generalized mass and stiffness for mode shapes

When the modal neutral file for the component is successfully created, it is ready to be inserted into the ADAMS program. This is done by choosing the Build - Flexible Body - ADAMS/Flex command. The damping ratio must be set to be zero when validating mode shapes and frequencies. Upon being inserted into the file, the component should be located in the exact same position as the equivalent rigid body component (Assuming the same global coordinate system is used and the unit convention is the same).

Although the flexible body representation may appear to look correct upon their insertion, a free-free analysis is performed to validate that the free-free (unconstrained) modes of the flexible body are correct. When validating the free-free modes, the damping ratio must be set to zero, otherwise ADAMS will choose a predefined value based on the frequency of the mode. Gravity should also be turned off unless it was accounted for in the NASTRAN model. To validate these free-free modes, the frequencies and the shapes of each mode are compared to the finite element model created in PATRAN as described in Section 4.7.5. Close correlation should be noted, otherwise there may be an issue with the number of normal modes being used or with the model itself. The first six modes will represent rigid body modes. Modes may differ slightly due to orthogonalization techniques used in the conversion process.

If the free-free mode validation is successful, the flexible body can be constrained in the ADAMS model. A constrained mode analysis can now be conducted. Constrained modes are validated using ADAMS/Linear. This involves conducting a static equilibrium calculation of the system, and once this is complete, the linear modes can be computed

111

and viewed. The modal frequencies and shapes can be compared for the constrained cases. Equivalent models must be created using NASTRAN, where the constraints used are created exactly as they are to be used in ADAMS. If a bushing element is used in ADAMS, an equivalent spring element must be used in NASTRAN (using the CELAS1 function). This is to verify that the constraints are applied correctly, and to determine if ADAMS is interpreting the degrees of freedom from the finite element models correctly. This is a very critical step when adding flexibe bodies to the system.

If deficiencies are found between results for either the free-free case or the constrained cases, likely causes include inadequate geometry meshes, or incorrect implementations of boundary conditions. Care must be taken to follow the methodologies in the above sections to assure that the NASTRAN files are created in a sound manner.

The mode shapes and frequencies must be in agreement before flexible body simulations can commence. The forces in the system must also be verified through a load path analysis to see if the loads transmitted to the flexible bodies are reasonable. This is done through a rigid body model validation. If the loads are unreasonable, the results for stress analysis and fatigue analysis will be irrelevant.

### 4.6.8 Modal Stress Recovery (MSR)

Once a modal analysis has been completed, the next step is to perform a modal stress recovery on the component. A modal stress recovery (MSR) is performed to calculate the stress and strain in a component(s), which is done using NASTRAN. For the stress and strain to be calculated on a certain component in ADAMS, specific coding must be inserted into the NASTRAN model to request these values. Kilroy {24} suggests that requesting modal stress and strain can increase the MNF file size by two or three times, which is why they are not requested initially while correlating mode shapes.

112

During the modal computation phase using NASTRAN, a stress component can be associated with each orthogonalized mode shape, which will allow the stress and stain to be computed based on modal deformation during a dynamic simulation in ADAMS. The following statements must be inserted into the case control section of the NASTRAN code that was created using the techniques from section 4.6.6:

- STRESS(PLOT)=ALL

- STRAIN(FIBRE, PLOT)=ALL

   These two functions, STRESS and STRAIN output the element stress and strain respectively. ALL means that the stress and strain for all elements will be output. The PLOT command dictates that the element stress for the requested set will be generated and placed in the binary file (.out), but the information will not be printed in a NASTRAN text file. The FIBRE command is required along with the STRAIN function when shell elements are used.

- GPSTRESS=ALL

- GPSTRAIN=ALL

   The commands GPSTRESS and GPSTRAIN request the grid point stresses for printing only. The ALL describer means that the stresses and strains are requested for all the VOLUME and SURFACE commands defined in the OUTPUT (POST) section as shown below.

- OUTPUT(POST) - This statement with the POST descriptor is required at the beginning of VOLUME and SURFACE command.

- SET 1=ALL - Defines a set of surface or volume elements to be used in the GPSTRESS and GPSTRAIN commands. Surfaces and volumes require separate SET commands, with unique identifiers.

- VOLUME 21 SET 1, DIRECT - This defines a volume for the calculation of grid point stresses or strains. The SET identifier references the SET command identified

113

above, and the DIRECT command requests the direct, mean pressure and von Mises equivalent stresses to be calculated. The number 21 simply refers to a volume identification number as does the number 22 in the SURFACE command.

- SURFACE 22 SET 2, FIBRE Z1, NORMAL Z - This defines a surface for the calculation of grid point stresses or strains. FIBRE Z1 means that that the stress is calculated at the back face of the shell element (-thickness/2). Other options include Z2 (frontal face), and MID which is the midplane of the shell element. NORMAL Z refers to the direction of the axis or surface normal.

Once this coding has been inserted, a normal modes solution can be solved. The NASTRAN .out file is then transferred into ADAMS in the same manner as described above in Section 4.6.7. To verify that the modal stress recovery has been performed correctly, a simple force can be applied to the component in ADAMS, and the same model can be created using NASTRAN. The resulting stress output from both files, as well as the component displacement should correlate closely between the two programs. If these results correlate closely, the component is ready to be inserted into a current model assembly as a flexible body. ADAMS/Durability allows the stress and strain contours to be plotted on the flexibly bodies while viewing dynamic simulations in ADAMS/Postprocessor. Stress, strain and deformations can be plotted for each node on the flexible body.

### 4.6.9 Limitations of ADAMS/FLEX

There are several limitations when using ADAMS flex that must be noted.

- Bushings, as well as rotational spring dampers (torsional), cannot be connected directly to a flexible element in ADAMS, as they are not yet directly supported. A single component torque cannot be directly applied to a flexible body either. Many of the components explored in the current research use bushing, requiring an alternative

114

technique to be used. To overcome these issues, a massless link, also referred to as a "dummy" part in ADAMS, is used to connect elements such as a bushings to the flexible body. A massless link is part that has zero or insignificant mass. The process in creating these massless links is presented in Section 4.7.10 in further detail.

- Only one SURFACE and/or VOLUME card is allowed per NASTRAN model.

- Only one superelement model can be used per NASTRAN model.

- When using ADAMS, flexible body deformation is a linear combination of modal deformation shapes. Care should be taken when modeling high deformation. To overcome deficiencies when modeling high deformation, it may be beneficial to break the component into several flexibly bodies which can be assembled in ADAMS.

## 4.6.10 Analysis of Flexible Vehicle Components using ADAMS

Flexible bodies are added in place of a rigid bodies one at a time. Each time a component is inserted it should be verified independently. Several flexible bodies were added to the ADAMS model being investigated in this research. The focus was placed upon the rear suspension system, as this was the area of interest pertaining to durability. The main components that were represented as flexible bodies include the 3-link upper and lower control arms, as well as the rear stabilizer bar.

All of these components started off as rigid body CATIA models. The CATIA models were modified and the geometry was altered as necessary, depending on how the components were loaded or constrained. The first step in the analysis was determining the boundary conditions on the parts themselves, how to define constraints that are necessary in attaching them to other bodies in ADAMS.

The lower control arms use four separate attachment points, including two for the bushing mounting locations in the front and rear of the arms, and two points that are used to connect the stabilizer bar. The control arms were then brought into PATRAN, where

115

they were meshed accordingly using tetrahedral elements, and then RBE2 elements were added to represent the bushings at each end of the control arms, and the connection points to the stabilizer bar.

NASTRAN files were created, one for the ADAMS model (.out) and one for the PATRAN model (.op2) for correlation purposes. The PATRAN file uses fixed single point constraints (SPC) at all of the attachment points, which represents how the lower control arms are attached to other bodies in the ADAMS model. The mode shapes and frequencies were observed in PATRAN and their properties were noted for comparison to the ADAMS model in the steps to follow. The ADAMS file had the appropriate modification based on the steps described in earlier section, and had the SPC's removed. The flexible body representing the lower control arm was opened on its own in ADAMS, constraints were applied as shown in Figure 4.15. In this diagram, a close-up is shown of the area that is attached to the stabilizer bar. The RBE2 elements are used to simulate the bolt being in place, as well as the contact between the two components. The mode shapes are confirmed using the techniques presented in Section 4.6.7.

The control arm was inserted into the full vehicle model by replacing the rigid body, and adding constraints to the existing model. The flexible body file (MNF file) was used for both the left and right control arms, as they are identical parts. The original file was created for the left side. In order to make the right side control arm flexible, the flexible body for the left side is imported into ADAMS and simply repositioned to the other side. This is a great benefit to using the superelement technique, because if another vehicle platform uses this part (as more and more manufacturers are using parts on several vehicles), it can be imported and repositioned in additional models if they exist.

116
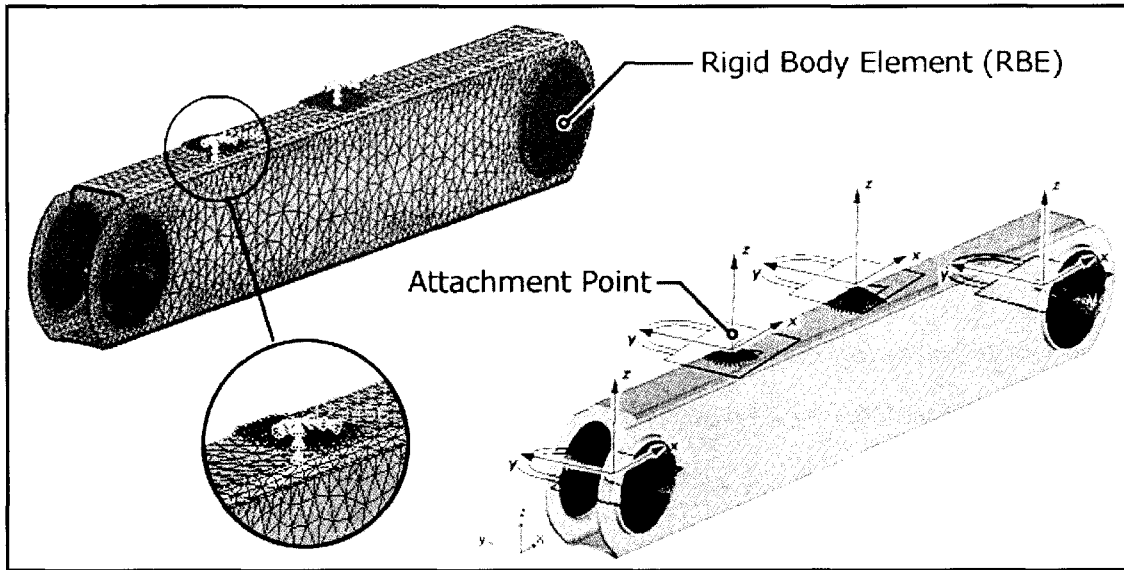
**Figure 4.15**: Flexible rear lower control shown in PATRAN on the left, and ADAMS on the right. Note the rigid body element representation is also shown in ADAMS, and that constraints are in place (where "padlocks" denote fixed joints). The lower control arm is attached to the full vehicle model in the same manner.

The geometry modification and meshing for the upper control arm was done in the same manner as used on the lower control arms. Any small holes in non-critical areas were removed, as were smaller fillets, in order to avoid having an overly fine mesh. The upper control arm uses three attachment points: one at the ball joint interface on the rear axle, and the other two are located at the interface to the body of the vehicle. RBE2 elements were used to represent the ball joint and bushing presence in the model. The NASTRAN coding was produced in the same manner as with the lower control arms, and the flexible bodies were inserted into model upon correlation and verification. An illustration of the upper control arm is shown in both PATRAN and ADAMS model in Figure 4.16. Ribs located on the bottom surface were retained as they help to stiffen the component (increase modal frequency values).

117
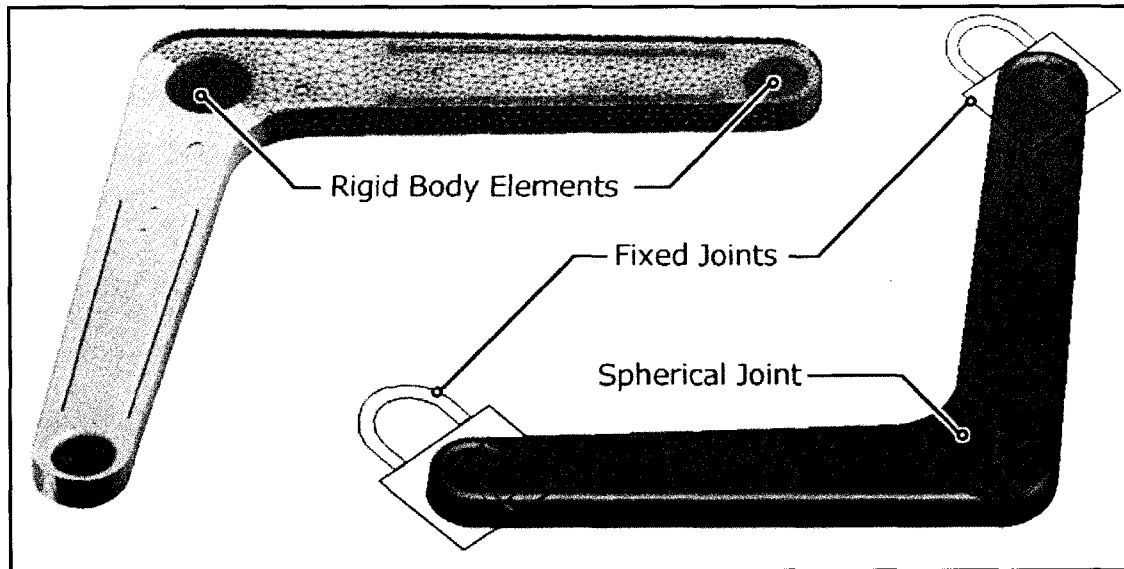
**Figure 4.16**: Flexible rear upper control arm shown in PATRAN on the left, and in the ADAMS environment on the right. Half of the mesh is shown on the PATRAN model to show the degree of detail. Note the constraints shown in the ADAMS model. The markers on the ADAMS model represent the attachment points of the flexible body.

Finally, the stabilizer bar was added to the model as a flexible body. This was done in attempt to reduce any stress concentrations in the lower control arm when using the rigid stabilizer bar, and also to give a better representation of the stabilizer bar operation itself (rather than simply using a torsional spring). Four attachment points were used created, that represent where the bar is bolted to the control arms on each side. Figure 4.17 shows the stabilizer bar model in ADAMS with the constraints added. Notice the end portion of the bar that is expanded, showing RBE allocation along the surface. The top of the bar is constrained as shown to represent the head of the bolt, and the lower edge is constrained to represent the contact between the surfaces.

118
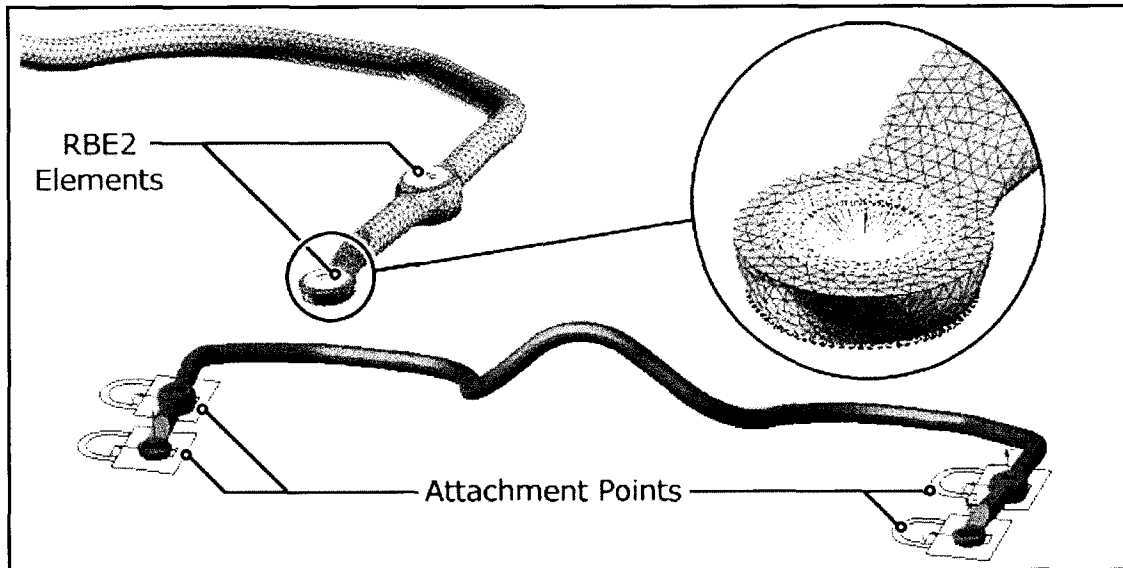
**Figure 4.17**: Flexible body representation of the rear stabilizer bar shown in PATRAN on the top, and ADAMS on the bottom. Four fixed joints are used to represent where the bar is bolted to the control arm. RBE2 elements are used to connect the nodes of the model near the near the attachment point to represent the constraints placed on the component by the bolts, as well as the contact between the bar and the lower control arm.

All of these flexible components can be used in ADAMS individually, or as a complete system of flexible bodies as shown in Figure 4.18. When attaching flexible bodies to one another, certain procedures are required, depending on the constraints being used. Fixing one flexible body to another requires that either a massless link be used, where the attachment points for each flexible body are connected to this link, or the 2 bodies - 2 locations option be used with the fixed joint itself. The process of adding massless links to a model is presented in Section 4.7.10. Numerical errors in ADAMS will result if a default 2 bodies - 1 location option is used when placing a fixed joint on the model.

119
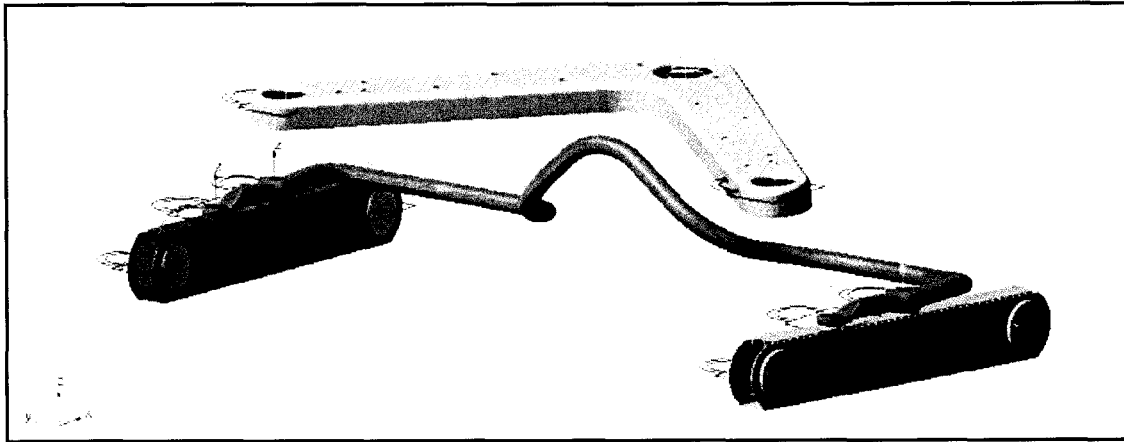
**Figure 4.18**: Rear suspension flexible body components as shown in ADAMS. The constraints show are the constraints used to attach these bodies to the rigid bodies in the existing vehicle model. The fixed joints fix the components to one another and not necessarily to the ground, as this allows them to take on relative movements. In the case of the fixed joints at bushing locations, this fixes the flexible bodies to the massless links.

## 4.6.11 Flexible Body Pointers

When adding a flexible body in place of a rigid body that contains bushings, there are a few steps that must be followed. There are also techniques that are used for which the parts can be changed without having to re-define the bushings and joints all over again which is time consuming. To start, a link of any size, which will become a "massless" link as described in Section 4.7.9, should be created near where the bushing interface is located (Exact position is not critical). Add a fixed joint attaching the external node (point where the bushing is defined) on the flexible body to the link created in the previous step. Next, display bushing information using ADAMS to determine which markers the bushing references. Rename the marker that the bushing attaches to the rigid body with, and change the name from the rigid body reference to the massless link that was just created. To make the link "massless", simply remove the geometry of the link, since ADAMS calculates the mass and inertia properties using the part geometry.

120

One item to note is that ADAMS uses modal information to determine the deflection of a flexible body, meaning the computation time is completely independent of the number of nodes on the body. Playback time and fringe plot observations will be affected by the number of nodes since all of the nodes are still referenced to the flexible body, and modal deformations in particular. Analysis using ADAMS/Post takes considerably longer to do when flexible bodies are used, and this time increases with the complexity of the model.

Rather than manually changing back and fourth between rigid and flexible bodies, certain inertia invariants, as described in Section 3.3.8, can be turned on or off to represent rigid or flexible behavior of a component when using flexible bodies. While simulation times may be greater due to the presence of the flexible body, it can save time and space by not having to switch between rigid and flexible bodies manually.

## 4.7 Process Automation

With literally hundreds of elements contained within this ADAMS model, it becomes increasingly difficult to rapidly change certain parameters in order to perform correlation studies and sensitivity analysis. Several tools have been created as part of the present research to assist in running simulations, serving to further speed up the process of computer analysis. Repetitive tasks have been addressed, and in many cases, computer coding has been generated to fully automate these tasks. A custom menu has been created specifically for this project and can be accessed just like any other menu on the header of the ADAMS/View program. Using this "SUV" menu as is illustrated in Figure 4.19, many different custom made functions can be accessed as will be discussed in the following sections. This makes simulation of the model user friendly, and allows simulation results to be analyzed much faster.

121

```
Help  SUV  Durability
              Edit              ▶
              Export            ▶
              Suspension        ▶   3-Link Rear
              Linear Modes          4-Link Rear
              Road Inputs       ▶
              Visualization     ▶
              View              ▶
```
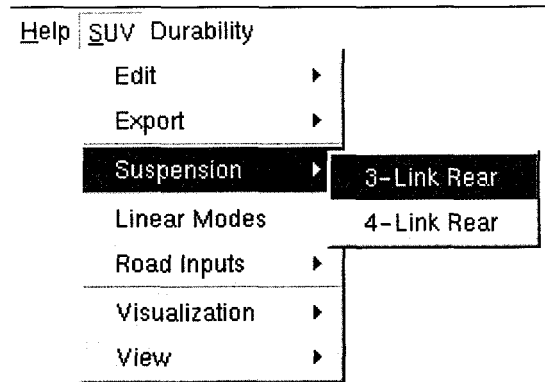
**Figure 4.19**: Illustration of the interactive menu created as part of the present research for navigating functions specifically created for the simulation of this vehicle. The menu allows for quick access to the bushing and input editor, file output menu, road input selection menu, and for changing the visual settings. Shown is the submenu for changing the rear suspension configuration.

### 4.7.1 Component Change Capability

It is very common in pre-production, and in the production phase to have several different configurations for components under consideration by designers. To execute a change such as a full rear suspension system with this project, would require prototypes to be built, new bushings to be developed, and would require the vehicle to be run through a durability cycle once again. It is easy to see that this would be time consuming, as well as being very costly, especially when the end result shows that the change actually has negative effects.

A menu in ADAMS has been created by the author that allows the user to rapidly change suspension configurations in literally seconds. This includes changing the physical links themselves and their related mass, inertia, and centre of gravity positions, as well as altering all of the bushing properties by simply selecting an option in the menu. A "group" was created in ADAMS for each suspension configuration, and coding was written to first activate the group containing the assembly to be analyzed, while deactivating any others. This way only one system can be active at a time. From this, the

122

visibility of the components is changed, so that only the suspension in consideration is visible on the screen. Using this philosophy, as many groupings of sub-assemblies can be added to the model as needed. The ADAMS menu allows these sub-systems to be activated and deactivated with ease, further reducing the simulation time, and allowing many more what-if scenarios to be investigated than would be physically possible.

Items were also placed on the menu to allow for the flexible bodies used in the rear suspension to be turned on or off. This allows simulations to be conducted with ease for rigid or flexible bodies, with the user only having to open one ADAMS model.

### 4.7.2 Road Change Capability

In performing durability and fatigue analysis, it is critical to expose the vehicle to all types of terrain, in order to exhibit many types of damaging input of varying frequency and amplitude to the vehicle. In order to do this, certain elements have to be activated and deactivated, recalling that each road course requires 12 separate inputs. Macros were created in order to overcome this, allowing the user to switch the road surfaces input to the model very rapidly. A total of eight roads are available for use in this model. This further allows for quick generation of stress-history plots to be exported to fatigue analysis.

Provisions were also made to remove all of the road inputs, allowing bushings to be added at the spindles to replicate tires. This is useful for performing linear analysis of the vehicle system, as well as for measuring the corner weights of the vehicle. This is also accessible from the aforementioned menu structure.

### 4.7.3 Input Parameter Dialog Box

Dialog boxes were also created for various input parameters such as for scaling inputs to the model, as well as scaling the mass and inertia of the full vehicle. Editing many of these values requires a great deal of experience using ADAMS, which limits

123

simulations to be conducted only by those who are well acquainted with the software suite. Having input editor capabilities like these allows users with less experience in ADAMS to effectively conduct complex simulations with ease. This further enhances the robustness of the computer model by making model input errors less likely to occur.

### 4.7.4 Bushing Parameter Dialog Box

Assessing the behavior of the model when certain component parameters are changed is the basis of sensitivity analysis. Bushings have proven to be among the most influential components on frequency outputs, and certain output parameters have shown to be quite sensitive to changes in stiffness and damping. The process of scaling bushings in the model is further complicated by the fact that each bushing requires 12 different values to characterize both stiffness and damping. In order to scale up bushing values, each of these values must be changed for each of the more than thirty bushings contained within the computer model. This is quite time consuming, and further increases the chances of introducing human error into the system. Using ADAMS dialog box creator, an interface was created as can be seen in Figure 4.20.

124

Front Suspension

Scaling Factors

| | Trans. | Rotate | Modify Values | | | |
|---|---|---|---|---|---|---|
| Upper Control Arms | 1.0 | 1.0 | LF | LR | RF | RR |
| Lower Control Arms | 1.0 | 1.0 | LF | LR | RF | RR |
| End Links | 1.0 | 1.0 | L1 | L2 | R1 | R2 |
| Clevis | 1.0 | 1.0 | L | R | | |

Rear Suspension

⊙ 3 Link  ○ 4 Link

| | Trans. | Rotate | | |
|---|---|---|---|---|
| Lower Control Arms: Body | 1.0 | 1.0 | L | R |
| Axle | 1.0 | 1.0 | L | R |
| Upper Control Arms: Body | 1.0 | 1.0 | L | R |

Change Multiple Scaling Factors

Change Scaling Factors  |1.0

☑ Front  ☑ Rear  ☑ Translational  ☑ Rotational

| OK | Apply | Cancel |

**Figure 4.20**: The bushing editor created within ADAMS environment used to perform sensitivity analysis of bushings fast and efficiently. All bushing parameters can be quickly scaled or edited with ease by entering the scale factors in the appropriate input boxes. Once "OK" or "Apply" is selected, the bushings are automatically scaled to the appropriate values.

This interface allows all of the bushings to be scaled from a central location, and they can be edited as necessary by depressing the appropriate buttons on the right hand side of the panel. All of the bushings can be scaled by using the input box at the bottom of the interface, requiring only one number to be input and a button to be depressed to scale every bushing in the model.

125

### 4.7.5 Body Visual Representation

In order to study the behavior of the body structure, particularly during linear analysis, the body structure was represented using shell files in ADAMS. Since the body of the vehicle remains a rigid entity, its main function in this analysis is to act as a visual representation. It can also be used to position accelerometers for measuring body acceleration at specific locations. The body surfaces were assembled using CATIA and ENOVIAvpm, and were imported into ADAMS as shell files. These shell files were referenced to the body in the ADAMS model. The body representation, as well as a visual representation of the tires and wheels of the vehicle are easily turned on and off through the navigational menu. Body structures carry proprietary rights and are considered trade secrets of the corporation, and subsequently will not be recreated in the body of this report.

### 4.7.6 Outputting Data in RPC III and DAC Output Formats

To facilitate external analysis of the measured data using nCode software, critical parameters of the vehicle's response are output to either DAC or RPC III files. A dialog box was created for this purpose that allows the user to select which virtual instrument data that they wish to export to a file, as shown in Figure 4.21. Once the appropriate entities have been checking off, they are automatically output to separate DAC files once "OK" or "Apply" is selected.

126
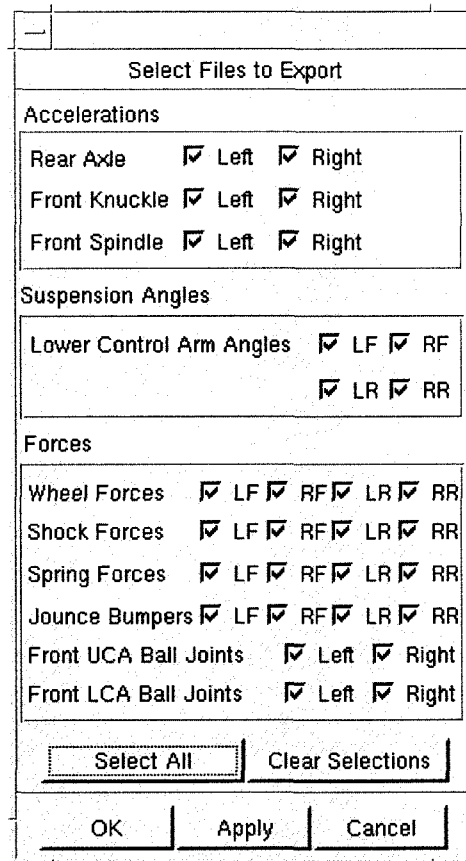
**Figure 4.21**: Interface created for automated output of DAC files from the ADAMS environment. This allows for more rapid data output with minimal effort. It also prepares the data and places it in an appropriate folder so that batch processing can be executed.

### 4.7.7 Batch File Processing

In Chapter 2, various software suites produced by nCode software were highlighted and their applications outlined. Batch files were created that reference the various nCode modules in order to analyze large datasets, and to automate repetitive processes. Text files were created using UNIX scripting, and from these, executable files were created that could be run from a command prompt. Three main files were created, as will be discussed briefly below.

The *file2si* function was created to modify the units of time history data from imperial to SI. A majority of the time history responses received from the RTS machine

127

were in imperial units. Literally hundreds of DAC files required conversion, which made automation necessary. This is done by referencing the arithmetic (MART) module from nCode within the batch commands.

The *time2psd* function was created to rapidly convert datasets from time to frequency domain using output DAC files that were created in ADAMS. This program takes all files in a certain directory and converts them to PSD data using a batch command that calls the nCode auto spectral density (MASD) function. The resulting PSD files are placed in a new folder. This program was also used to convert the raw and edited datasets once the units had been changed using the *file2si* command.

The *plot* function is used to overlay time and frequency domain datasets quickly and efficiently. The user is prompted to select an output file to plot from a list of over 30 possible plots. When a file is selected, the program then prompts the user whether they want to plot an ADAMS comparison (to compare separate ADAMS simulations) or to plot ADAMS results against physical data. Once the file and plotting selection have been made, the program executes the multi-file display (MMFD) module from nCode, and overlays all of the datasets on one plot. The scales are automatically adjusted, and the type of dataset is listed in the command window, which dictates whether the data is raw, edited, remote, or virtual simulation results. The PSD plots that are presented in the results section in Chapter 5 are generated using this function.

128

# CHAPTER 5  MODEL SIMULATION AND VALIDATION / RESULTS

## 5.0 General

This chapter presents the findings of the conducted analysis for this vehicle using virtual simulation. Model validation techniques and results are explained in detail. Different input configurations are highlighted including combinations of force and displacement input. Suspension configuration comparisons are made, and the effects of adding flexible bodies into the model are outlined.

## 5.1 Model Input Methods

Four unique methods exist in applying input to the virtual model. The possible input configurations to the model include:

- Vertical Displacement, Longitudinal Force, Lateral Force
- Vertical Displacement, Longitudinal Displacement, Lateral Force
- Vertical Displacement, Longitudinal Force, Lateral Displacement
- Vertical Displacement, Longitudinal Displacement, Lateral Displacement

129

Vertical displacement was used in all cases, as this was shown to be an effective methods according to Ferry {16}. These were also used because no opposing vertical displacements exist, which would be the case with the lateral and longitudinal directions.

All of the above input schemes were attempted, with the first scheme giving the most favorable results. This configuration will be discussed in detail in the sections to follow as a result. The final input method, which uses full displacements, was primarily used to drive the virtual test rig as is described in Section 5.6.2. Simulations involving displacement input in the lateral and/or longitudinal direction were found to give the most realistic visual representation, but also tended to over-estimate the forces in the model. This is undesirable especially when stress and fatigue analysis is involved. The objective was to closely correlate the forces in the components, in order to replicate the stress and strain in these components.

### 5.1.1 Displacement Input

Displacements are fixed in time, meaning that a body driven by displacement must be in a given position at a prescribed time. Each displacement input that is used as model input removes one degree of freedom from the system. Recalling that each rigid body has three translational degrees of freedom, three separate unique displacements can be used as input for a rigid body. If more than three are used, or if these three are not applied in mutually perpendicular directions, the model will "lock-up" in ADAMS. Lock-up occurs when there is no mathematical solution in ADAMS, which will cause a simulation to terminate.

Several advantages and disadvantages were found when using displacement input are as follows, where the comparison is made with respect to using force input:

*Advantages*

- The position of a component in the prescribed direction is fixed in time.

130

- Initial conditions do not affect motion in the direction of displacement input since displacement is fixed in time.

- Component accelerations correlate with less difficulty.

*Disadvantages*

- Constrained body motions tend to over-estimate body forces, especially when opposing displacements are used (as with lateral and longitudinal directions).

- Force elements "absorb" deflections creating unrealistically high forces in the components when opposing displacements are used, especially when only rigid bodies are implemented in the model.

- The steering system is very sensitive to displacement input. Using too high a stiffness for the springs (restricting the system from moving) will cause the simulation to fail due to lock-up.

- Displacements can be difficult to measure in the physical model, making virtual model inputs difficult to acquire.

### 5.1.2 Force Input

Force input can also be used to drive the virtual model, which allows an alternative to displacement input. Unlike displacement input, force input does not remove degrees of freedom from the system. Forces are applied moving with the body to a certain marker. As the model moves, the force is applied in a direction relative to the vehicle, not to the ground. The forces used for model input come directly from the load cell output on the physical testing apparatus, as well as from the wheel force transducers (WFT). When using force input, stiffness and damping were added to the model at each corner, which controlled the "drift" of the model. Without the stiffness and damping, the model would tend to translate and yaw off into space, since there are no external forces

131

resisting or constraining the movement of the vehicle. Several advantages and disadvantages were found when using force input as follows:

*Advantages*:

- Unconstrained body motions avoid the over-estimation of body forces.

- Component forces correlate with less difficulty.

- Avoids model lock-up in ADAMS, which results in a model that is more stable.

*Disadvantages*

- Model tends to drift off into space (unrealistic visualization).

- Model requires stiffness and damping to be applied at each corner to prevent model drift. This can affect the dynamic behavior of the system, depending on the parameters used.

- If sensor coordinate systems are defined with respect to the global system, the measured responses will also drift proportionally.

- Difficult to determine absolute displacement of spindles on the RTS rig as the model drifts.

- Sensitive to initial conditions (since the position of the body is not fixed in time).

- Component accelerations are more difficult to correlate, and are very sensitive to the flexibility of the part, which is often not considered.

## 5.2 Road Test Simulator Concerns

The road test simulator functions based on applying input to computer controlled hydraulic actuators to excite a vehicle. The system itself is very complex in operation, and incorporates a network of computer controllers, sensors, and hydraulic systems. Many of the following issues were also reported by Ferry {13}, who notes several additional discrepancies.

132

The drivetrain and powertrain are not operational during the durability testing on the RTS machines. This means any forces and/or torques that would normally be induced on the vehicle, would not be present during laboratory testing. The machines must compensate for lateral weight shift due to drive torque, as Gillespie {17} notes this is predominant in solid axle rear-drive vehicles. This drive torque will also transfer forces to the body through the engine/transmission body mounts. Drivetrain and powertrain operation can also act to dampen accelerations that would otherwise be present in the system. Gillespie {17} explains that drivetrain and powertrain systems are often designed to provide a vertical resonance frequency near the front wheel hop frequency, which he states is in the range of 12-15 Hz.

Several other factors arise in relation to the vehicle being tested on a proving ground. Aerodynamic effects, which tend to apply a pitching moment to a vehicle, are not present. Other factors, such as temperature and humidity can also play large rolls in the behavior of components. The atmospheric conditions that the test vehicle is exposed to at a proving ground can be quite different than the environment experienced in a laboratory. Bushings and especially dampers tend to heat up during usage, which can act to affect their dynamic behavior. Elastometric components in general can be quite sensitive to these conditions.

Numerous issues arise when attempting to use displacement input to the virtual model using local responses provided by the RPC software package. The displacements that are ideal to use for the virtual model are those measured at the spindle of the vehicle. The problem that arises with this is that the physical displacement is measured at the hydraulic actuators, and a mathematical relation is used to approximate this displacement at the spindles using the rig's geometry. This relation is only an approximation, since there is coupling of the motions in each direction. The vertical direction is the least affected. As discussed earlier, to further complicate matters, the exact displacement at

133

the spindles is unknown due to the measurement techniques used by the MTS machine. This acts to change the displacement into the system, which further affects the recorded forces and accelerations. The greatest problems occur in the lateral direction, which is shown in Figure 5.1.
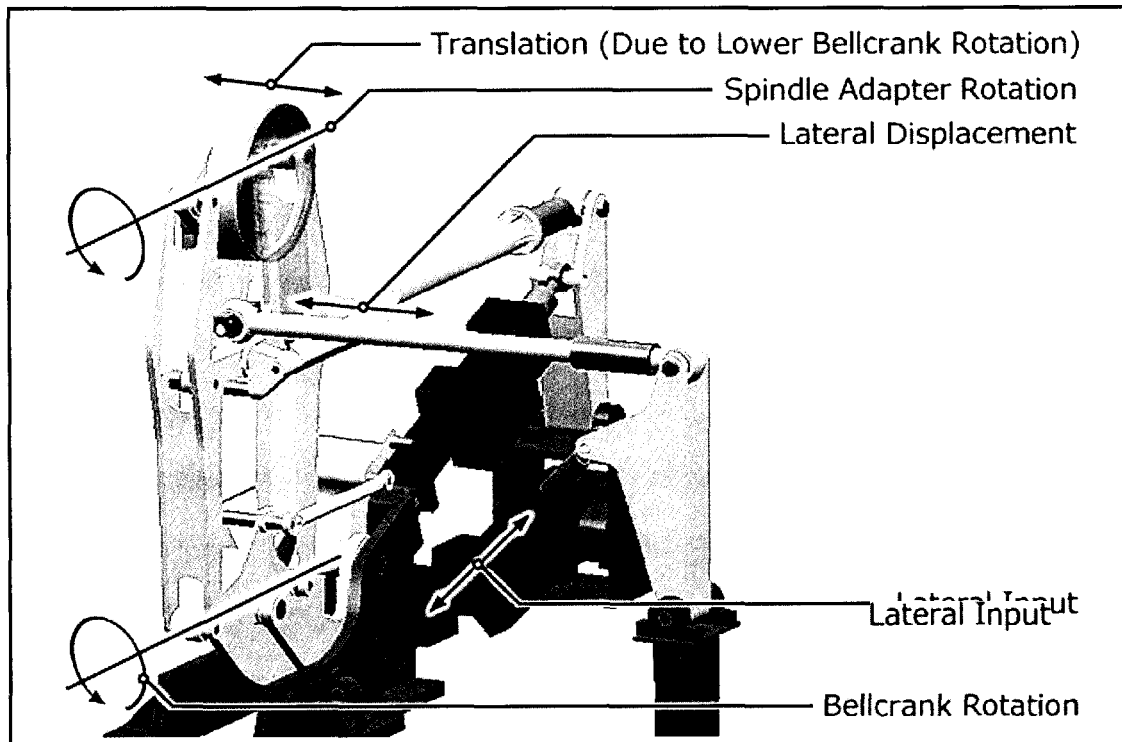


**Figure 5.1**: CATIA drawing of the MTS 329 RTS machine, showing the transmission of motions in the lateral direction. The lateral motion of the simulator is transmitted into the vehicle through a combination of vertical strut translation (due to the rotation about the bellcrank) and a rotation of the spindle adapter. Partial transparency has been added to the spindle adapter in this illustration.

The lateral direction is the most susceptible to errors in using displacement as an input. Figure 5.1 shows the front profile of one corner of an MTS 329 RTS machine. The lateral input is applied approximately to the tire patch of the vehicle. As the lateral displacement is input, its motion is transmitted into the machine as a translation of the vehicle laterally (due to the rotation about the bellcrank), and a rotation of the vehicle spindle itself. Independent and solid axle suspensions are both susceptible to this movement, with the independent suspension tending to be more sensitive to the rotation.

134

This relative movement depends on the stiffness of the components, the stiffness of the bushings on the vehicle, and on the rig itself. The use of further instrumentation, including the absolute displacement and rotation of the spindle adapter may provide a means of driving the virtual model in the lateral direction. The usage of an MTS 329LT 6 DOF machine may allow these movements to be better characterized, as is documented in Section 6.3 as future work.

## 5.3 Model Correlation

The most important phase of this research project is in the correlation of the computer model. This confirms whether or not the virtual model behaves similarly to the physical vehicle. For every relevant channel that was measured on the RTS machine, there was an equivalent virtual sensor placed on the ADAMS model. Two main types of correlation were performed. Static validation is used to confirm that the mass of the parts are correct, as well as their relative weight distribution on the vehicle. Dynamic validation involves simulating a vehicle over a certain road course and adjusting specific input and component properties, to test their sensitivity, as well as to tune the outputs to the desired responses.

Initial simulations showed that the vertical movements of the vehicle are not very sensitive to longitudinal and lateral input methods and vise versa. Preliminary results indicated the position at which the inputs are applied affected the vertical movement of the independent front suspension quite significantly. The lateral input was applied at approximately the tire patch (below the spindle rotation axis), which is shown in Figure 5.1. The reason that this made a significant difference is that this front suspension configuration is able to rotate about a longitudinal axis. This would not have been the case if the front suspension were a solid axle, as simulations showed that the rear axle

135

assembly was not very sensitive to the position of the lateral input. This is because the entire rear axle was treated as a rigid entity.

The results shown in the following sections use vertical displacements, longitudinal forces, and lateral forces input, unless otherwise noted. The vertical displacement and the lateral force input were taken from the local responses from the RTS rig. The longitudinal force input was taken from the WFT output from the remote responses measured on the vehicle. In the correlation plots to follow, the desired response is the data measured at the proving ground, the remote response is the information recorded during testing on the RTS machine, and the ADAMS model refers to the virtual simulation results. The results presented were "normalized" by dividing each value by the highest magnitude in each separate plot. This was done to avoid revealing any confidential information, while at the same time allowing for relative comparisons to be made between ADAMS and physical test data.

An illustration of the ADAMS model showing the location of the inputs to the system can be seen in Figure 5.2, which shows the sensor locations on the vehicle in addition. Bushings were added at all four corners as shown in this diagram, to stabilize the motion of the vehicle model during simulations. These act to resist the model from translating excessively in the longitudinal and lateral directions, and resist yawing about the vertical z axis. These bushings have stiffness and damping added in the lateral and longitudinal directions which can be edited using dialog boxes that were created in ADAMS for the purpose of this project. These values were adjusted by using trial and error approaches. Damping was not required in the vertical direction, as the model was driven using displacement input. Ferry {13} also presented a similar method for constraining the motion of the vehicle. Figure 5.2 also shows the displacement input as illustrated by the blue colored arrows, while the longitudinal and lateral forces are shown with white colored arrows.

136

| Virtual Model Inputs | Virtual Instrumentation | Force Transducers |
|---|---|---|
| ⬆ Displacement | Accelerometers | 5. LCA Ball Joint |
| ⇧ Force | 1. Steering Knuckle | 6. UCA Ball Joint |
| | 2. Lower Control Arm | 7. Jounce Bumpers |
| | 3. Rear Axle | 8. Shock Absorbers |
| | | 9. Springs |
| Stabilizing Bushings | RVDT's | 10. WFT's |
| | 4. LCA Angles | 11. LCA Axial Forces |
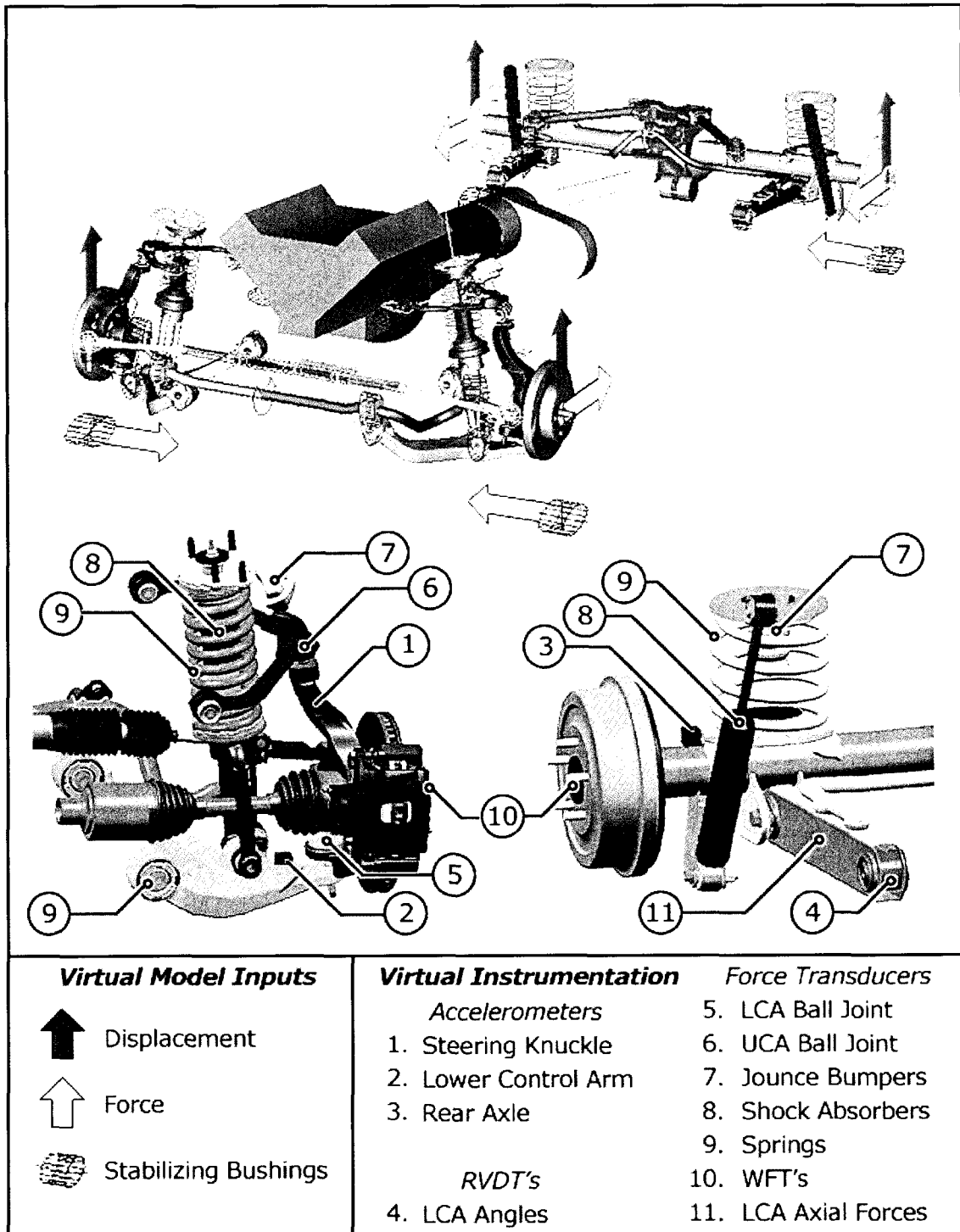
**Figure 5.2**: Illustration of the ADAMS virtual model as well as calibration sensor locations on the vehicle. The top illustration was produced in ADAMS and shows the locations of the inputs to the system. The lower diagrams are from CATIA and show the actual location of the sensors on front and rear suspensions of the vehicle. These sensor channels were measured on the proving ground as well as on the virtual model.

137

### 5.3.1 Static Validation

Corner weight analysis was done on the ADAMS model to confirm that the mass and centre of gravity properties are correct in the model. This also confirms that the weight distribution is correct, which also confirms that the centre of gravities for the components are in the correct locations. In order to do this, bushings were placed at all four corners and were given stiffness and damping properties similar to actual tries. The model was simulated to reach its equilibrium state at the FRL rating, and the vertical forces on the bushings were measured. At the proving ground and at the VIMF facility, scales are placed under the vehicle to measure the weight at each corner. With these results, the weight distribution of the vehicle can be calculated. Results confirmed that the mass of the virtual vehicle reflected that of the actual vehicle at the VIMF and proving ground facilities. The steady state response of the system can be seen in Figure 5.3. These are the corner weights without the weight of the tires at each corner.
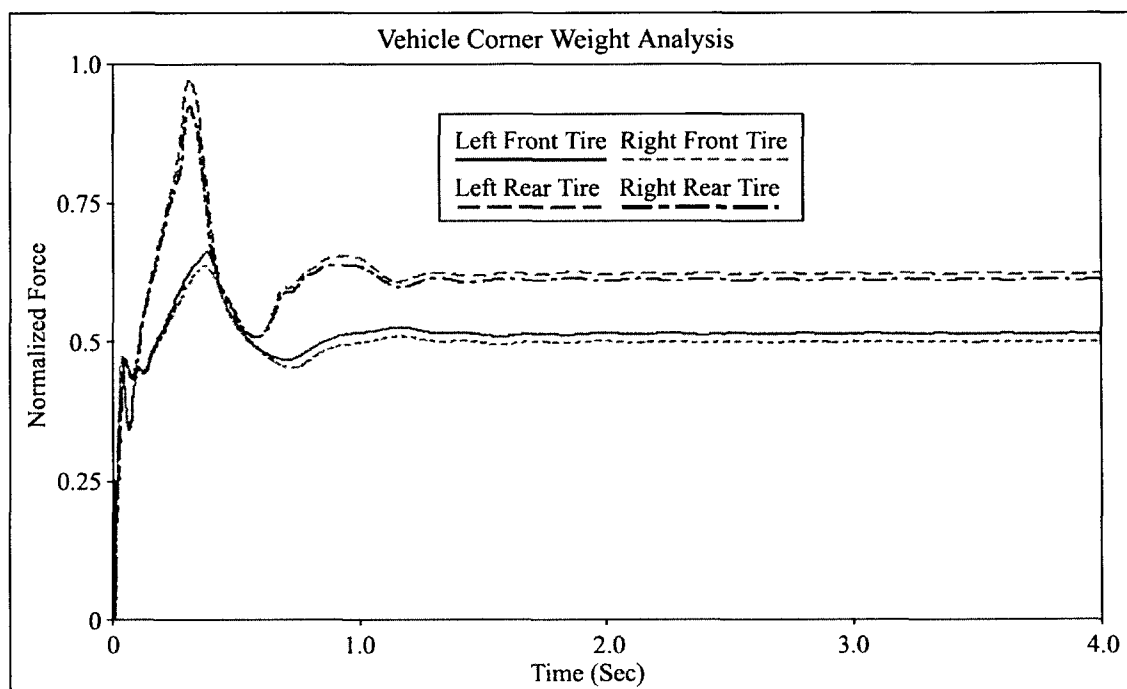


**Figure 5.3**: Normalized vehicle corner weight analysis at full rated load (FRL). Both the vehicle weight and weight distribution correlate well. The initial overshoot is due to the fact that the model starts out at curb position and sinks to full rated load and settles to equilibrium.

138

### 5.3.2 Dynamic Validation

The road course that was known to cause the most damage to vehicles was chosen as input to allow the critical frequencies as well as amplitudes to be experienced by the vehicle system. A simulation time of 50 seconds is used, which was chosen based on the capabilities of the computer system, and the requirements of the model. A sampling rate of 409.6 Hz is implemented, such that the time steps match the resolution used in the physical testing. The inputs to the model use this resolution and instabilities in interpolation can result if a smaller amount of time steps are used due to the higher frequency content in the signals. The simulation results were correlated by comparing the time history data output from physical tests to virtual tests. Data was compared in the time domain and in the frequency domain where applicable.

The responses were converted from the time domain to the frequency domain using nCode's MASD program which is executed using used defined batch codes as described in section 4.7.7. This program converts the signal using a Fast Fourier Transform (FFT), and also allows the data to be presented as power spectral density (PSD) plot. Documentation from nCode {32} states that any periodic function can be expressed as a summation of a number of sinusoidal waves of varying frequency, amplitude and phase. An FFT is used to express each individual sinusoidal wave as a spike in the frequency domain, and as the difference in frequencies between them tends to zero, these spikes tend to merge into a continuous function. A PSD plot is obtained by taking the modulus squared of the FFT, which acts to highlight the amplitude of the frequency content within a signal.

ADAMS/View post-processor is used for overlaying and comparing the data in the time domain, while the MMFD module within nCode's software suite is used to overlay data in the frequency domain for correlation purposes. The plots shown in the following sections are shown as results from opposite corners of the vehicle. This was

139

done to give a representation of data from both sides of the vehicle from front to back, as similar results were shown for both sides of the vehicle in the front and rear.

### 5.3.2.1 Vibration Modes Analysis

Linear modes of the vehicle were analyzed to determine the ride characteristics of the vehicle as an additional means of correlation. Linear modes represent the mode shapes and the natural frequencies of the components as a system. This was performed to determine whether the movements of the rigid vehicle model compared to that of published expected values. Bushings were placed at the spindles to simulate an actual tire being in place, and were coupled to the ground. Approximate values for tire stiffness were used as the bushing parameters. The critical vibration modes are shown in Table 5.1 shown below for the three link rear suspension.

| Critical Vibration Modes | |
|---|---|
| Linear Mode Description | Frequency (Hz) |
| Front Wheel Hop | 14.43 |
| Rear Wheel Hop | 10.87 |
| Body Roll | 2.28 |
| Body Pitch (about front) | 1.37 |
| Body Pitch (about rear) | 1.12 |
| Engine/transmission vertical | 14.92 |

**Table 5.1**: Listing of several predominate linear mode frequencies of the vehicle model. Bushings were added to the model at the wheel spindles to approximate a tire being in place, where the bushings were assigned stiffness values similar to actual tires.

In comparison, Barak {3} notes that the wheel hop frequency for a solid axle is generally 10-12 Hz, where the ADAMS model of the rear axle assembly falls within this range with 10.87 Hz. Gillespie {17} notes that in general, front wheel hop frequency is in the range of 12-15 Hz, where the ADAMS model predicts 14.43 Hz. The front independent suspension has a higher frequency since the unsprung weight is much less

140

than that of a solid axle assembly. As mentioned earlier, Gillespie {17} states that the engine/transmission vertical frequency is designed to be close to the front wheel hop frequency which is true in this case, as the two values only vary by 0.5 Hz.

Barak {3} affirms that pitch modes are commonly in the range of 1.2-1.6 Hz, which is close to the 1.37 Hz pitch mode about the front suspension, and 1.12 Hz pitch mode about the rear suspension values predicted by the ADAMS model. He also states that body roll is in the range of 1.5-2.0 Hz, which is slightly lower than the 2.28 Hz that was predicted by ADAMS. These values correlate well with published values, and any variance in these ideals is likely due to the fact that overall vehicle flexibility was not considered in this model, and that many component values are a linearized approximation.

### 5.3.2.2 Body Relative Movement

Once the linear mode frequencies were analyzed and confirmed, the next stage is to correlate the body movement relative to the suspension using test data. Control arm angles can be used for this task. Two key factors in validation of control arm measurements are phase and magnitude. This will determine when the control arms are moving in time, and to what extent they are moving. Figures 5.4 and 5.5 illustrate the movements of the right front and left rear control arm angles respectively. These plots are shown in both time and frequency domain. Both of these figures show close correlation throughout all channels. The desired and remote responses as shown in the PSD plots are nearly identical, which can be attributed to the fact that they are used as control channels. The ADAMS model simulations are also very close in comparison, which confirms that the suspension is moving relative to the body in the same manner as the physical vehicle, both in magnitude and phase.
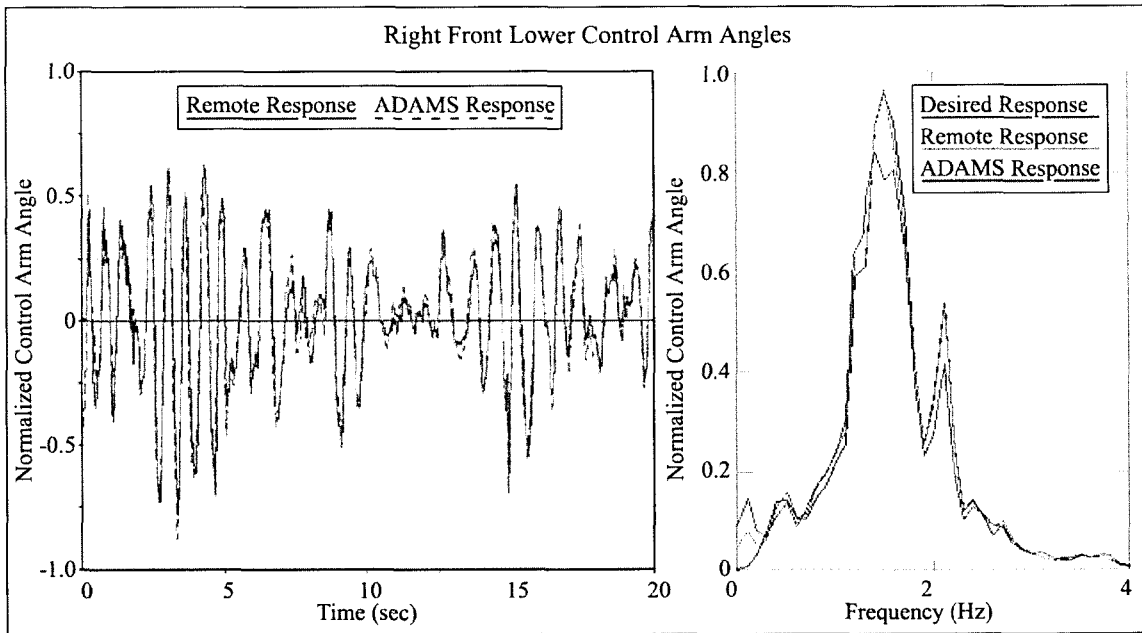
**Figure 5.4**: Illustration of right front lower control arm angles in both the time domain and in a PSD plot. Time domain plot shows close correlation in both phase and magnitude, and frequency domain also shows close correlation. The time domain plot shows the first 20 seconds of the simulation, while the frequency representation is over the entire 50 second simulation.
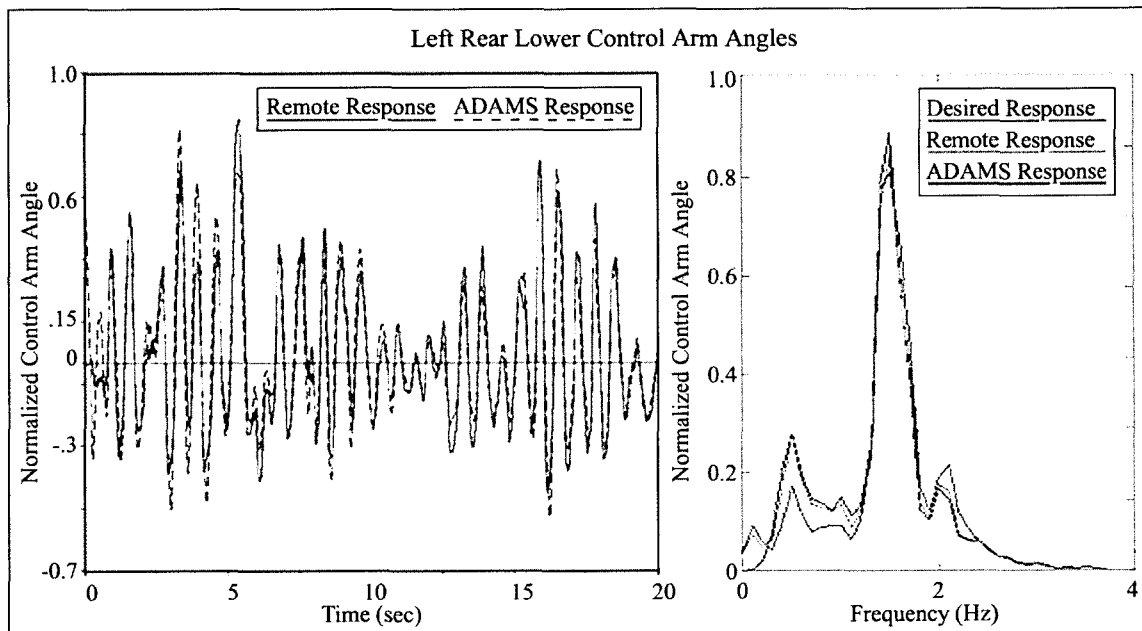


**Figure 5.5**: Illustration of left rear lower control arm angles in both the time and on a PSD plot. Time domain plot shows close correlation in both phase and magnitude, and frequency domain also shows close correlation. The time domain plot shows the first 20 seconds of the simulation, while the frequency representation is over the entire 50 second simulation.

142

### 5.3.2.3 Load Path Analysis

Analyzing the loads placed on the vehicle is an essential part of durability analysis, since the loading on components will directly affect the stress and stain placed on them, and will affect the fatigue life of the components. There are several locations on the test vehicle for which the loadings were measured during data acquisition. All of these available loading channels were used to correlate the virtual model. Recorded data includes shock absorber forces, spring forces, ball joint forces, jounce bumper forces, control arm forces and WFT forces.

Jounce bumper readings serve two main purposes for correlation. The first is to determine when and if the jounce event is occurring, and the other is to determine magnitude of the force that is transmitted to the body of the vehicle. The parameters that affect jounce events the most are vertical displacement input, spring and shock absorber rates, and torsional stiffness of the bushings. Jounce bumper forces were also found to be quite sensitive to stabilizer bar rates.

The jounce bumpers results, as shown in Figure 5.6, show close correlation between physical and virtual results. The timing of each jounce event is nearly exact. The magnitude is slightly lower in the ADAMS model than is physically shown. There are many factors, including spring rates, shock absorber rates, and jounce bumper rates that directly affect these results. The rates provided by the manufacturers were given as a linear rate, when in reality the elastomeric components would behave non-linearly. If the bushings were to stiffen up with displacement, this may result in higher forces transmitted to the body like in the physical case. The point at which the jounce is achieved was also approximated by measuring distances on CATIA drawings which would also affect the displacement of the bumpers. The jounce events occur more often in the rear of the vehicle as expected, since it is at full rated load (FRL).

143
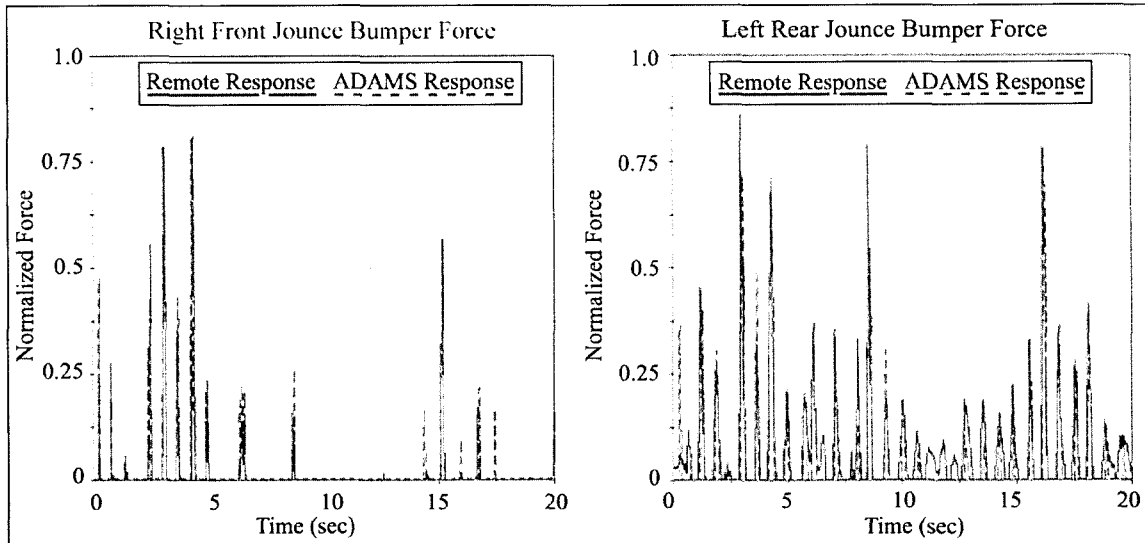
**Figure 5.6:** Normalized left rear jounce bumper forces as a function of time showing the transmission of forces to the body at full jounce. This plot shows close correlation between force and magnitude, showing the virtual vehicle's movements closely match those of the physical one. Model input is vertical displacements, lateral forces, and longitudinal forces.

Springs and shocks are another input channel that is used to correlate body movement and forces. Figures 5.7 and 5.8 show the plots for the front and rear suspension, which include both the springs and shock absorbers. The frequency content of the physical results in comparison the virtual results are close for both figures. The ADAMS model underestimates the maximum force magnitude in the right front springs

by $\sqrt{\dfrac{0.96}{0.74}} = 1.14$, while the force in the right front shock absorbers is overestimated by

$\sqrt{\dfrac{0.90}{0.70}} = 1.13$. The left rear spring forces were predicted exactly, while the virtual model

overestimates the shock absorber force by $\sqrt{\dfrac{0.95}{0.72}} = 1.15$. These values correlated well

within an acceptable level. The rates of the springs and shocks were not altered or scaled from their factory specifications.

144
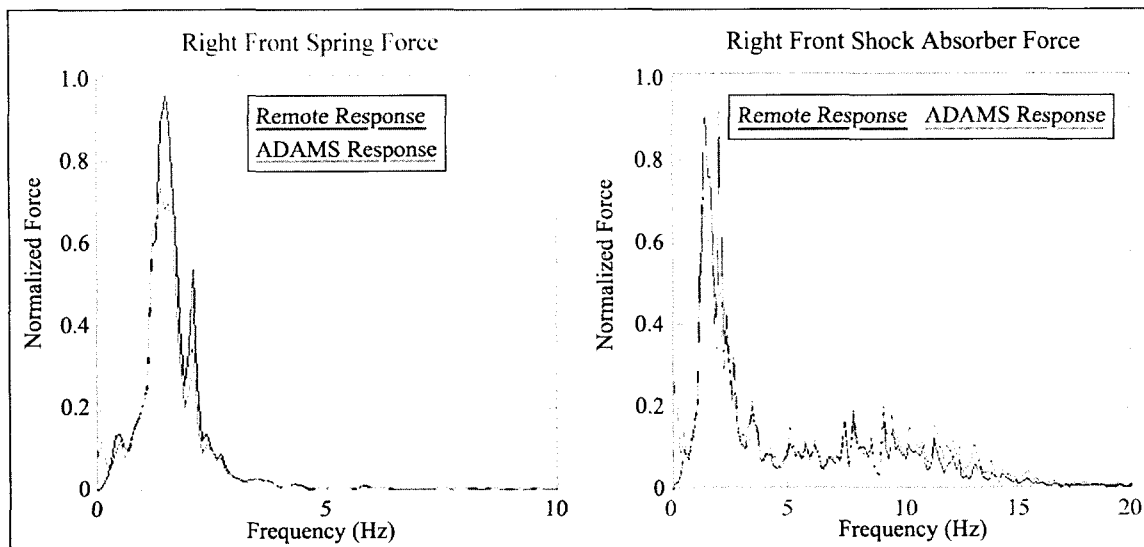
**Figure 5.7**: Right front spring and shock absorber forces shown on a PSD plot in the frequency domain. Both plots show similar trends in correlation in both magnitude and frequency. The ADAMS response is slightly less in magnitude for the springs, and slightly higher for the shock absorbers.
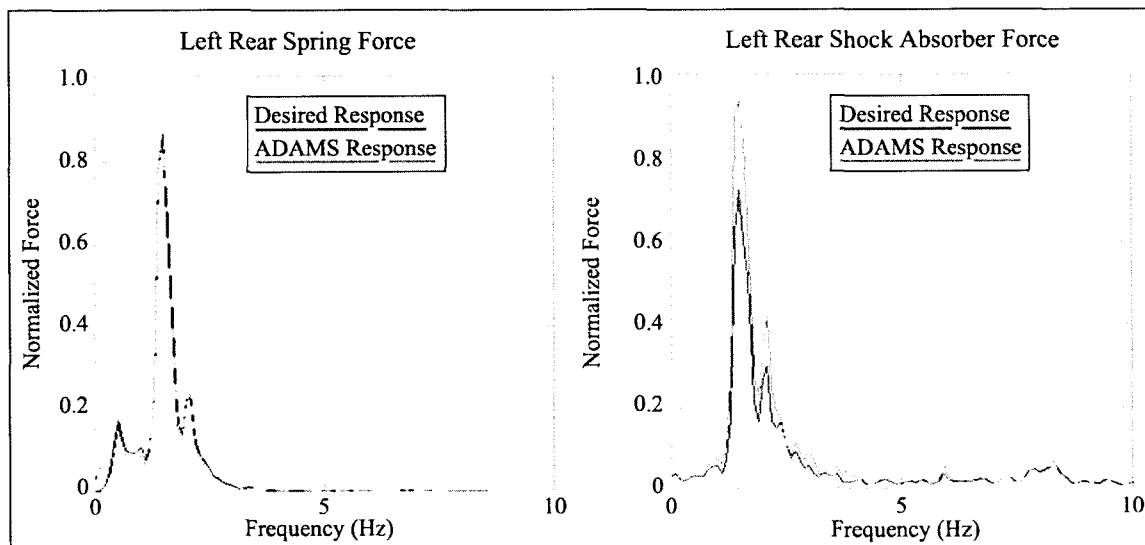


**Figure 5.8**: Left rear spring and shock absorber forces shown on a PSD plot in the frequency domain. Both plots show similar trends in correlation in both magnitude and frequency. The responses for the right rear spring correlate closely, while the ADAMS model again slightly overestimates the response.

The test vehicle was instrumented to measure the forces in the upper and lower ball joints. The longitudinal forces were recorded for both the front upper and lower ball joints, and the lateral forces for the lower control arm. These values were only recorded on the MTS rig and were not recorded on the proving ground, although the

145

instrumentation was in place. Figure 5.9 illustrates the measured longitudinal forces on

the upper and lower ball joints. Both plots show very close correlation for the higher

magnitudes at lower frequencies from 0-5 Hz. Variance exists at higher frequencies, but

at the frequencies above 5 Hz, the magnitudes are much lower in comparison.
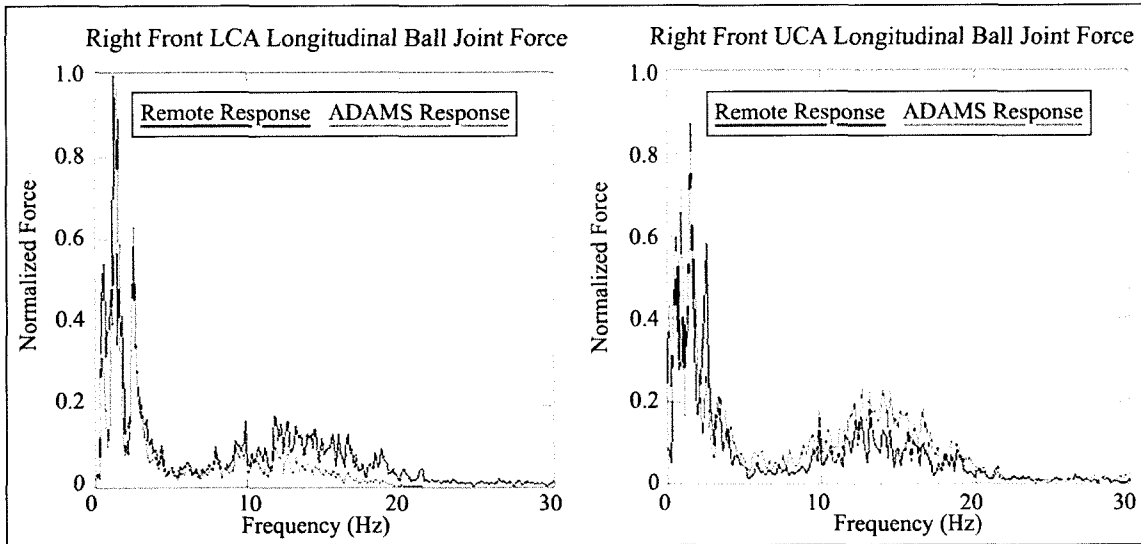


**Figure 5.9**: Comparison of remote response and ADAMS predicted longitudinal forces
for both the upper and lower control arm ball joints show on PSD plots. Close
correlation is noted for both plots at lower frequencies. The values are
slightly lower for the ADAMS response at the LCA, while the predicted
values are higher for the UCA at higher frequencies.

The lateral forces are shown in Figure 5.10 for both the right front lower control

lateral ball joint and the lateral forces in the right front WFT forces. The ball joint shows

strong correlation between channels, while the WFT forces are slightly less than the

desired responses. The differences in the wheel force transducers are partially due to the

stiffness and damping being added to the system for stabilization. Also, note that the

desired value at the proving ground is actually lower than the ADAMS response, as well

as the remote response. The forces measured in the vertical and longitudinal directions

using the WFT's are used as correlation channels, but the lateral forces are not.
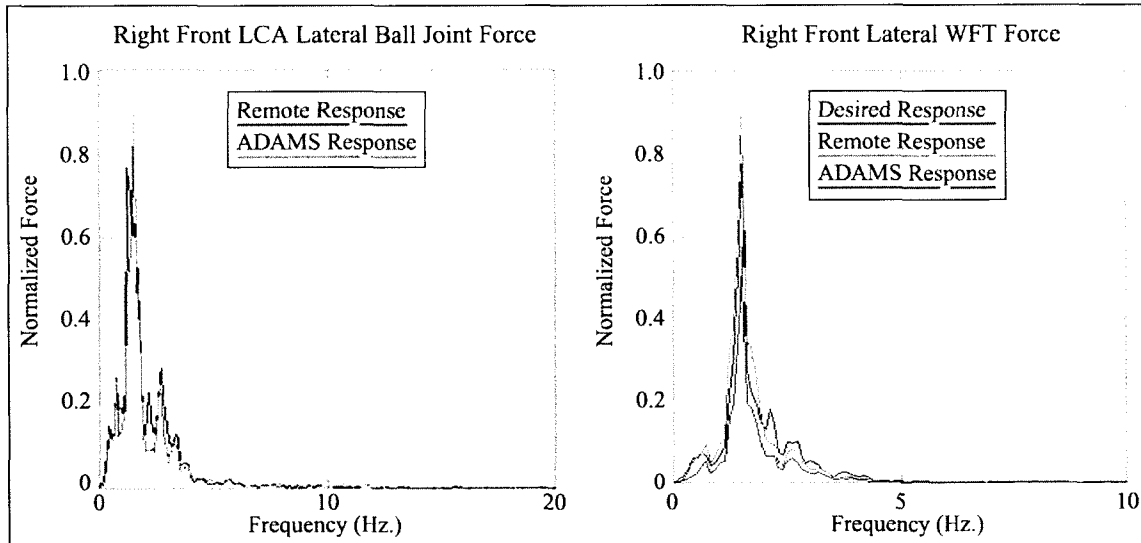
**Figure 5.10**: Assessment of the left front lateral ball joint forces and the lateral wheel force transducer. Both plots show relatively close correlation for the forces in the system across the frequency band shown. The magnitude of the WFT forces is slightly less for the lateral direction due to the stiffness and damping of the bushings being used to stabilize the model.

The right front vertical and longitudinal WFT forces are shown in Figure 5.11. Both of these plots show close correlation between the remote and ADAMS responses. Close correlation is noted for both channels, in both magnitude and frequency content. The response for the vertical confirms that the weight distribution is correct, and also helps to confirm that the inertial values are also correct, as this is difficult to characterize otherwise. Both of these channels were used as correlation channels.

The longitudinal forces in the left rear lower control arm and WFT are shown in Figure 5.12. The forces in the lower control arm were also referred to as axial loadings in previous chapters. Both of these channels correlate well, with the ADAMS force being slightly higher at lower frequency and slightly lower at higher frequencies for the axial LCA force.

147
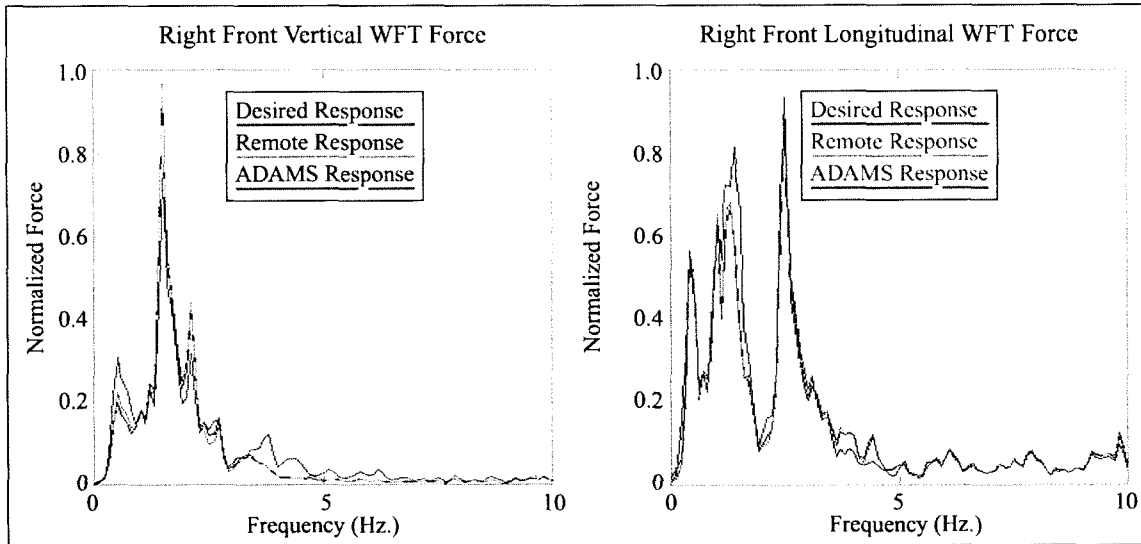
**Figure 5.11**: Comparison of right front vertical and longitudinal wheel force transducer (WFT) forces. Both plots show similar trends in correlation in both magnitude and frequency across the frequency band. Minor differences in the longitudinal direction are partially due to the stiffness and damping used to restrain the system.
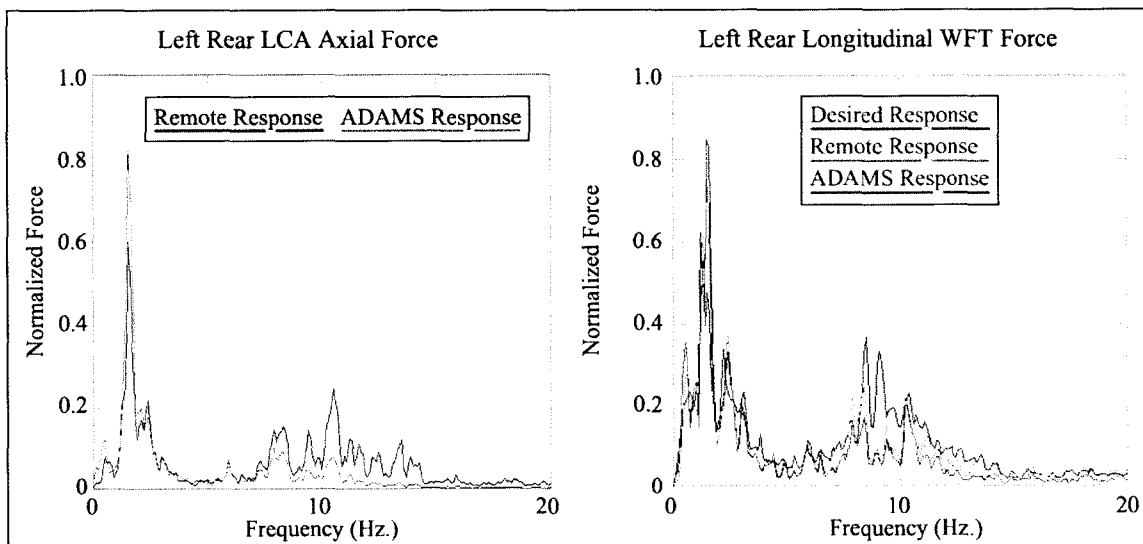


**Figure 5.12**: Left rear axial LCA force and WFT force comparison on PSD plots. The magnitude of the LCA axial force ADAMS response is higher at lower frequencies and lower at frequencies above 5 Hz. The longitudinal WFT forces match closely between remote and ADAMS responses, while the desired is slightly higher.

The final two WFT forces in the lateral and vertical directions are shown in

Figure 5.13. Both of these again show strong correlation, with the exception of the

magnitude of the lateral direction, due to the opposing forces from the bushings used to

148

stabilize the model. The lateral WFT forces are not used as control channels, which helps

to explain why there can be a difference in the remote and desired responses in the lateral

direction, but not in the longitudinal and vertical directions.
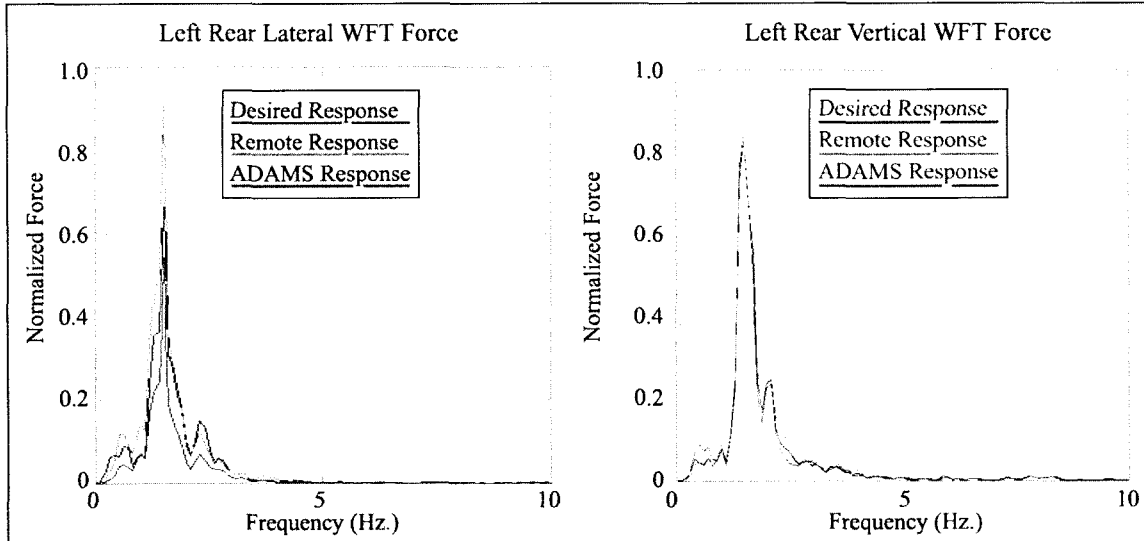


**Figure 5.13**: Left rear lateral and vertical WFT forces comparison on PSD plots. The lateral WFT force is lower due to the stiffness and damping that are added to stabilize the model. The vertical WFT force correlates nearly exactly, which further confirms the weight and weight distribution of the vehicle.

From the plots presented in this section regarding the load path analysis, several

conclusions can be made. The ADAMS model was found to correlate well with results

measured both on the MTS rig itself, and with desired results, where applicable. Forces

were predicted to within 15% using this ADAMS model, which represents every "load"

related sensor on the test vehicle that was measured. The differences appeared mainly in

vertical and lateral related channels. Differences in the lateral channels are probably due

mostly to the stabilizing bushings that were used in the model. It may be beneficial to

add the lateral WFT forces as control channels while performing iterations, as

deficiencies were found between remote and desired responses. Currently, only the WFT

moment (about a longitudinal axis, $M_x$) is used to control forces in the lateral direction.

Based on the jounce bumper force results, the lower control arm results, and the spring and shock forces, it is felt that the movement of the body (sprung weight) in relation the suspension (unsprung weight) is representative of the actual vehicle.

## 5.3.2.4 Acceleration Analysis

An acceleration analysis was done simultaneously with the load path analysis while conducting simulations. Acceleration analysis is used to determine the predominate frequencies of vibration that a component experiences during a test. The location and orientation of the accelerometers on the physical model were reproduced on the virtual model. Two accelerometer readings were compared; one on the rear axle, and one on the front steering knuckle of the front suspension. Two sensors were instrumented for use at the proving ground, while only one was measured on the RTS rig. The accelerometer on the steering knuckle which was recorded on the rig was used for this reason.

The right front vertical and lateral accelerations on the steering knuckle are shown in Figure 5.14. As expected, the vertical channels correlate nearly perfectly, while the lateral accelerations are also similar, although the ADAMS model tends to over predict the acceleration by approximately $\sqrt{\dfrac{0.70}{0.48}} = 1.21$ at 1.75 Hz. This increase is also likely due in part at frequencies above 10 Hz as in the longitudinal acceleration, where steering effects are a major factor as shown in Figure 5.15.

The longitudinal acceleration on the front steering, shown on Figure 5.15, proved to be quite difficult to correlate. The movement of the steering system is difficult to predict without having the vehicle modeled on a virtual rig, or having actual steering sensor responses from the RTS rigs to use as input. The springs added to the system to approximate the steering effects inherently add to the frequency content at the steering knuckle. The longitudinal rear axle acceleration is also shown in the same plot.

150
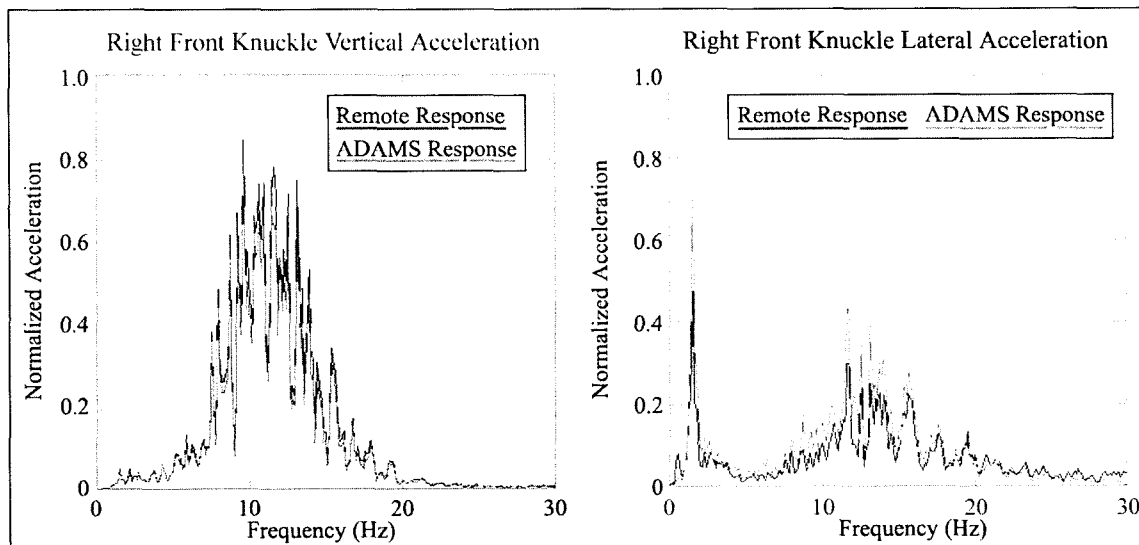
**Figure 5.14**: Comparison of right front vertical and lateral acceleration on PSD plots. These values are measured on the knuckle of the vehicle (component that pivots about the ball joints). These plots show excellent correlation in the vertical direction, and the ADAMS model tends to over-estimate the acceleration magnitudes in the lateral direction. The frequency content and trends are very close to both plots.
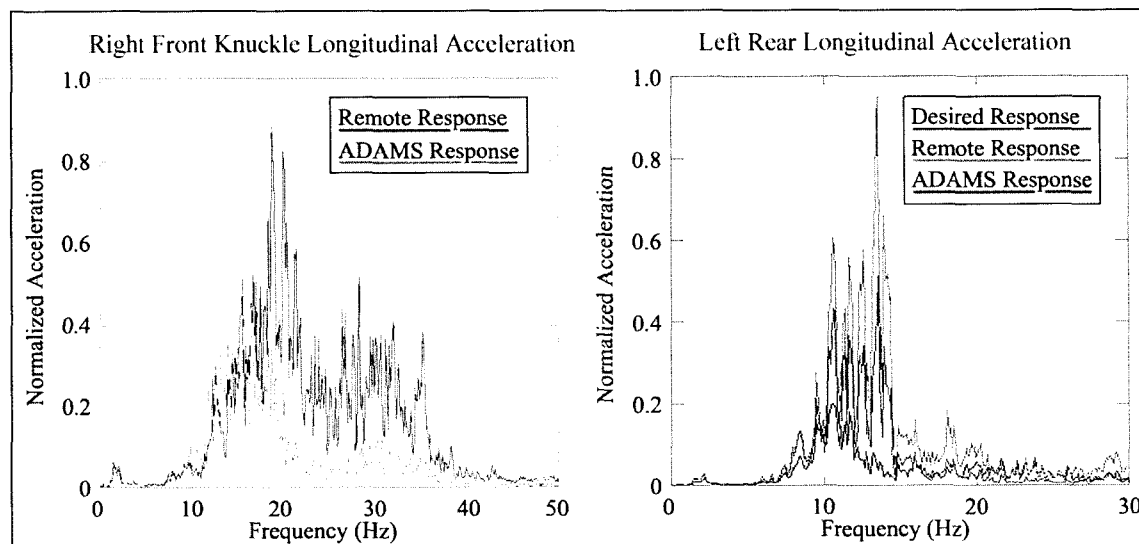


**Figure 5.15**: Comparison of right front and left rear longitudinal accelerations on PSD plots. These values are measured on the knuckle of the vehicle (component that pivots about the ball joints). Higher frequency content was present in the ADAMS model, which is partially due to steering effects. Recommendations regarding the front steering are presented in Section 6.2. The ADAMS response for the rear longitudinal acceleration correlates fairly well with the remote response, where the desired response is considerably less.

151

{16}, especially concerning lateral acceleration when damping is added to the model. In that research, lower frequency regimes correlated well, while regions above 10 Hz were damped out considerably in the ADAMS model for the lateral direction. The other issue is the flexibility of the rear axle. In reality, the rear axle (including axles, brakes and backing plates) is susceptible to slight deformations, which will affect the remote responses in relation to the ADAMS model. In the ADAMS model, there are no force elements in the rear solid axle that offer any form of compliance in the lateral direction. Another possible reason is that the coil springs on the rear axle have stiffness in the lateral direction, while in the ADAMS model the lateral stiffness would not exist. To account for this, a spring could be attached laterally to connect the body to the rear axle.

There lies a fine line between the correlation of forces and the correlation of accelerations. As parameters such as bushing stiffness are adjusted, both on the suspension components themselves, as well as the bushings used to stabilize the model, forces may correlate well in certain sensors, while others may shy away from the required values. The results presented are produced after running many simulations and adjusting of the appropriate parameters. This is done by adjusting the parameters and analyzing the effects on these changes. Based on these changes, corrections are made, and simulations are re-run. Figure 5.17 shows the values used for the stiffness and damping for the full vehicle shown on a custom dialog box that was created within ADAMS. Stiffness and damping was only used in the lateral and longitudinal directions (force input direction).



| Input Stiffness/Damping ("Anti-Drift") | | | |
|---|---|---|---|
| | Front | | Rear | |
| | k | c | k | c |
| Longitudinal | 0.5 | 0.1 | 0.1 | 0.5 |
| Lateral | 2.0 | 0.75 | 0.5 | 2.0 |

**Figure 5.17:** Final Bushing stiffness and damping values used in the full vehicle model using vertical displacements, and longitudinal and lateral force input. Stiffness and damping was used in the lateral and longitudinal directions.

153

## 5.4 Rear Suspension Comparison

Changes in suspension geometry act to affect the kinematic movement in the rear of the vehicle, which causes the suspension to travel along a differing path under dynamic movement. The degree to which this movement changes, and the relative stiffness of the components used will dictate the changes in forces and accelerations on the system. Since the forces and displacements are still applied as the same point on the vehicle, and the magnitudes are still the same, it is expected that the greatest changes will be observed in the body movements, and the forces transmitted to the body assembly (sprung mass). A comparison of vibration modes between the two suspension configurations are shown in Table 5.2.

| Critical Vibration Mode Comparison | | |
|---|---|---|
| Linear mode description | 3 Link Frequency (Hz) | 4-Link Frequency (Hz) |
| Body pitch (about front) | 1.37 | 1.34 |
| Body pitch (about rear) | 1.12 | 1.12 |
| Body roll | 2.28 | 2.25 |
| Front wheel hop | 14.43 | 14.43 |
| Rear wheel hop | 10.87 | 10.35 |
| Tramp (primarily front) | 17.79 | 17.66 |
| Tramp (primarily rear) | 18.06 | 18.89 |
| Side shake, engine roll (coupled) | - | 20.02 |
| Wind-up | 21.8 | 20.9 |
| Side shake | - | 21.08 |
| Rear axle yaw | 26.7 | 27.92 |

**Table 5.2**: Comparison of linear mode frequencies between 3-link and 4-link suspension assemblies. The alterations that were made were changing of suspension links, geometry, as well as the bushings used in these links. Bushings were added to the model at the wheel spindles to approximate a tire being in place, where the bushings were assigned stiffness values similar to actual tires.

In comparison, the values shown in Table 5.2 are quite similar in magnitude for the wheel hop, body roll and yaw frequencies. This is likely due to the fact that the

154

properties of the force elements were not changed drastically, and the same body mounting points were used. Axle tramp, which is similar to wheel hop, except the wheels move vertically out of phase, was similar for both suspensions. Axle wind-up (rotation about the spindle axis), and axle yaw were also very similar. One significant difference is in the side shake mode which is prominent in the four link, but not in the three link. Side shake refers to the movement of the axle in the lateral direction. This is due to the additional degrees of freedom (and compliance) added by removing the ball joint and adding bushings as in the case of the four link suspension.

A comparison was made on the effects of changing suspension systems by monitoring the forces and accelerations on the body near the point where the control arms attach to the body. An accelerometer was placed on the virtual model just above the upper control arm mounting location with a global axis being used. The accelerometer located on the rear axle, which is the same one used on the actual test vehicle was also monitored for acceleration.

The acceleration of the left rear axle and the body in the lateral direction is shown in Figure 5.18. From this figure, it can be said that the vertical acceleration on both the body and axle assembly is basically unchanged, where the body vertical acceleration only changes minimally. This is due to the fact that displacement input is used.

The left rear longitudinal axle and body accelerations are shown in Figure 5.19, while the corresponding lateral accelerations are shown in Figure 5.20. Both of these figures illustrate that the acceleration in the rear if the vehicle is quite sensitive to the change in suspension configuration. The longitudinal axle direction shows a dramatic increase in acceleration between 20-30 Hz, while the longitudinal body acceleration shows a slight increase above 20 Hz. The acceleration in the lateral direction shows an increase in acceleration in between 15-20 Hz, while the body acceleration remains unaffected.

155
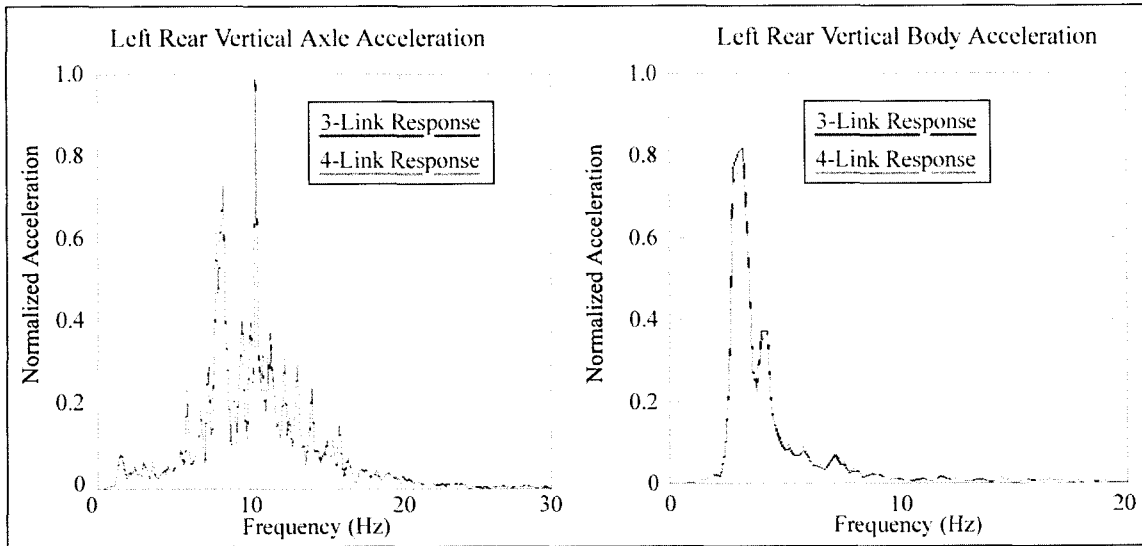
**Figure 5.18**: Comparison of left rear axle and body vertical accelerations using 3-link and 4-link suspension systems on PSD plots. Very little change is noted in these directions.
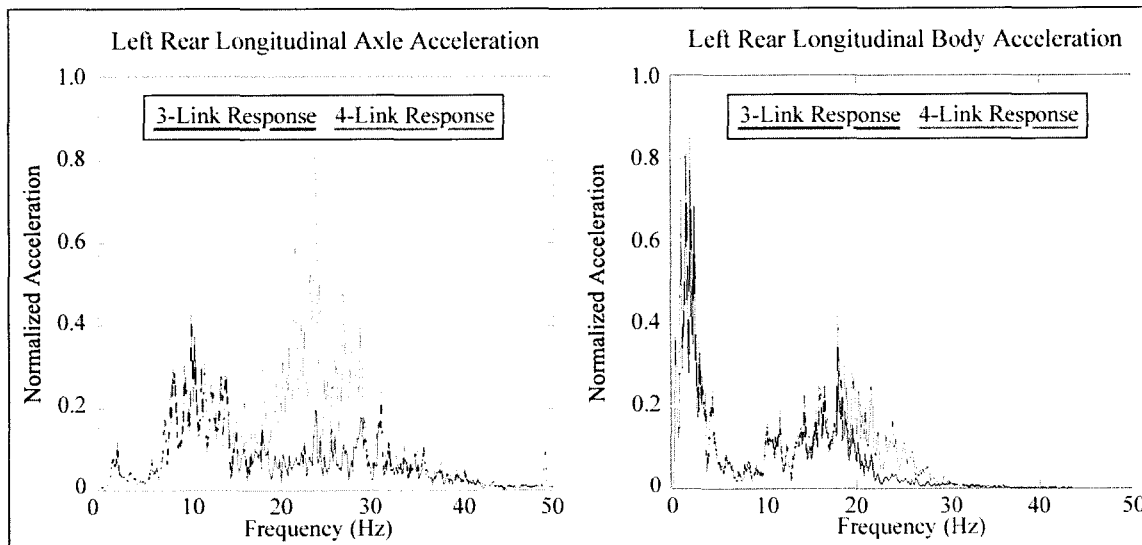


**Figure 5.19**: Comparison of longitudinal axle and body accelerations between three link and four link suspension configurations on PSD plots. A notable increase is shown between 20-30 Hz on the rear axle, while a slight increase in this regime is shown on the body. Outside of these regions, the response remains the same.

156
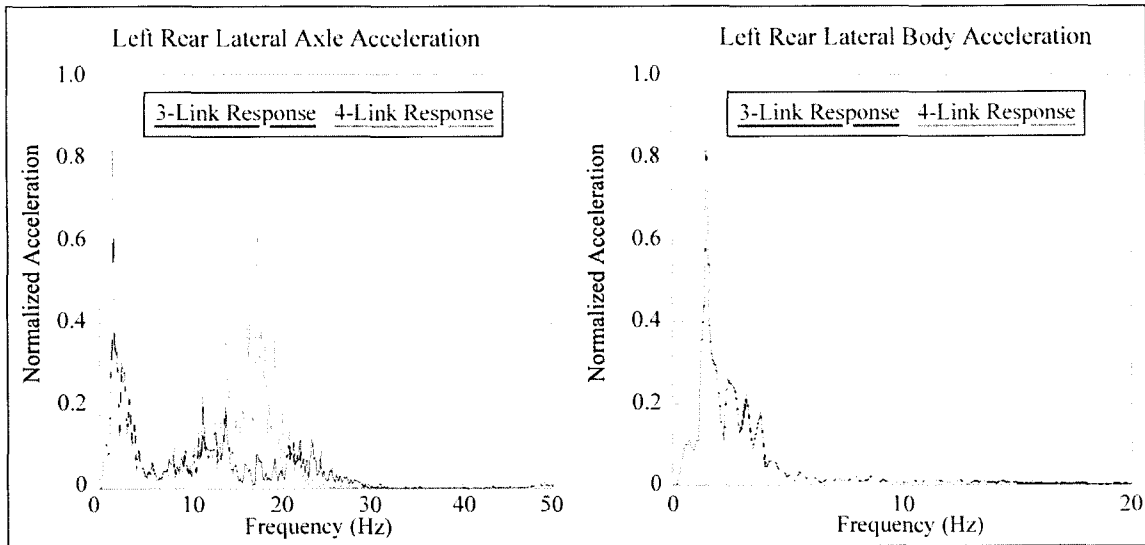
**Figure 5.20**: Comparison of lateral axle and body accelerations between three link and four link suspension configurations on PSD plots. Increases in acceleration are noted in the longitudinal direction around 20 Hz region, but this time at slightly lower than 20 Hz. The body acceleration remains unaffected.

The vertical UCA and LCA body forces are shown in Figure 5.21, where a drastic decrease is noted in the UCA vertical forces. The forces in the LCA essentially stay the same. This is clearly a result of bushings being added in place of ball joint in the rear.
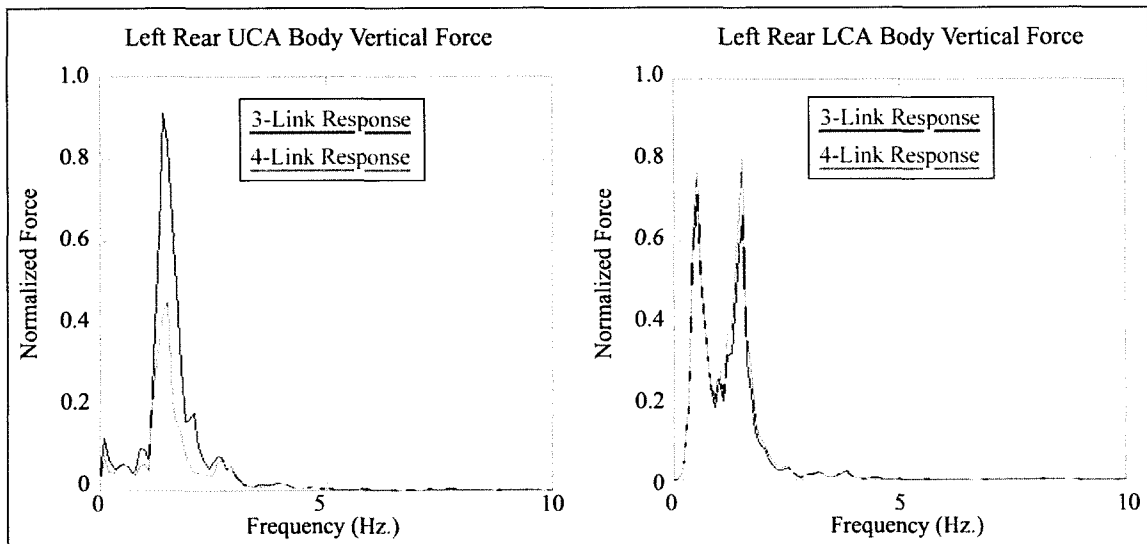


**Figure 5.21**: Comparison of vertical UCA and LCA vertical body reaction forces between three link and four link suspension configurations on PSD plots. A large decrease was shown in the vertical direction where the UCA connects to the body, where the LCA body force remained essentially the same.

157

The longitudinal and lateral forces are shown in Figures 5.22 and 5.23 respectively. These show forces at the body for both the upper and lower control arms.
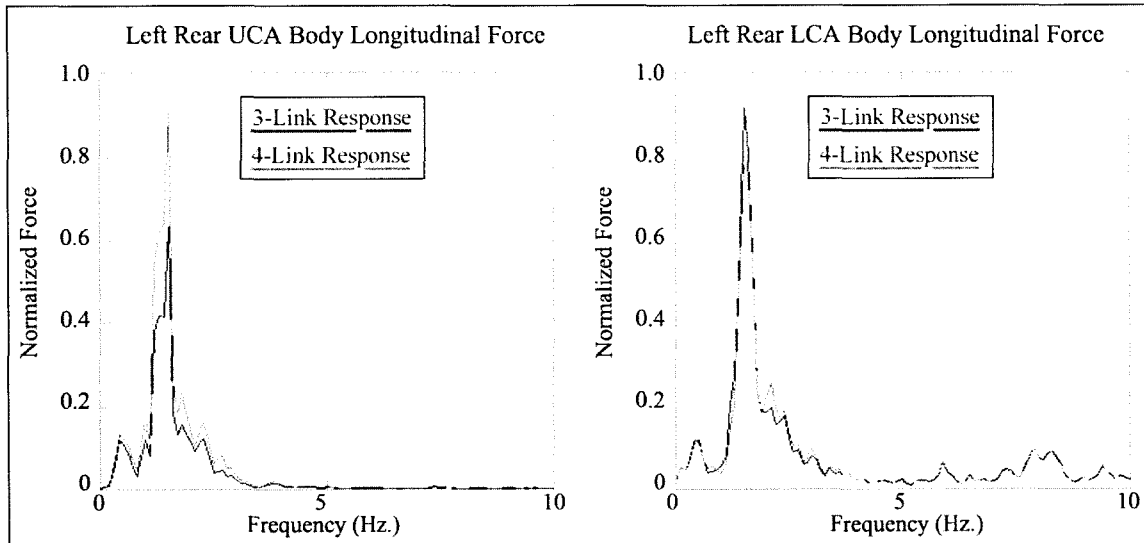


**Figure 5.22**: Comparison of vertical UCA and LCA longitudinal body reaction forces between three link and four link suspension configurations on PSD plots. The four link suspension showed an increase in longitudinal forces in the UCA body region, while a decrease in force was shown at the LCA longitudinal interface.
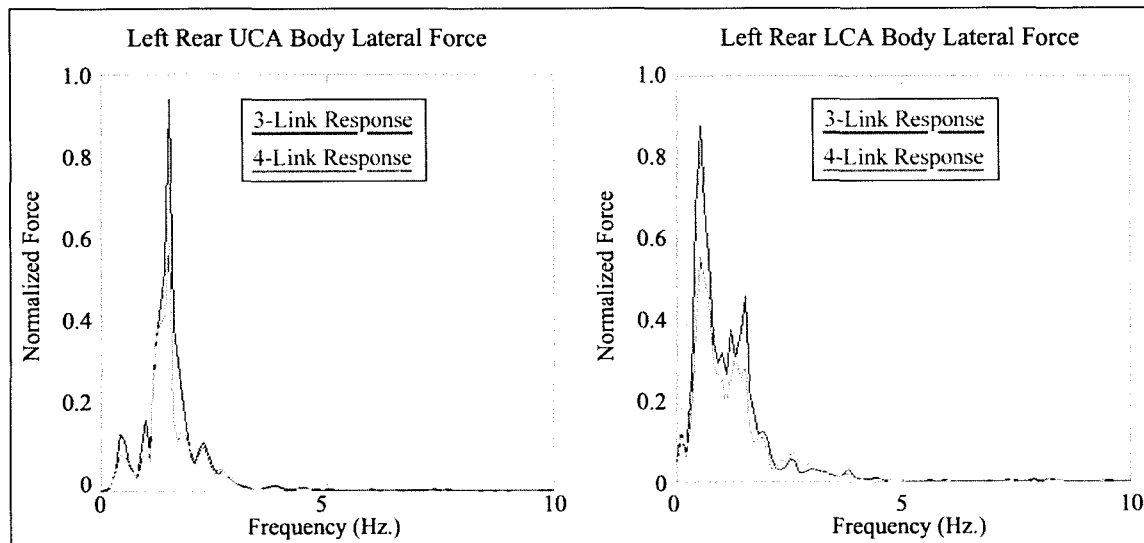


**Figure 5.23**: Comparison of UCA and LCA lateral body reaction forces between three link and four link suspension configurations on PSD plots. The four link suspension configuration demonstrated a decrease in forces for both the LCA and UCA lateral body forces. This is partially due to the revised geometry, as well as the bushing addition on the upper control arms.

158

The force plots shown in Figures 5.22 and 5.23 demonstrate an increase in force with the four link arrangement in the longitudinal direction for the UCA, and a slight decrease at the LCA. The lateral direction shows a decrease in forces for both the UCA and LCA in the lateral direction. This can be attributed to the compliance introduced by the addition of bushings in place of the ball joint in the upper control arm. This is also evidenced by the presence of a side shake mode as observed in ADAMS.

Referring back to the linear modes analysis from Table 5.2, an investigation shows that several different linear modes lie in the 20-30 Hz region. A majority of the linear modes pertaining to the rear suspension lie within this range. It is clear that these modes do affect the acceleration of the rear axle. They are difficult to directly relate to certain frequency regimes, as there is not a tire interface on the RTS rig, but this may help to explain these differences.

Based on these results, it would appear as though the forces produced in the rear suspension are significantly different when the suspension systems are changed. It may not be advisable to use these drive files to run durability simulations with a revised four link geometry using three link drive files for this reason. It would be beneficial to drive the model using data acquired on the proving ground and RTS rig with the actual four link suspension for an additional comparison.

## 5.5 Flexible Body Effects

Once the rigid body model had been correlated to an acceptable level, flexibility was investigated. As noted in Section 4.7.10, only the components in the rear 3-link suspension were considered in this research. This analysis includes simulation of a single flexible body (upper control arm), and then finally the entire rear suspension assembly as noted earlier in Chapter 4.

159

Once a model had been created in PATRAN, both for post-processing in ADAMS and in PATRAN, the mode shapes and frequencies were compared. This gives reassurance that the constraints are applied correctly in ADAMS, and are interpreted the same as in NASTRAN. This also confirms that the mode shape orthogonalization was done correctly using the ADAMS/Flex toolkit translation module. Table 5.3 shows a comparison between modal frequencies in PATRAN and ADAMS. The first ten modes out of the 20 that were requested are shown. The results in this comparison matched very closely, where the modal frequencies varied by 0.58 Hz at the most.

| Mode Frequency Comparison | | |
|---|---|---|
| Mode | PATRAN (Hz) | ADAMS (Hz) |
| 1 | 470.08 | 470.11 |
| 2 | 484.29 | 484.38 |
| 3 | 760.64 | 760.67 |
| 4 | 828.85 | 828.85 |
| 5 | 886.53 | 886.59 |
| 6 | 894.08 | 894.12 |
| 7 | 963.49 | 964.07 |
| 8 | 942.38 | 942.50 |
| 9 | 1024.0 | 1024.52 |
| 10 | 1054.1 | 1052.30 |

**Table 5.3**: Flexible normal mode frequency analysis comparing the first 10 modal frequencies shapes from both PATRAN and ADAMS for the rear three link upper control arm. As can be seen, mode shapes correlate nearly exactly, confirming that the DOF are correct in ADAMS. .

An illustration of the mode shapes and frequencies are shown in Figures 5.24 and 5.25 for ADAMS and PATRAN respectively. As noted in Table 5.3, the modal frequencies correlate very well, and these figures confirm that the mode shapes corresponding to each frequency match. These diagrams show the first mode (eigenvector) in both software packages. As evidenced by these illustrations, the shapes of the modes also match exactly.

160
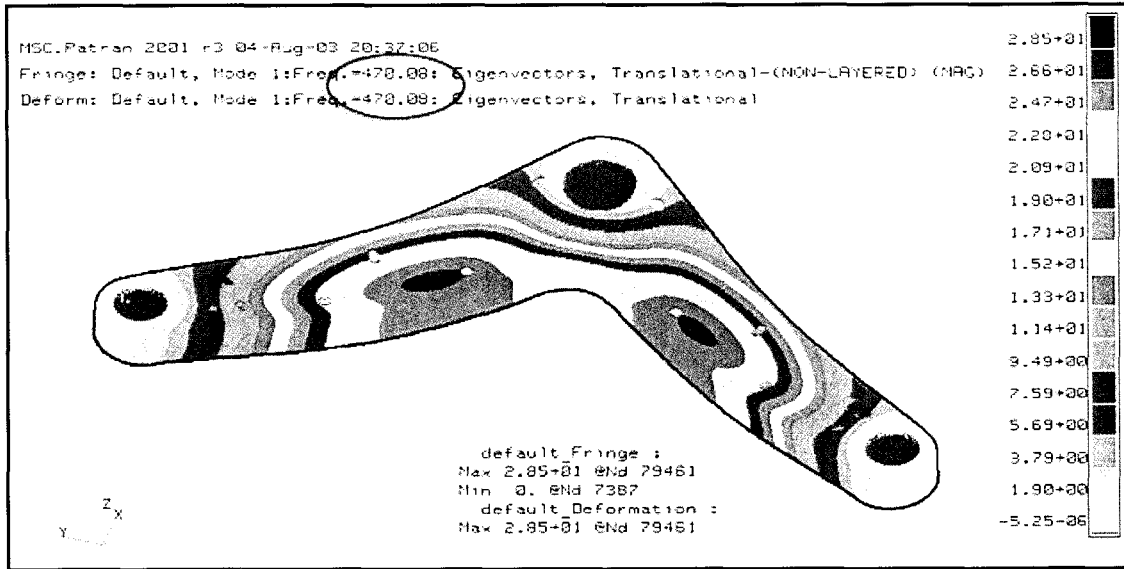
**Figure 5.24**: Illustration showing the 1$^{st}$ mode of the rear upper control arm in PATRAN. The first mode, as shown previously in Table 5.3, is 470.08 Hz. Both the mode shapes and frequencies match in comparison between ADAMS and PATRAN.
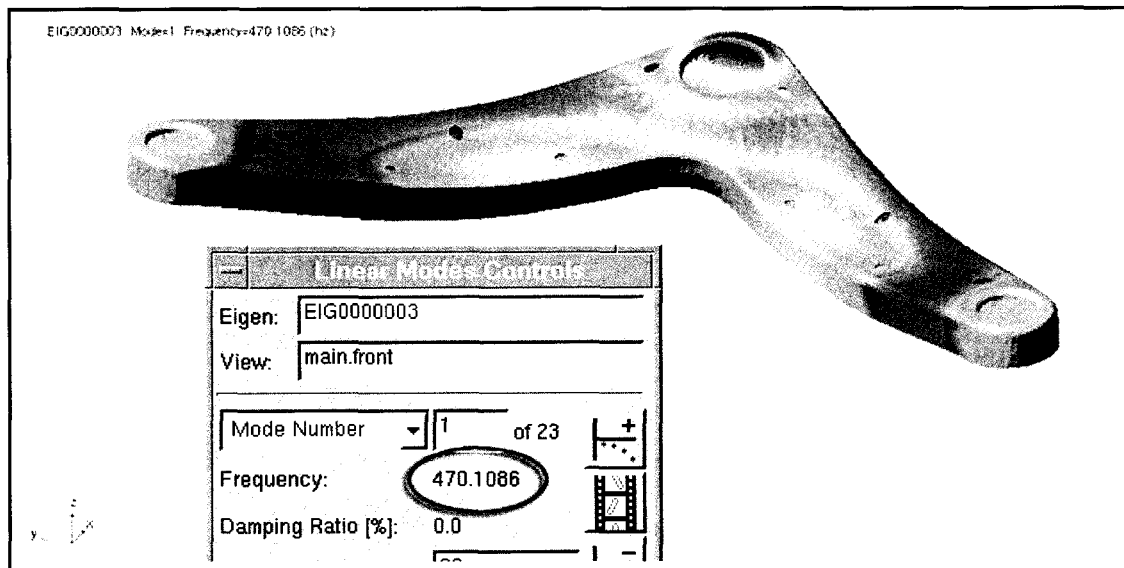


**Figure 5.25**: Illustration showing the 1$^{st}$ mode of the rear upper control arm in ADAMS. The first mode, as shown previously in Table 5.3 is 470.11 Hz. Notice how the shape of this mode closely resembles that of the PATRAN results shown Figure 5.23.

The validated flexible upper control arm was exchanged with the rigid ones in the

ADAMS model, and simulations were re-run using identical inputs to observe results.

161

The flexible bodes were constrained to the full vehicle model the same was as they were constrained when correlating the modes.
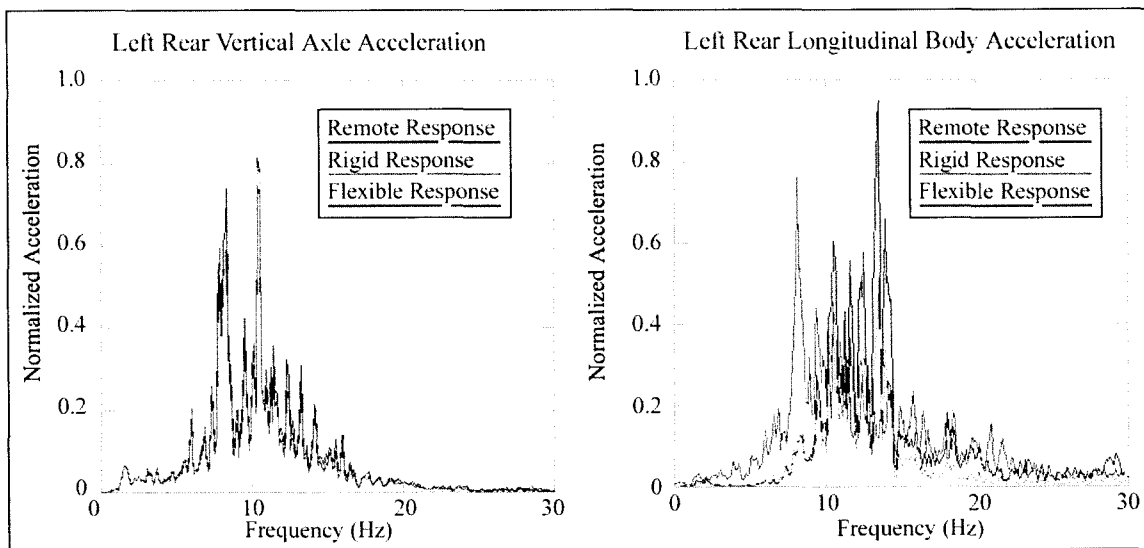


**Figure 5.26**: Effect of the upper control arm flexibility on the left rear vertical and longitudinal axle accelerations. The remote response is included to show the correlation with respect to the actual results. Vertical results match flawlessly, while the addition of flexible bodies introduces a signal at around 9 Hz in the longitudinal direction.
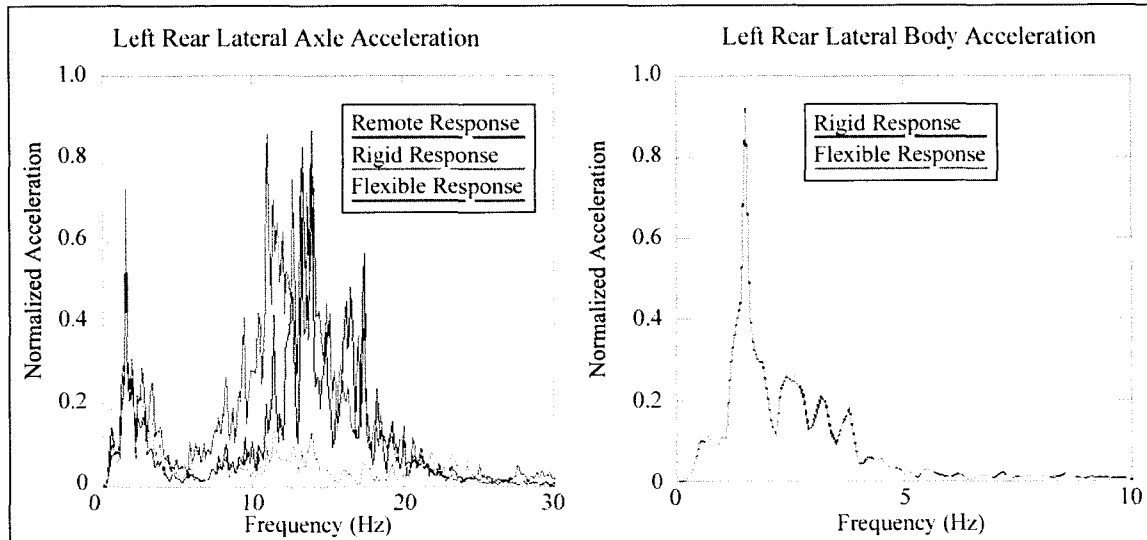


**Figure 5.27**: Comparison of left rear rigid body and flexible body lateral accelerations for the axle and the body respectively. The upper control arm flexible body implementation introduces content between 5-10 Hz for the axle lateral acceleration, while the magnitude at approximately 15 Hz more closely matches the remote responses in comparison to the rigid body response. Rear lateral body acceleration remains unaffected.

162

The left rear vertical and longitudinal body accelerations are shown on Figure

5.28. As is shown, the vertical acceleration is affected minimally, while the flexible body

implementation introduces frequency content between 10-15 Hz.
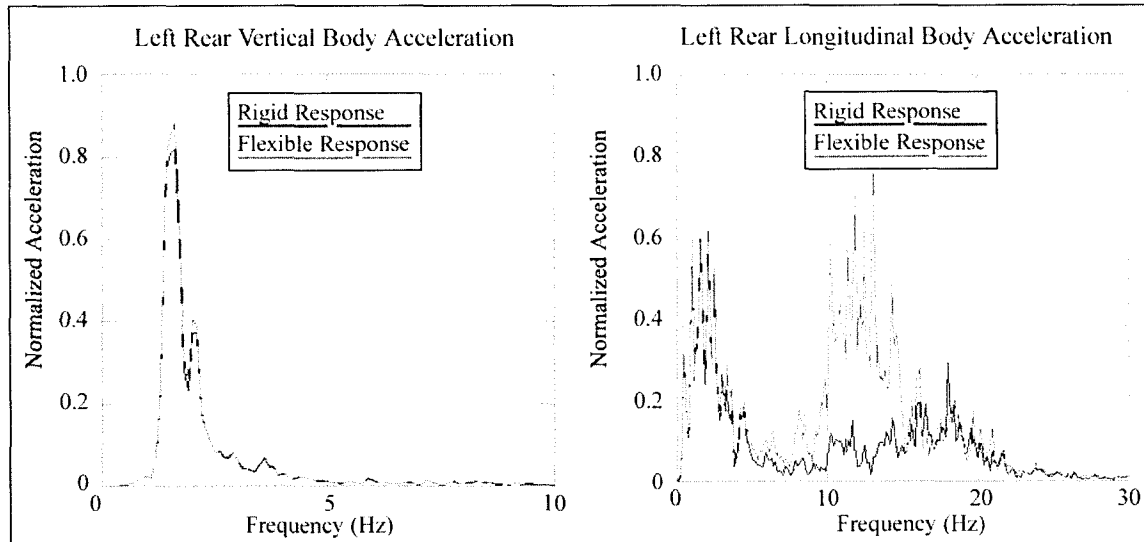


**Figure 5.28**: Comparison of left rear rigid body and flexible body vertical and
longitudinal body accelerations for the axle and the body respectively. The
vertical body acceleration reduces only slightly. The upper control arm
flexible body implementation introduces frequency content between 10-15 Hz
for the body longitudinal acceleration, while the content remains the same for
the rest of the frequency band.

The lateral forces in the left rear UCA and LCA are shown on Figure 5.29, while

the responses for the longitudinal direction are shown on Figure 5.30. Both of these plot

show very little change in the forces transmitted to the body of the vehicle. This makes

sense, since the deformation of the flexible body is minimal, which results in a negligible

change in suspension geometry due to deformation. As was shown in the previous

section regarding suspension geometry, forces can change drastically based on similar

suspension geometries.

163
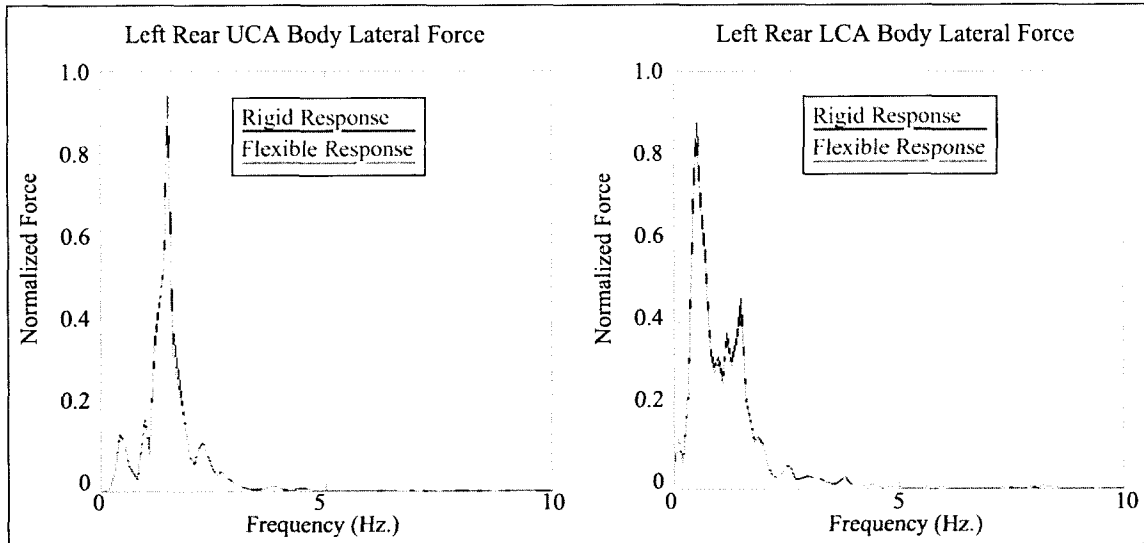
**Figure 5.29**: Comparison of left rear UCA and LCA lateral forces using rigid and flexible bodies. As can be seen in both cases, the forces remain essentially unchanged when flexibly is introduced into the system.
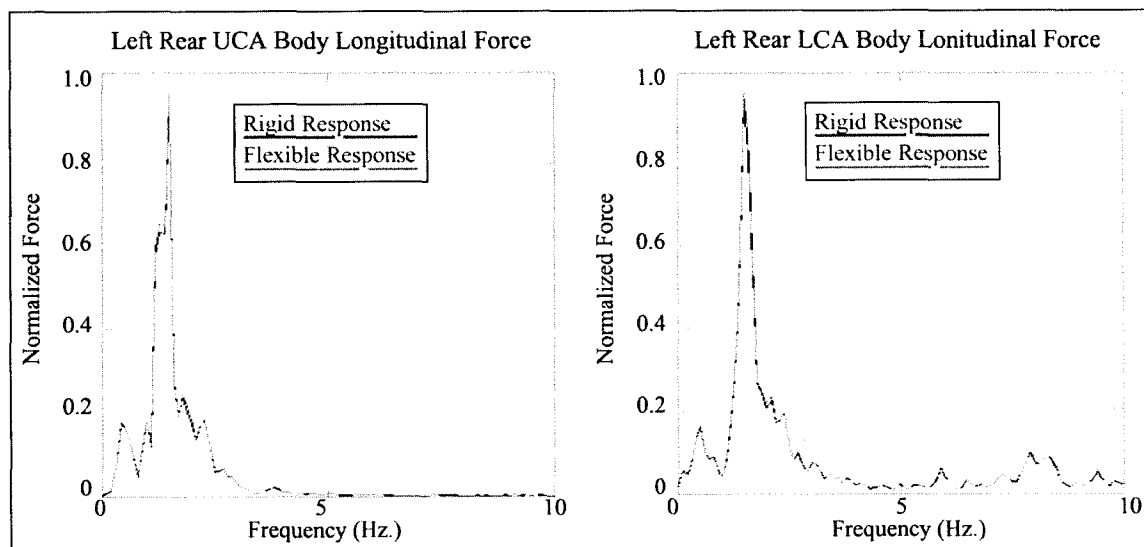


**Figure 5.30**: Comparison of left rear UCA and LCA longitudinal forces using rigid and flexible bodies. As shown in both cases, the forces remain essentially unchanged when flexibly is introduced into the system.

An illustration of the flexible body under dynamic loading is shown in Figure 5.31. The fringe on the right shows the von Mises stress in the UCA. Unfortunately, no strain gauges were available for any of the parts for the purposes of correlation, so the flexibility cannot be validated similar to the rest of the model.

164
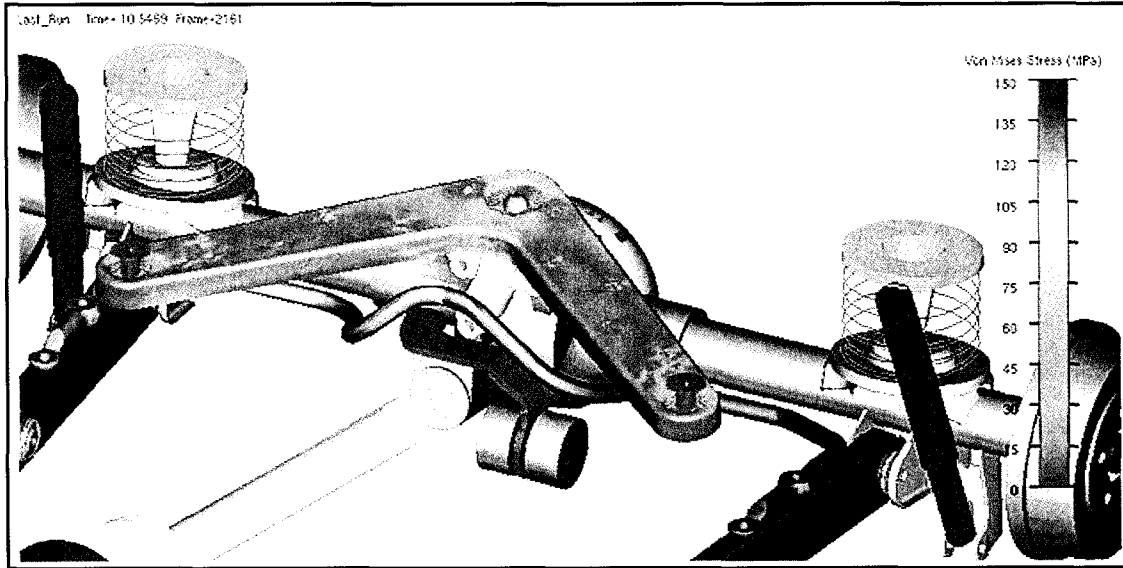
**Figure 5.31**: Rear suspension system shown in ADAMS showing the stress distribution in the flexible upper control arm. Unfortunately, no strain gauges were located on this specimen on the test vehicle, so a precise correlation could not be performed. Note the local stress concentrations around the small holes stamped into control arm itself.

Since the results based on the addition of the UCA as a flexible body proved to be promising, the stabilizer bar was used in the model as a flexible body while the other components were left as rigid bodies. A comparison of values is shown in Figure 5.32, where the lateral and longitudinal accelerations are shown. The vertical direction is not shown, because as expected, the output remains unchanged. The longitudinal direction show very little effects of the addition of the flexible stabilizer bar. The lateral direction on the other hand shows that the flexibility improves the correlation dramatically across the entire frequency band. The only frequency that is not duplicated is in the 14 Hz range. Based on these results, it is apparent the addition of the stabilizer will improve the lateral acceleration results in the model.

165
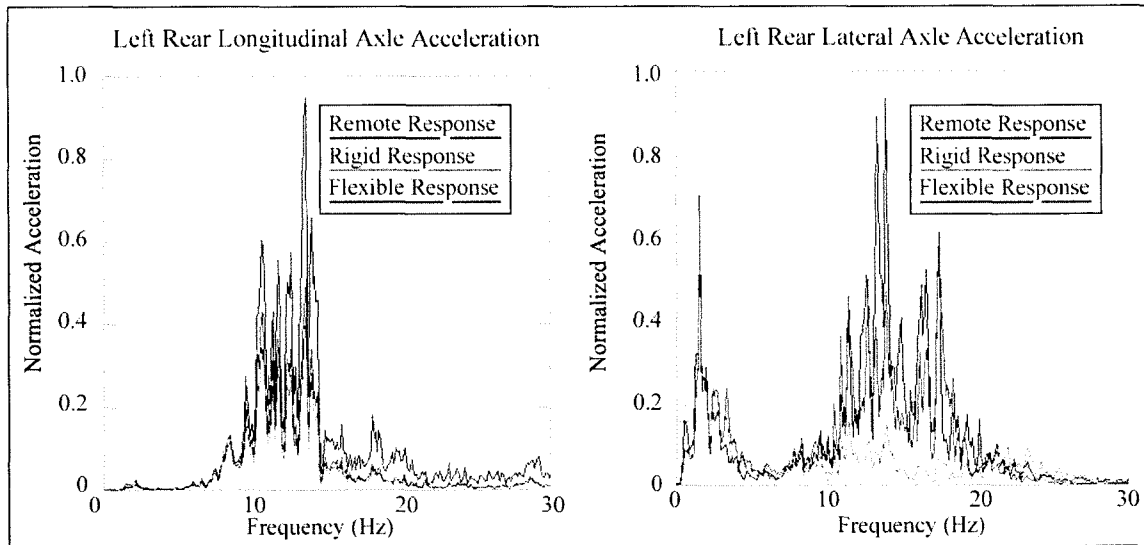
**Figure 5.32**: Comparison of left rear rigid body and flexible body longitudinal and lateral accelerations for the axle assembly. The longitudinal acceleration remained essentially the same, while a drastic change was noted in the magnitude in the lateral direction. By adding the stabilizer bar into the model, the lateral channel was now placed in close correlation to the remote response.

After inserting the UCA and stabilizer bar into the model, the entire rear suspension assembly was attempted in ADAMS. The simulation time increases this time by a factor of 8-10 in comparison to a single flexible body. Problems occurred in the amount of memory required by ADAMS, and the simulations often failed as a result. The times could likely be decreased if the finite element meshes were refined and optimized. This in itself is very time consuming, but would be interesting to see how much of an effect that refining the model, or reducing the number of mode shapes would have on the simulation and post-processing times. Although a comparable 50 second simulation could not be created, Figure 5.33 was generated to show how powerful ADAMS can be at calculating the stress profiles and stress concentrations during a dynamic simulation. A vehicle that contains strain gauges on the components to be treated as flexible bodies would give the ability to verify how close the stresses and strains actually are. This is obviously beyond the scope of this research, but may provide insight into potential future projects in this regard.

166
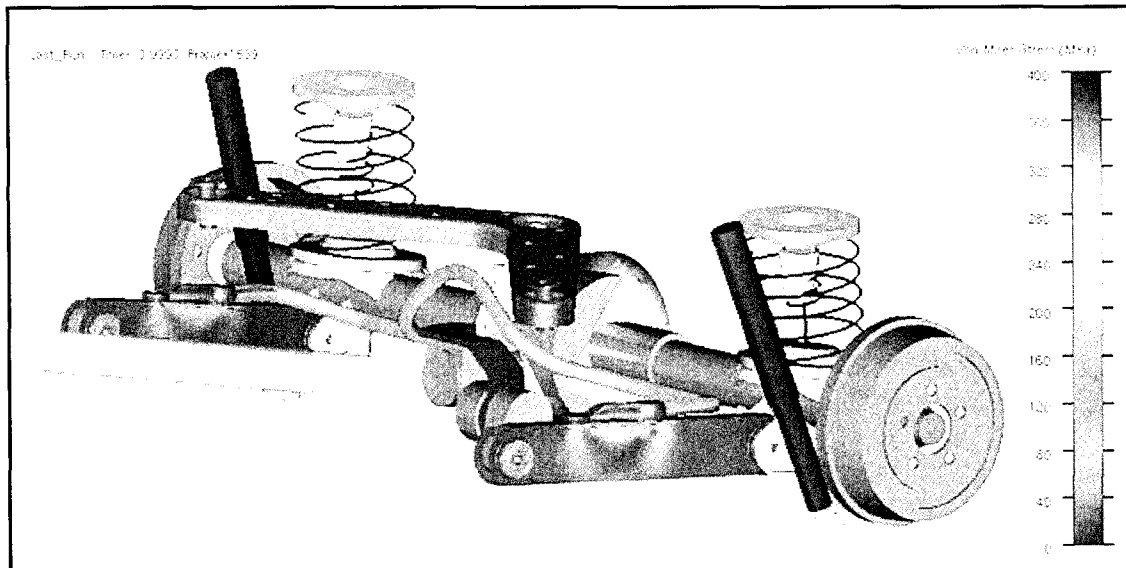
**Figure 5.33**: Rear suspension system shown in ADAMS showing the stress distribution in the flexible bodies incorporated into the rear suspension system. Note the stress distribution below the attachment point of the stabilizer bar to the LCA..

As shown in Figure 5.33, the stabilizer bar shows a higher stress along the entire bar. This is perfectly normal as the bar in is torsion, and is made of spring steel which has a much higher yield than regular hot or cold rolled steel. Norton {33} states that spring steel (tempered alloy strip) has an ultimate tensile strength of approximately 1700 MPa (246 ksi).

In reality, the interface between the stabilizer bar and lower control arm would not be a rigid connection as was modeled in this research. Preloads are also involved when a fastener is used to connect one part to another, which would also be difficult to simulate using ADAMS, unless a residual force (preload) is added. This may be an appropriate area to investigate the usage of contact between flexible bodies in future research projects. Fastener connections and related preload investigations may also add to the refinement of this model in this respect. Literally every suspension component could be treated as a flexible body in this model, but that would be very time consuming, and is well beyond the scope of this research.

167

## 5.5.1 Drawbacks to using Flexible Bodies

By adding a flexibly body into the system, the simulation time can easily double or triple based on comparisons made with equivalent rigid models (Test run using one flexible body only). This is simply the time required to run a model, with no post-processing that involves stress analysis. As noted in earlier chapters, contact was avoided in this model due to the amount of time required to solve contact related problems. If contacts were to be included in models incorporating flexible bodies, the simulation time would be even larger.

Model playback is considerably slower in comparison to rigid bodies. It was found that the amount of nodes on the body does not affect the simulation time in comparison to another similar flexible body with less nodes using the same number of mode shapes. Post processing also takes a great deal longer to perform, and increases even more so if multiple flexible bodies are used. The post processing phase is a major downfall to flexible body simulation in ADAMS, as the amount of time it adds to analysis is high. Performing tasks as simple as changing the title of an animation can take upwards of ten minutes, when the change would be done instantly in the case where rigid bodies are used. This was witnessed when running a simulation of merely 10 seconds in duration, where a 50 second simulation using the full sampling rate could take a considerable amount of time to process. Each flexible body that is added will cause all of these associated times to increase proportionally.

Alternatively, it may be beneficial to perform a modal stress recovery (MSR) using FEA programs such as ANSYS or NASTRAN. Once a simulation is run in ADAMS, the ADAMS/Durability module allows flexible body modal deformations to be exported as modal deformation files (.mdf) for use in these FEA programs. When using NASTRAN, a DMAP "alter" function, *msr_v2001.alt*, is used to translate the modal deformation file so it can be solved using NASTRAN. The results can then be viewed in

168

an appropriate post-processor, such as PATRAN, to observe stress and strain outputs. With the more recent acquisition of ADAMS by MSC, the bridge between ADAMS and a dedicated FEA program will inevitably grow stronger in the near future.

There is also a considerable amount of time required in creating finite element models for use in these flexible body simulations. Techniques for meshing components come with time and experience. This requires the skill level of the ADAMS user to move up to a higher level in order to incorporate these effects.

Many publications lead the reader to believe that creating an actual flexible body suitable for use in ADAMS is straightforward. This process is complex in nature and is by no means straightforward. A lack of documentation regarding this matter further complicates this issue. It is hoped that the detailed descriptions included within this thesis can serve as a valuable resource in the creation of flexible bodies.

## 5.6 Modeling the Road Test Simulator

The objective of incorporating the MTS 329 rig into the computer model was to be able to directly input displacements from the three hydraulic cylinders into equivalent cylinders in the computer model. Recall from Section 4.6.4, the input that is given by the local responses is the approximated displacement of the spindles. To excite the virtual rig, the cylinder displacements are used. To get the actual physical cylinder displacement, the calculations that MTS uses to calculate the spindle displacement were reversed, and consistant scaling factors were determined. The local response displacement inputs to each of the cylinders were multiplied by these scaling factors in the vertical, lateral, and longitudinal directions, which gave the input necessary to drive the virtual model.

The road test simulator was modeled into order to gain insight into how to correctly apply inputs to the vehicle in the computer model, and also to explore how the

169

machine itself constrains vehicle motion. This would help to show any indications of whether significant system coupling between the vertical, longitudinal, and lateral channels were present.

### 5.6.1 Building the Virtual RTS Rig Model

To build an accurate computer model of the RTS equipment, detailed drawings of the components were acquired from MTS Corporation {30}, and geometric models were prepared in CATIA. The weights of the components were estimated based on the geometry and material properties, as the actual weights were not available. CAT/ADAMS was used to transfer this model into ADAMS. Once in ADAMS, revolute joints, spherical joints, and prismatic joints were used to constrain the motion of the test rig. Bushings were also used to allow the necessary movements to prevent the model from locking up. The values for the bushings were estimated, as the purpose of this operation was to observe the motions of the rig, and how they affect the frequency of the vehicle system. Bushing properties were not available from the manufacturers, and if the facilities exist in the future, bushings should be tested in-house to allow for an accurate model to be assembled.

The RTS rig can be driven using forces or by specifying displacements at the hydraulic cylinders, as would be done on the physical model itself. The vertical direction is driven by displacement only, while the longitudinal and lateral directions can be driven by either force or displacement. A visual representation of the MTS 329 test rig can be seen in Figure 5.34, and a summary of the ADAMS model can be seen on Table 5.4.

170
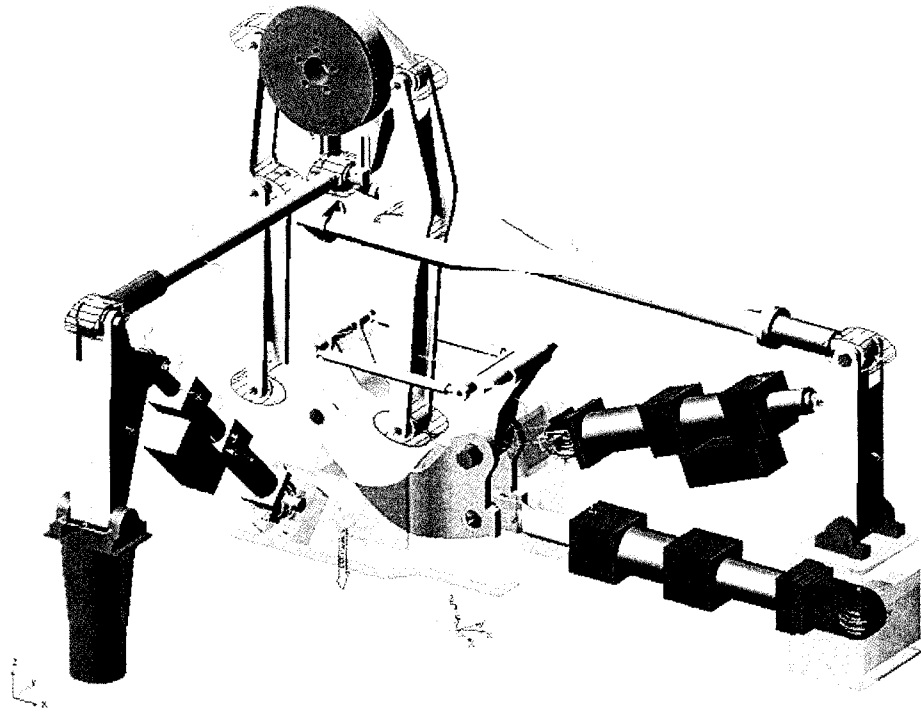
**Figure 5.34**: ADAMS model of a MTS 329 series road test simulator. This model was created entirely in CATIA, and can be controlled vertically by displacement, and by force or displacement in the lateral and longitudinal directions. Transparency has been set to specific parts for clarity.

| Summary of MTS 329 Road Test Simulator Properties in ADAMS | |
|---|---|
| Item Description | |
| Moving parts | 20 |
| Revolute joints | 5 |
| Spherical joints | 8 |
| Translational joints | 3 |
| Fixed joints | 6 |
| Input motions | 3 |
| Bushings | 9 |
| **Degrees of Freedom (DOF)** | 35 |

**Table 5.4**: Summary of the ADAMS model statistics for an MTS 329 Road Test Simulator illustrating one corner only. Multiply these values by 4 to get the entire rig at all four corners, as it would be in the laboratory. This is assuming that the rig is driven through the 3 translational joints at the hydraulic actuators.

171

### 5.6.2 Full Displacement Input

Full displacement input process removes the most DOF (3 per corner) from the system, and fixes the position of the spindles in time. The spindles are still free to rotate, and model will not drift into space due to these constraints.

One issue that arises when attempting to use displacement input is with the rear suspension of the vehicle. The rear axle assembly is being treated as a rigid body, and as a result can only be driven in certain directions using displacement input in each direction. The greatest problem occurs in the lateral direction, where opposing displacements have to be used. Since the axle is not flexible, using opposing displacements will not work, and will cause the simulation to "lock up" meaning that these conditions are not possible to solve numerically.

A solution that was derived in this case was to use a massless part at one end of the axle assembly that is constrained to move along the centerline of the axle tubes using a translational joint. A spring connects the "dummy axle" to the axle assembly itself and is used to absorb the difference in the lateral displacements.

One problem with this type of input is with the lateral and longitudinal directions. By using displacement input, the spindle positions are fixed in time. When using a rigid body model, the only portions of the model that allow compliance are the bushings, and spring elements. This does not pose a problem in the vertical direction, but does in the longitudinal and lateral directions where opposing displacements are used. In these directions, the bushings are forced to displace a certain amount regardless of the force that is generated within them, due to the fact that displacement input it used. The only way to reduce these forces is to scale the displacement input, or to reduce the stiffness of the bushings. By scaling the input displacements, the acceleration is also scaled accordingly, which affects these results.

172

### 5.6.3 Adding the Road Test Simulator to the Vehicle Model

The ADAMS model of the MTS 329 test rig was then added into the system to simulate the operation of the vehicle when driven by the RTS machine. An additional model had to be created in CATIA and ADAMS to make a mirror image of the assembly along the longitudinal plane of the vehicle, which gives a left and right hand side to the machine. This gave a "half-rig" assembly. To create a full rig, the half rig was copied, rotated 180 degrees, and then positioned so that it lined up with the spindles of the vehicle. The vehicle was attached to the rig using revolute joints about the spindle centreline. This was done because the vehicle is run on the machine in neutral gear, which allows the spindles to rotate freely. If the vehicle model was to be attached to the spindle using a fixed joint, the rig model will tend to impose a moment on the suspension assembles, which does not occur in reality (unless braking torque is used).

This model, which is shown in Figure 5.35 was assembled to analyze vehicle movement when the motion is constrained by the rig. The properties of this model are shown in Table 5.5. The objective was to determine whether applying simple loadings at the spindles (x,y,z directions) was sufficient to represent the test rig. Studies into the actual operation and function of the rig were well beyond the scope of the present research project, as accurate component properties were not obtainable. Difficulties arose when running this model due to the amount of processing time, and the large amount of disk space required in monitoring the movements of the entire assembly during long duration simulations.

The model created can be used as a powerful research tool, and can be used for any simulations involving this RTS machine, since it is not limited to the vehicle being tested. Further correlation for the rig itself is required for validation, and is presented in more detail as a future work proposal in Chapter 6.

173
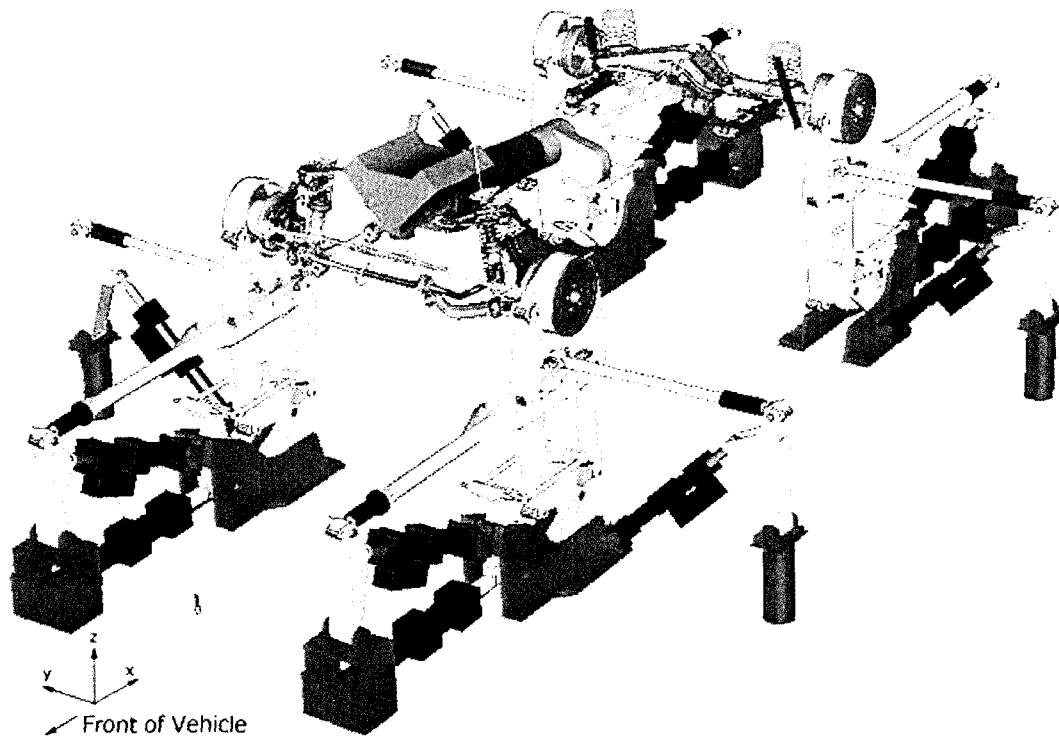
**Figure 5.35**: ADAMS model representation of a full vehicle mounted on an MTS 329 series passenger car spindle coupled road test simulator. This model is controlled using primarily using vertical displacement, but can be controlled using input forces.

| Summary of Model Properties for a Full Vehicle Model Mounted on a Virtual RTS Rig in ADAMS | |
|---|---|
| Item Description | |
| Moving parts | 143 |
| Revolute joints | 42 |
| Spherical joints | 25 |
| Translational joints | 17 |
| Fixed joints | 49 |
| Point-Curves | 2 |
| Input motions | 12 |
| Bushings | 61 |
| **Degrees of Freedom (DOF)** | 186 |

**Table 5.5**: Summary of the ADAMS model statistics for a test vehicle mounted on an MTS 329 Road Test Simulator. The spindles are attached to the rig at each corner using revolute joints. These values are stated assuming the rig is driven though the 12 translational joints at the hydraulic actuators.

174

# CHAPTER 6  CONCLUSIONS AND RECOMMENDATIONS

## 6.0 General

This chapter outlines the findings of the current research, and how they relate to

the proposed objectives.  Recommendations have been given on how to improve results

with both this simulation, and with any further simulations to be conducted of this nature.

Objectives for future work have also been addressed, building on what was discovered in

the current project, as well as directing this technology towards other areas of research.

## 6.1 Conclusions

A multibody dynamics model of a compact sport utility vehicle (SUV) has been

created and validation studies have been performed for the purpose of this research.

CATIA, ADAMS, and NASTRAN software suites proved to be very effective in the

creation of this model, as many aspects regarding the behavior of the "virtual" vehicle

closely represented that of the actual vehicle.

One proving ground road course was used primarily for correlation studies, and

the road chosen was known to be damaging to the vehicle.  By choosing the most

damaging road, frequencies and amplitudes that are most influential on the durability of

the vehicle can be tested and validated using the virtual model.  The model was tested

175

using data collected at full rated load (FRL) at a proving ground, as this places the highest stress on components due to the larger vehicle weight, reduced suspension travel, and jounce conditions as result of this.

Static validation of the vehicle model showed that the mass distribution of the virtual vehicle matched that of the physical test vehicle, by comparing the corner weights of the vehicle at FRL. Various types of input methods to the virtual model were tested while performing dynamic simulations. After conduction simulations and comparing virtual to physical results, the method using vertical displacement, longitudinal forces, and lateral forces produced the closest correlation. Ideally, a full displacement input would have been preferred due the nature in which it constrains the model, however, adequate input data was not available for usage. Several methods for acquiring input data in the form of displacements have been recommended in Section 5.2.

Dynamic simulations showed very strong correlation in channels relating to the vertical movements of the vehicle. These include the forces in the springs, shocks, jounce bumpers, as well as the control arm angles themselves. Vertical forces accelerations account for over 75% of the damage incurred during durability testing according to many engineers in the related field, which signifies the importance on the verification of this particular data.

Correlation in the lateral and longitudinal directions proved to be much more difficult. The rear lateral and longitudinal accelerations as measured on the axle correlated well, as did the lateral accelerations in the front. The longitudinal accelerations measured virtually on the front of the vehicle differed from the remote responses partially due to steering movement, since the accelerometers were located on the steering knuckles. The knuckles are free to rotate, so a spring was used to restrict movement, but tended to excite higher frequencies. By recording the movement of the steering of the vehicle while on the RTS rig, closer correlation may be possible. The

176

difficulty in correlating lateral and longitudinal accelerations was also noted by Ferry{17}, and is likely the reason that close correlation was not reproduced in any publications regarding this subject.

The control arm angles for both the front and rear of the vehicle correlate nearly exactly, further confirming that the relative motion of the body (sprung mass) relative to the suspension (unsprung mass) is accurate.

The correlation of this model often presents a sacrifice when adjusting parameters. Often times, adjustments are made where the acceleration results improve dramatically, while the forces would vary by several orders of magnitude. The results presented here are the result of many simulations that were conducted, and represent the best compromise of both acceleration and forces that were attainable based on performed simulations.

All of the force sensors that were used on the test vehicle at the proving grounds were also monitored in the ADAMS model. Strong correlation was shown for these virtual force sensors, where each sensor predicted accurate forces to within 15% of the recorded physical forces based on comparisons using PSD plots in frequency domain. Having the forces in the model correlate is crucial in attaining valid results for stress and strain in flexible bodies, and is also critical if a fatigue life prediction (FLP) is to be done on the components.

Methods of process automation in ADAMS were devised to address the need to rapidly change component configurations. These not only change the graphics displayed to the user, but also change the component properties, such as stiffness and damping, so that design studies can be evaluated. Other menus were created to change road inputs, and also to quickly scale the values of component properties such as bushings and stabilizer bars. Techniques were also devised to automate the processing of virtual model output.

177

These automation methods not only reduce the amount of time in running simulations, but also make the model more user friendly, such that users other than the original creator of the model can reproduce simulations fast and effectively. The ability to create these flexible interactive menus in ADAMS serves as a very powerful tool to optimize the usage and operation of each specific model.

Two different rear suspension configurations were analyzed using ADAMS, where suspension vibration modes, forces and acceleration were compared between the two designs. Simulations dictated a reduction in forces transmitted to the body, which confirms that it may be necessary to use independent datasets in order to assess durability concerns, since the forces and accelerations are significantly different.

Documentation regarding the creation of flexible bodies from start to finish for use in ADAMS was found to be virtually non-existent. As a result, methods for creating them were explored and documented. This research highlights the methodology used in the creation of flexible bodies using CATIA, ADAMS and NASTRAN software, and explains general guidelines involved in their creation. A step by step methodology is presented, with the intent of having a start to finish procedure self-contained within this document.

Flexible bodies were successfully implemented into the ADAMS model in the form of rear suspension components. Simulations were run using the rear upper control arm as well as the rear stabilizer bar. The simulations showed that the addition of flexible bodies dramatically altered the acceleration of the rear axle assembly, while a majority of the forces remained unchanged. The addition of the stabilizer bar greatly increased the correlation in the lateral direction, which may help to explain why there was a difference compared to the rigid model. While many other components could have been meshed and analyzed using ADAMS, this research provides a backbone from which

178

to build, both with the rigid body model, and with complete documentation regarding the addition of flexibility into the system.

Numerous critical assumptions were made throughout this research project. It was assumed that the component properties, such as springs, shock absorbers, and bushings were correct based on the information provided from the manufacturers. Many of these values were represented as linear approximations in the ADAMS model, which inevitably will affect the results, but this greatly decreases simulation times. In many cases, only basic linear approximations of component properties are available. Less significant concerns such as vehicle alignment and manufacturing tolerances were also not considered in this research project. Several recommendations and future work regarding this research project have been suggested in the sections to follow.

## 6.2 Recommendations for Future Work

**Further Instrumentation**: In order to monitor the motion of the body and the powertrain assembly, further instrumentation should be used in the form of accelerometers. These would allow the bushings to be tuned separately for the engine, as well as for tuning the motion of the body structure. The model used in the current research only allowed for the acceleration measurement of the front and rear suspension assemblies alone. The only sensors available to validate the motion of the body in the current testing are the control arm angles, as well as the spring and shock forces. These only allow for validation in the vertical direction. This provides very little feedback about the effect of bushing stiffness or stabilizer bar rates on body motion.

To facilitate the validation of flexible bodies, strain gauges should be strategically placed on the vehicle on any component that is to be replaced by a flexible body. This way, a node can be created on the flexible body in the ADAMS model, which can be

179

compared to the physical strain gauge data at a point, to confirm whether the stress and strain values are in close comparison.

While running virtual simulations without incorporating a virtual RTS rig, it is difficult to predict the steering behavior of the vehicle. Vehicles tested at the proving grounds do have existing sensors to monitor steering response, but these channels are not monitored while testing on the RTS rigs. If these channels were monitored, they could be input into the ADAMS model to accurately predict steering behavior. This would allow for easier correlation of lateral and longitudinal accelerations on the steering knuckles, and would reduce the number of unknowns in the model.

Accurate positioning information regarding sensor placement is also critical when correlating virtual models.

**Measuring Spindle Absolute Displacement:** If a means could be devised in order to measure the absolute displacement of the spindles, this would give the true displacements of the system, independent of the coupling effects within the MTS rig itself. This would allow the models to be driven purely with displacement, eliminating the need to use stabilizing bushings or force input. If absolute spindle displacement is to be used with independent front suspension, the rotation of the spindle (about a longitudinal axis) would also be required. This rotational information would only be necessary for the rear axle if flexibility effects are considered.

MTS uses optical sensors (lasers) to measure the absolute displacement of the spindles on some of their Kinematics and Compliance (K&C) machines. If a similar method could be devised using the 329 machine, this would positively confirm the spindle position, making the ADAMS models much easier to drive with displacement input. Any error introduced in calculated displacement at the spindles will increase or decrease the forces in the vehicle dramatically as noted in the previous chapter.

180

**Create a Database of Component Properties:** A large potion of the time spent on this project was spent determining the mass and inertial properties of separate components, as well as seeking rate properties for components in-house and from suppliers. Now that the data is cataloged on spreadsheets for this vehicle and several others, it would be very beneficial to transfer these values to a database for easy access and retrieval of information. This would reduce the amount of redundant time spent seeking mass and/or rate properties for specific components. Several datasets do exist on the internal network from which some of the information on this project was drawn. With this in mind, a database using software such as Microsoft Access would not only help researchers locally, but it would assist globally within the company.

**Validation of the MTS Road Test Simulator:** To conduct accurate simulations using the MTS RTS 329 machine, the bushing parameters will have to be determined. Each bushing parameter on the machine can be determined through the manufacturer, or by using in-house testing methods. Since the RTS machine has four similar quadrants, the bushing properties will be the same for each. Correlation for the virtual rig should be performed using a half-rig set-up. Using the half-rig will reduce the amount of moving parts in the system, and in particular the body, which will greatly reduce the amount of variables, as well as the degrees of freedom. Elementary tests can be executed by running simple known inputs, such as sine sweeps or white noise, and forces and acceleration can be monitored through instrumentation of the component. An identical model can be devised in ADAMS using the existing model that has been created as part of this thesis.

The geometry of the RTS machine has been created in CATIA using construction drawings from the manufacturer. The weight of the separate components should be confirmed by weighing the components themselves, which will allow the density of the objects in the model to be adjusted as to closely approximate the mass and inertia

181

properties of the rig itself. Looking ahead even further, ADAMS/Controls and ADAMS/Hydraulics packages may be used to drive the rig if preliminary results prove to be promising. The definitive objective of this process is to be able to completely replicate the RTS process, with the only input being the proving ground data. This way, initial drive files could be predicted virtually, which would greatly increase the efficiency of the physical RTS process, and may give insight in how to improve current strategies used by the RTS engineers.

The main point of interest is in characterizing the motion of the test rig in the lateral direction, as it determined by the movement of the spindle adapter. It may be useful to instrument the rig itself to monitor the rotation of the spindle adapter on the testing apparatus. Digital inclinometers may prove to be useful for this task, where one can be placed on the spindle adapter, and another can be placed on the vertical strut. This would aid in determining the rotation of the spindle relative to the vertical upright of the MTS machine while testing the vehicle on the rig. Using similar techniques, the rotation of the spindle adapter about a vertical axis may be used to determine the movement of the vehicle's spindles (steering effects).

**Accurate Component Characterization:** Non-linear elements including bushings and dampers proved to be very difficult to accurately represent in the current research. Several other researchers have presented other potential methods, which reduces the dependence on suppliers for data, and may allow components to be tested in-house. Dzierżek {14} showed that accurate results can be attained for bushings using finite element methods. Durali et al. {13} presented neural network approximations to model non-linear behavior of a vehicle using ADAMS. MTS Corporation has devised EDM (Empirical Dynamics Method), and Barber {4} has demonstrated EDM methods to characterize bushings and dampers accurately using "blackbox" methods. Other means of characterizing components including the building of testing apparatuses may also

182

make determining a set of accurate component data possible. It may also be beneficial to devise methods of testing the friction in components, such as ball joints, to observe the effect that this may have on the system. This could save a great deal of time, and may provide more reassurance in the validity of the component properties being used in computer models. Having accurate component properties is the key to precise model correlation.

**Vehicle Dynamics Simulation**: The model presented in this research is an accurate model containing mass and inertial properties of the critical components of the vehicle, which makes it suitable for other related dynamic simulations. If a tire model is applied to the vehicle, through such means as ADAMS/Tire or through user defined methods, ride and handling could be investigated. This would involve inputting effective road profiles in order to excite the system. In this case, more attention could be given to the effects of suspension alignment, as this model was assembled at curb position, and did not take into consideration alignment variances including toe, caster, or camber.

The model was purposely built with many extra parts connected with fixed joints in ADAMS to facilitate components to be easily inserted with minimal modification to surrounding systems. This may allow for additional sub-systems, such as the braking system to be investigated, which could include such entities as anti-lock braking simulations. Braking simulations could be conducted to investigate squat and dive characteristics, and effects of brake biasing could be researched. This model can also be useful in clearance studies as well.

**Vibration Analysis:** Testing for vibration fatigue of individual vehicle components requires an accurate set of vibration data to exist. If vehicles do not have accelerometers or load sensors placed on them during proving ground or laboratory testing, and additional vehicle will have to be tested. ADAMS allows the acceleration of any point to be monitored, and also allows one to output this information in DAC or RPC

183

III format. This data could potentially be used to drive physical fatigue set-ups, as well as virtual model testing of such items as brackets, hardware and even interior components.

**Body Flexibility Effects:** The definitive complement to this model would be the addition of a flexible Body in White (BIW) structure. This would involve creating the body structure as a flexible body, allowing it to strain with loading. This would be difficult to model, and the boundary conditions would be complicated. Key areas of interest would be where suspension components were mounted, such as shock towers, spring perches, and control arm mounting brackets. This would allow for early prediction of the body structure, including sheet metal and spot-weld failure. The main drawback to this would be the computational time involved on top of what is already required, and the complexity of creating such a model. It may be beneficial to represent the body as a torsional stiffness, in attempt to approximate these flexible effects. Common values of torsional stiffness for these vehicles could be used as a starting point.

**Virtual Proving Ground:** In the future, the objective is to apply the current research to the creation of vehicles in the virtual realm before a prototype is ever produced. This poses a problem, where the techniques proposed rely on having data provided based on input from the RTS rigs. This data is acquired from test vehicles on the proving ground and on the RTS rigs. During the virtual prototyping cycle, this data will not exist, since a physical vehicle itself will not exist. The model created in this research could be used along with an accurate tire model to represent the full vehicle model. Once a tire model is incorporated, the vehicle can be run over virtual road profiles, which would also have to be generated, based off the road courses at a proving ground.

**Four Poster Adaptation:** Since correlation proved to be straightforward in the vertical direction in this research, this model may potentially be used to conduct virtual

184

simulations on the four post simulator. A four post simulator only uses vertical input to the system using electronically controlled hydraulic actuators, and is typically used in BSR (Buzz, Squeak and Rattle) testing. There are no lateral or longitudinal input channels involved in this type of simulation. This would involve introducing an appropriate tire model into the system (a simple bushing may even work), since this machine applies forces directly the tire of the vehicle. Virtual model inputs can be used in a similar way as in this research, and can be retrieved from physical MTS test data. Information recorded in this type of virtual simulation would be beneficial for both durability and for NVH (Noise, Vibration, and Harshness) testing.

**6 DOF MTS 329LT (Light Truck) Rig Correlation:** Issues with the movement of the RTS rig in the lateral direction proved to be difficult to characterize due to the coupled motion of the rig, as well as the instrumentation used. The MTS 329LT 6 DOF rigs have two additional actuators that connect directly to the vertical struts in order to apply additional moments to a vehicle. The displacement that is recorded from the actuator movement will allow for the monitoring of the lateral motion of the vertical struts as well as the rotation of the spindle adapter that connects to the spindle of the vehicle. The movement of a virtual vehicle may be easier to characterize using this type of rig compared to the 4 DOF machine as used in this research.

**Durability Analysis:** The next logical step in the process now that flexible bodies have been implemented is to perform a fatigue life prediction (FLP) on the components to estimate their life expectancy. To get an accurate prediction of the durability of the component would require the vehicle to be simulated over several other road courses, as well as at other payloads. Simulations can be run in ADAMS, and results can be exported for use in programs such as FE-Fatigue. Ultimately, calculated fatigue lives can be compared to actual failures in the laboratory and proving grounds for correlation purposes.

185

1.  Adams, V. , Askenazi, A., "Building Better Products with Finite Element Analysis", Onward Press, 1999.

2.  Ambrósio, J.A.C., Gonçalves, J.P.C., "Complex Mulitibody Systems with Application to Vehicle Dynamics", Multibody System Dynamics, Kluwer Academic Publishers, 2001.

3.  Barak P., "Chassis & Suspension Component Design For Passenger Cars & Light Trucks", SAE Seminars, 2000.

4.  Barber, A.J., "Accurate Models for Bushings and Dampers using the Emperical Dynamics Method", Modeling Integration Products and Services, MTS Systems Corporation 1999.

5.  Blakely, K., "MSC/NASTRAN Basic Dynamic Analysis", The MacNeil-Schwendler Corporation, 1996.

6.  Caffrey, J.P., Lee, J.M, "MSC/NASTRAN Linear Static Analysis", The MacNeil-Schwendler Corporation, 1994.

7.  Campbell, R.M., "Analysis - When and When Not", SAE International Technical Paper 982011, 1998.

8.  Catelani, D. "Rules about FEM modelization for a correct interface to ADAMS and ADAMS/FLEX", Mechanical Dynamics Italy Inc, ADAMS Knowledgebase, 2002.

9.  Craig, R.R., Bampton, C.C., "Coupling of Substructures for Dynamic Analysis", AIAA Journal, 6(7): 1313-1319, 1968.

10. Craig, R.R., "Coupling of Substructures for Dynamic Analysis: An Overview", AIAA Dynamics Specialists Conference, Atlanta, GA, April 5, 2000.

11. Crolla, D.A., "Vehicle Dynamics – Theory into Practice",   Journal of Automobile Enginering, IMechE, 1996

12. Dittman, K.J., Albright, F.J., Leser, C., "Validation of Virtual Prototypes via a Virtual Test Laboratory", Eden Prairie, MN, USA, July 29, 2002.

13. Durali, M., "A Neural Network Approximation of Nonlinear Car Model Using ADAMS Simulation Results", SAE International Technical Paper 2001-01-3324, 2001

14. Dzierżek, S., "Experiment-Based Modelling of Cylindrical Rubber Bushings for the Simulation of Wheel Suspension Dynamic Behavior", SAE International Technical Paper 2000-01-0095, 2001.

15. Ewanochko, T.W., Nelson D., Esaki M. and Pesheck E., "Integrated Durability Analysis Using ANSYS, ADAMS and FE-Fatigue", Integrated Durability Analysis - 16th European Mechanical Dynamics User Conference, 2001.

16. Ferry, W.B., "Combining Virtual Simulation and Physical Vehicle Test Data to Optimize Automotive Durability Testing", M.A.Sc. Thesis, University of Windsor, 2002.

17. Gillespie, T.D., "Fundamentals of Vehicle Dynamics", Society of Automotive Engineers International, Warrendale, PA, 1992

18. Gockel, M.A., "MSC/NASTRAN Handbook for Superelement Analysis", The Macneil-Schwendler Corporation, 1982.

19. Grote, P., Sharp, M., "Defining the Vehicle Development Process", MTS Systems Corporation, 2001.

20. Grenier, G.C., Eisenlord, D.J., Leese, G.E., "Integration of Fatigue Analysis and Laboratory Simulation Requirements in the Field Data Acquisition Process", SAE International Technical Paper, 870805, 1987.

21. Harris B., Negrut D. "ADAMS Theory in a Nutshell", Department of Mechanical Engineering, The University of Michigan, Ann Arbor, Michigan, USA, 2001.

22. Hibbeler, R.C., "Engineering Mechanics, Statics and Dynamics", Eighth Edition, Prentice Hall, 1998.

23. Heydinger, G.J., Durisek, N.J., Coovert, D.A.Sr., Lawrence, R.D., Nowjack, J.A., Guenther, D.A., "An Overview of a Vehicle Inertia Measurement Facility", 27th International Symposium on Automotive Technology and Automation, Aachen Germany, 1994.

24. Kilroy, K., "MSC/NASTRAN Version 70 Quick Reference Guide", The Macneil-Schwendler Corporation, 1997.

25. Krishna, M.M.R., Kroppe, W.J., Anderson, S.V., "Flexibility Effects of Control Arms & Knuckle on Suspension – A Finite Element Vs. Rigid Body Comparative Analysis", SAE International Technical Paper 2000-01-3446, 2000.

26. McConville, J.B., "A survey of FEA-Based Stress Recovery Methods in ADAMS – Aircraft Model Case Study", North American ADAMS Users Conference, 2001

27. Mechanical Dynamics, Incorporated (MDI), "Using ADAMS/Flex", ADAMS/Solver Online Electronic User's Guide, Mechanical Dynamics Incorporated, 2002.

28. Mechanical Dynamics, Incorporated (MDI), "Using ADAMS/Solver", ADAMS/Solver Online Electronic User's Guide, Mechanical Dynamics Incorporated, 2002.

29. Meirovitch, L., "Methods of Analytical Dynamics", McGraw-Hill Company, 1970

30. MTS Systems Corporation, Vehicle Dynamics Division, "Series 329 Road Test Simulator Test System Manual", MTS Systems Corporation, USA, 1998.

31. Nasser, A.L., Dey, A., Tyron, R., "Simulation Tool for Predicting Warranty and Total Owenership Cost, SAE International Technical Paper 2002-01-0338, 2002

32. nCode Inc, Dynamics and Fatigue Group, "Vibration Fatigue", nCode Incorporated, 1997

33. Norton, R. L., "Design of Machinery, Second Edition", McGraw-Hill Company, 1999.

34. Ottarson, G., "ADAMS/Flex Theoretical Background", Mechanical Dynamics Incorporated, 2000.

35. Rao, P.S, Roccaforte, D., Campbell, R., Zhou, Hoa, "Developing and ADAMS Model of an Automobile Using Test Data", SAE International Technical Paper 2002-01-1567, 2002.

36. SAE International, "Vehicle Dynamics Terminology", SAE Standard J670e, Society of Automotive Engineers International, Warrendale, PA, 1976.

37. Shabana, A.A., "Flexible Multibody Dynamics: Review of Past and Present Developments", Kluwer Academic Publishers, Multibody Dynamic Systems 1: 189-222, 1997.

38. Shabana, A.,A., "Computational Dynamics", Second Edition, John Wiley and Sons, 2001.

39. Shabana, A.,A., "Dynamics of Multibody Systems", John Wiley and Sons, 1989.

40. Subramanyam, V., Monkaba, V., Alexander, T., "A Unique Approach to All-Wheel Drive Vehicle Dynamics Model Simulation and Correlation" SAE International Technical Paper 2000-01-3526, 2000.

41. Suh, K., Lee, Y., Yoon, H., "Dynamic Stress Analysis of Vehicle Frame by Flexible Multibody Dynamics Simulation", SAE International Technical Paper 2001-01-0032, 2001

# Appendix: Sample Flexible Body Creation Using ADAMS, PATRAN and NASTRAN software Suites

## A.1 General

The following section highlights the creation and validation of a flexible body using PATRAN, NASTRAN, and ADAMS software suites. A simple flat plate model was created using PATRAN software and contains 128 shell elements as shown in Figure A.1. This plate, which measures 98mm by 48mm by 1.5mm thick, was loaded using a static load of 20 N force which was applied to the tip of the plate in the center (Node 44). The back edge of the place was constrained by using an RBE2 element, where the independent node (attachment point in ADAMS) has all 6 DOF constrained using an SPC. A simulation was run in both NASTRAN (SOL 101 – Linear Static) and ADAMS, and the results are compared. A complete NASTRAN file is included at the end of this Appendix, and represents the coding used to generate and output file suitable for translation into ADAMS.

While this model may seem simple in nature, the techniques used in the creation and validation are similar to what is used to define a more complex component.
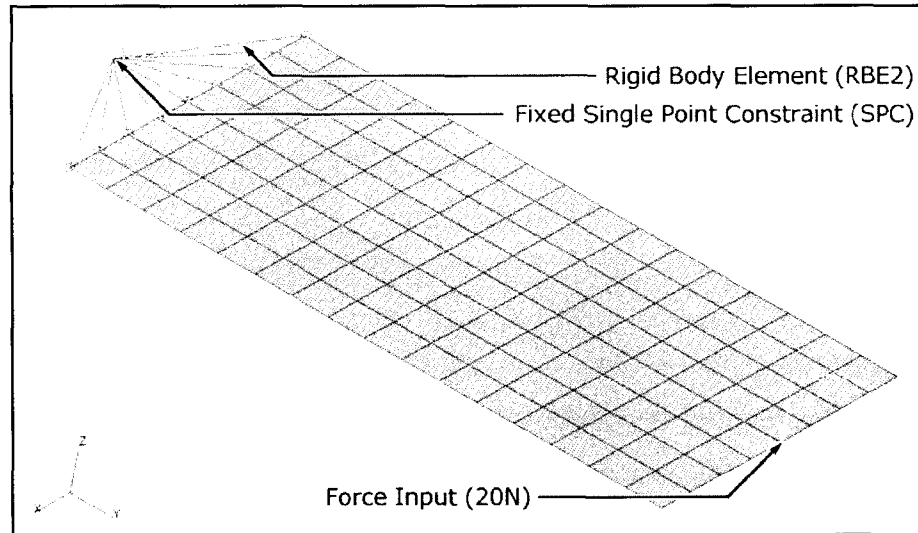
189

Figure A.1: Illustration of flat plate model using shell elements. A force of 20 N is applied at a single node at the tip of the 1.5mm thick plate. A multi-point constraint (MPC) in the form of and RBE2 element is used to restrain the back edge, while a single point constraint (SPC) is used on the independent node of the RBE2 element to fix all 6 DOF

## A.2 Results/Discussion

A constrained mode shape comparison was done as shown in Figures A.2 and A.3, where results are shown for the first mode (bending) in both PATRAN and ADAMS respectively. As is shown, the mode shapes and frequencies (134.95 Hz) are the same. Modal damping was disabled in these calculations.

The displacement of the plate was compared using PATRAN and ADAMS, and the results are shown in Figures A.4 and A.5. PATRAN reported a deflection of 2.13 mm at node 44, while ADAMS reported 2.124 mm at the same node. Node 44 is located at the tip of the plate. The deflection of the node in ADAMS was determined by placing a marker on the node, and the using ADAMS/Post to view the results.

The results of a linear static stress analysis are shown in Figures A.6 and A.7. The maximum von Mises stress was observed to be 101 MPa at Node 20 in both cases. Note that Node 20 is located on the back edge in the center, and also note that the stress contours are similar as well.
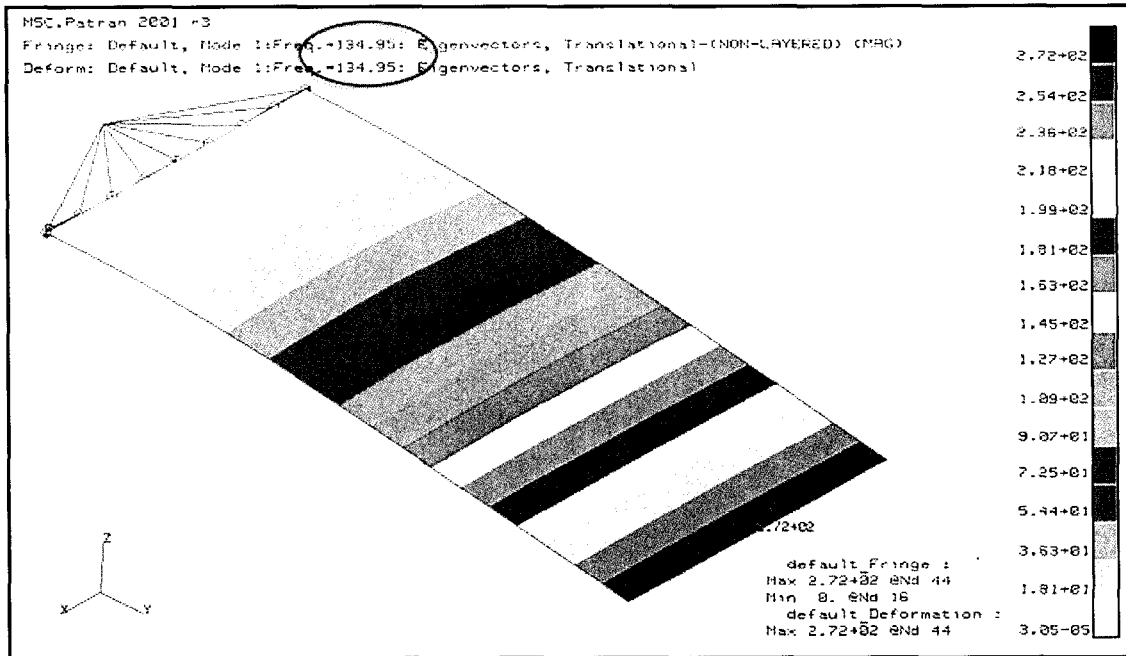
**Figure A.2**: Image showing a constrained normal mode analysis in PATRAN, where the first bending mode is shown. As shown in the image, the frequency is 134.95 Hz. The first step in the correlation process is validating these modes to confirm that the constraints are being treated the same in both programs.
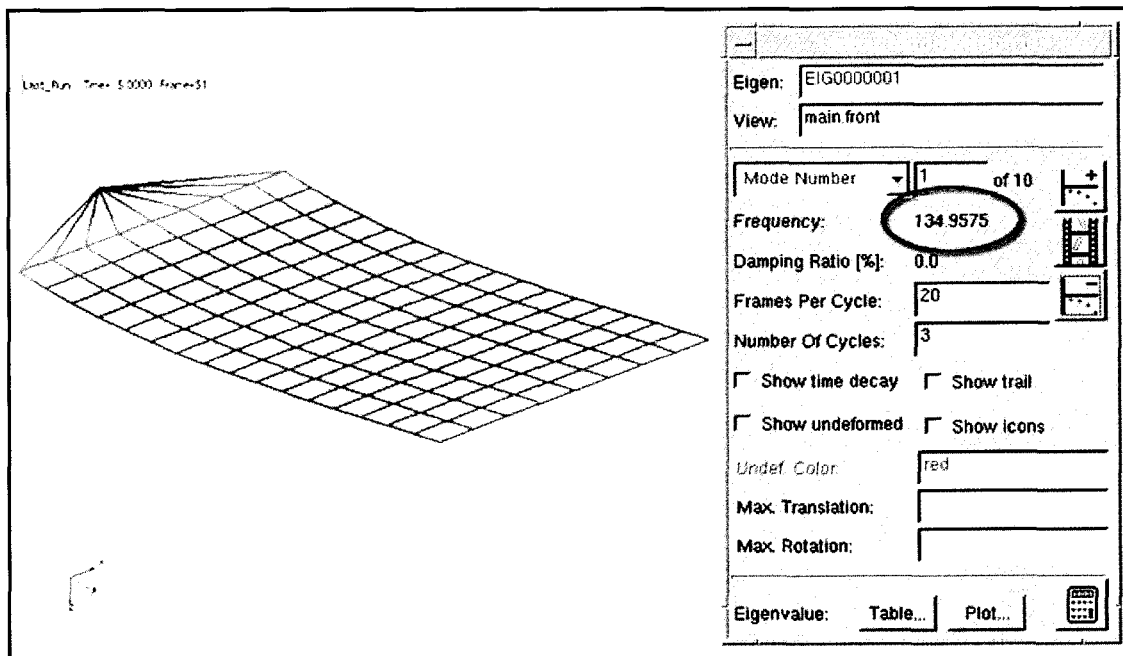


**Figure A.3**: Image showing the same constrained normal modes analysis as in Figure A.2, but this time using ADAMS software. The frequency predicted in ADAMS was 134.95 Hz, which is the same as in PATRAN above. These models use zero damping.

191
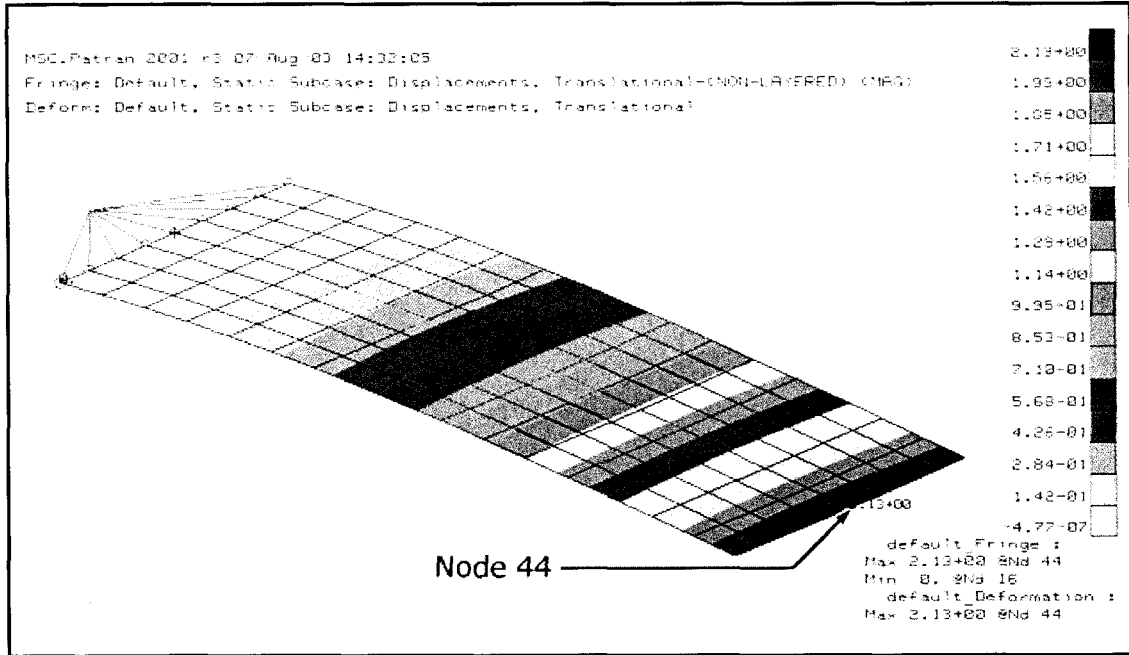
**Figure A.4**: Deflection of the flat plate model as shown in PATRAN. The undeformed shape is shown as a dotted line, while the contours are highlighted as a fringe, where the maximum deflection is noted as being 2.13 mm at the tip. This maximum deflection is measured at node 44 on the model.
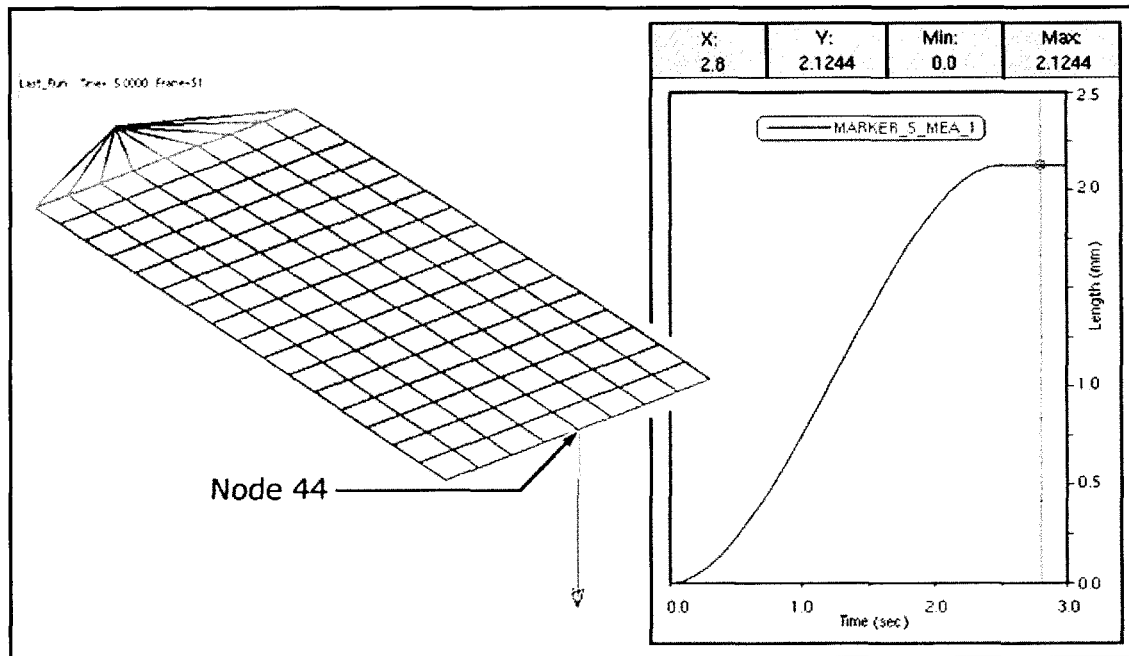


**Figure A.5**: Deflection of the flat plate model as shown in ADAMS/Post. A marker was added to node 44 in ADAMS, and the corresponding displacement plot is shown. A maximum displacement of 2.124mm was recorded, which is very close to the 2.13mm deflection observed above in Figure A.4.

192
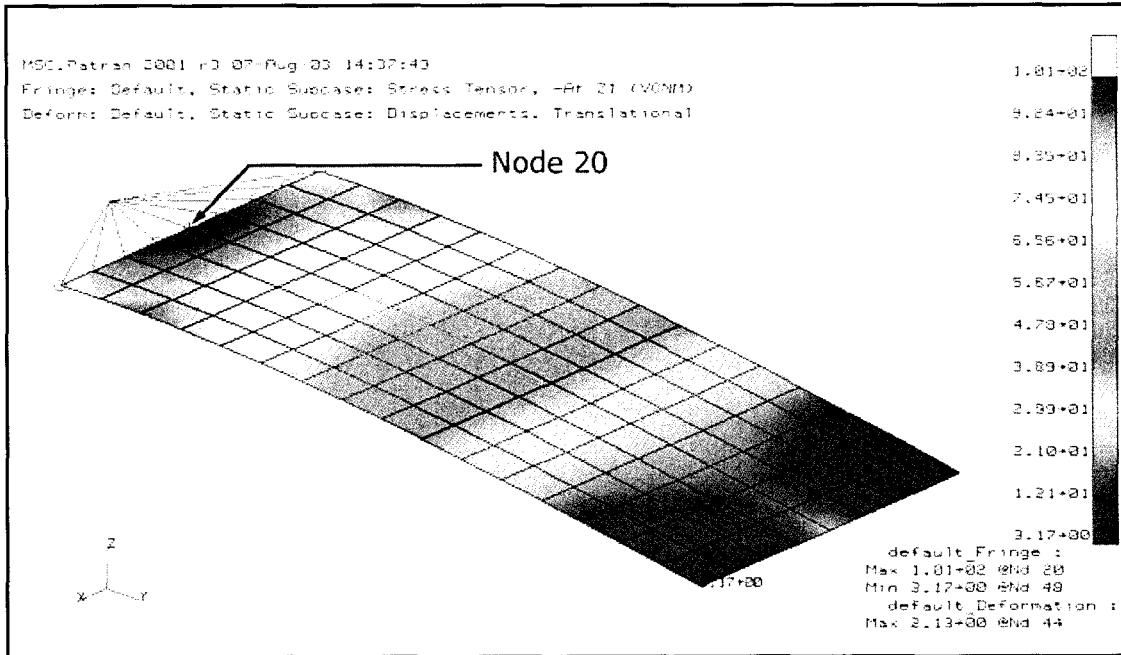
**Figure A.6**: Fringe plot showing the stress contours along the deformed flat plate in PATRAN. The maximum von Mises stress calculated was 101 MPa and was located at Node 20 as shown in the above plot.
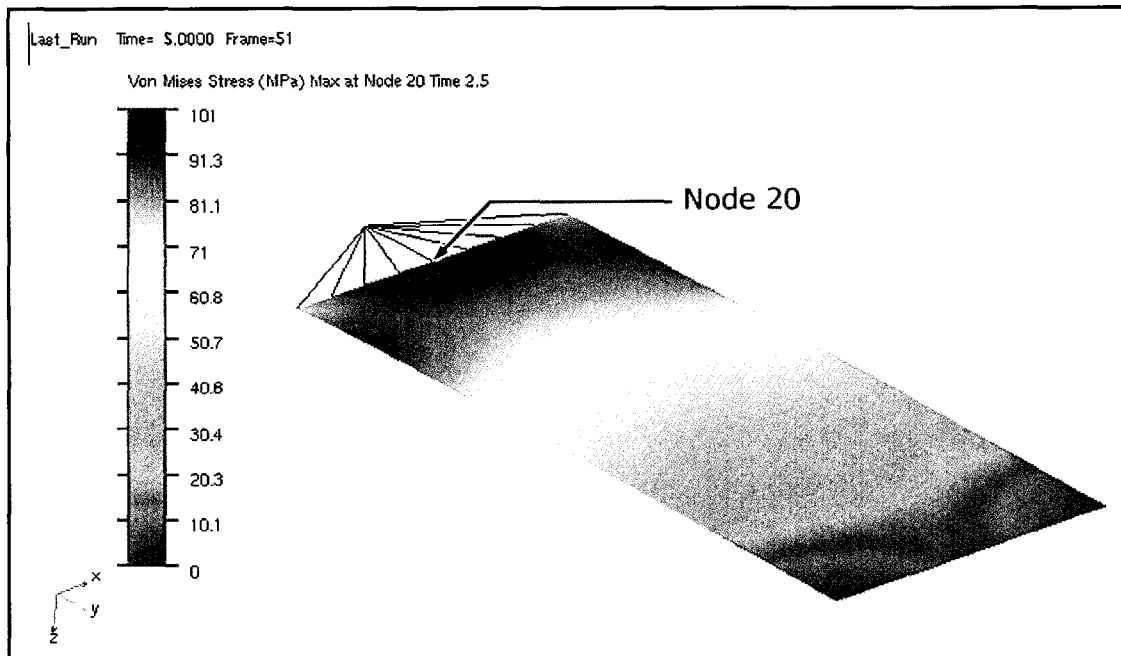


Figure A.7: Fringe plot of the same conditions in ADAMS, shown using the ADAMS/Durability plug-in for plotting these contours. A von Mises stress of 101 MPa was calculated at node 20, which is the same as listed above in Figure A.6. Note how the contours are similar in nature, although the colours represent different values in relation to contours, and the ADAMS contours are blended with a gradient.

193

The attached file, *plate_stress.bdf*, is a fully commented example of a FEM model created using NASTRAN code for use in ADAMS. Note that in NASTRAN, a dollar sign, "$", denotes that the solver does not execute any coding after its placement on a particular line.

```
$ Flat Plate Model created by Craig Wood
$
$ NASTRAN input file created by the MSC MSC.Nastran input file
$ translator ( MSC.Patran 2001 r3 )
$
ASSIGN OUTPUT2='plate_stress.out' STATUS=UNKNOWN UNIT=20 FORM=UNFORMATTED
$
$ Normal Modes Analysis, Database
$
SOL 103                $ NASTRAN normal modes solution
$
INCLUDE 'mnfx.alt'     $ DMAP alter function used to translate FEA data
$
CEND
SEALL = 100            $ to define all superelement operation on superelement 100
SUPER = 100            $ to define ID of the superelement
$
METHOD = 10            $ Define EIGRL card (eigenvalues calculation)
$
STRESS(PLOT)=ALL       $ Requests element stress output
STRAIN(PLOT)=ALL       $ Requests element strain output
GPSTRESS=ALL           $ Requests grid point stress output
GPSTRAIN=ALL           $ Requests grid point strain output
OUTPUT(POST)
SET 1=ALL              $ Defines a set of elements for a SURFACE
SURFACE 2 SET 1, FIBRE Z1, NORMAL Z      $ Defines a set of plate elements
$                                          defined by the SET command
$
BEGIN BULK
$
DTI, UNITS, 1, mgg, NEWTON, mm, SECOND  $ to assign units for ADAMS
$
PARAM,FIXEDB,-1             $ to avoid calculation on the residual structure
PARAM,AUTOSPC,YES          $ to fix singularities problems
PARAM,GRDPNT,0             $ to debug mass matrix in the NASTRAN .f06 file
PARAM,OLDSEQ,3
$
$ Define the superelement where the external point is node 154 (therefore
$ exclude this node from SESET command).  The number 100 is the unique
$ superelement identifier
$
SESET,100,1,THRU,153
$ Could alternatively use CSUPEXT, 100,154
$
$ Define DOF to use for modes
$
SPOINT,161,THRU,170        $ defines 10 modes, 10 DOF
$
SEQSET1,100,0,161,THRU,170       $ Assign the SPOINT to the Superelement 100
$
$ Define the eigenvalues calculation, where the number of modes equals the
$ number of SPOINTS defined above, in this case 10 modes.  The first 10
$ references the method as described above, and the second 10 is the modes.
```

194

```
$
EIGRL     10                            10        0
$
$ The external nodes must belong to elements with 6 degrees of freedom
$ RBE2, RBAR, CBEAM, CQUADR, CTRIAR
$ no CBAR, CQUAD4, or CTRIA3
$
$ Elements and Element Properties for Shell elements (1.5mm thick)
PSHELL    1         1         1.5       1                   1
$ Define elements, CQUAD4 shell elements in this case
CQUAD4    1         1         16        17        49        15        0.        0.
CQUAD4    2         1         17        18        50        49        0.        0.
$
$$$ A total of 128 elements are used in this model $$$
$
CQUAD4    127       1         142       143       146       147       0.        0.
CQUAD4    128       1         143       144       145       146       0.        0.
$ Referenced Material Records
$ Description of Material (Steel):
MAT1      1         200000. 78988.9 .266      7.86-9  1.17-5
$
$ Define rigid body elements (RBE)
$ This particular RBE attaches nodes 16-24 (dependant nodes) to node 154
$ (independant node).  All DOF of freedom are preserved as denoted by 123456,
$ which represents the translational and rotational DOF.  Node 154 is an
$ external (attachment) node.
RBE2      129       154       123456  16        17        18        19        20
          21        22        23        24
$ Define Nodes of the Entire Model
GRID      1                   24.       90.       0.
GRID      2                   24.       84.       0.
$
$$$ A total of 154 nodes are used in this model $$$
$
GRID      153                 0.        72.       0.
GRID      154                 0.        -12.      0.
$ Loads for Load Case : Default
$ Note that loads would go here, but are not required in superelement
$ analysis, unless residual forces are desired in the structure.  Gravity is
$ also omitted.
$
$ Displacement Constraints of Load Set : Default
$ Single point constraints would go here, but are also not required in
$ superelement analysis.  The DMAP alter will ignore them.
$
ENDDATA
```

James Craig Wood was born on April 21, 1978 in Halifax, Nova Scotia, Canada. He

graduated in 1996 from Fredericton High School in Fredericton, New Brunswick,

Canada. He attended the University of New Brunswick, which is located in Fredericton,

New Brunswick, where he earned his Bachelor of Science in Mechanical Engineering

with Honours in 2001. In 2001, Craig was awarded an NSERC Postgraduate Scholarship

and chose to pursue his education further at the University of Windsor, located in

Windsor, Ontario, Canada. He is currently enrolled as Masters candidate at this

institution, and is scheduled to graduate in the summer of 2003.